

**Design and optimisation of a composite space frame chassis including  
experimental and computational analysis**

**by**

**MIKHAIL NARSAI**

**Submitted in fulfilment of the academic requirements of**

**Master of Science**

in Mechanical Engineering

School of Engineering

College of Agriculture, Engineering and Science

University of KwaZulu-Natal

Durban

South Africa

November 2017

Supervisor: Prof. Sarp Adali

Co-Supervisors: Ms Kirsty Veale, Dr Jared Padayachee

**EXAMINERS COPY**

# COLLEGE OF AGRICULTURE, ENGINEERING AND SCIENCE

## DECLARATION 1 - PLAGIARISM

I, Mikhail Narsai, declare that

1. The research reported in this dissertation, except where otherwise indicated, is my original research.
2. This dissertation has not been submitted for any degree or examination at any other university.
3. This dissertation does not contain other persons' data, pictures, graphs or other information, unless specifically acknowledged as being sourced from other persons.
4. This dissertation does not contain other persons' writing, unless specifically acknowledged as being sourced from other researchers. Where other written sources have been quoted, then:
  - a. Their words have been re-written, but the general information attributed to them has been referenced
  - b. Where their exact words have been used, then their writing has been placed in italics and inside quotation marks, and referenced.
5. This dissertation does not contain text, graphics or tables copied and pasted from the Internet, unless specifically acknowledged, and the source being detailed in the dissertation and in the References sections.

\_\_\_\_\_ Date \_\_\_\_\_

Signed: Mr Mikhail Narsai

As the candidate's supervisor I agree to the submission of this dissertation.

\_\_\_\_\_ Date \_\_\_\_\_

Signed: Prof. Sarp Adali

As the candidate's co-supervisor I agree to the submission of this dissertation.

\_\_\_\_\_ Date \_\_\_\_\_

Signed: Ms Kirsty Veale

As the candidate's co-supervisor I agree to the submission of this dissertation.

\_\_\_\_\_ Date \_\_\_\_\_

Signed: Dr Jared Padayachee

## COLLEGE OF AGRICULTURE, ENGINEERING AND SCIENCE

### DECLARATION 2 - PUBLICATIONS

The paper titled “Destructive Testing of Composite Tubes and Computational Comparison of Failure Theories” is in preparation to be submitted to the Research and Development (R&D) Journal of The South African Institution of Mechanical Engineering (SAIMechE). I am the primary author of that paper and information in it overlaps with information in this dissertation. All experimental work and result interpretation is done by me.

\_\_\_\_\_ Date \_\_\_\_\_  
Signed: Mr Mikhail Narsai

## **Acknowledgements**

Firstly, thanks to all my supervisors for continued guidance and technical assistance. Thanks in particular to Ms Kirsty Veale for her support throughout the year and for the efforts made in this undertaking.

Secondly, thanks to Mr Lincoln Govender for his efforts and expertise during my work at the Durban University of Technology.

Thirdly, thanks to Mr Lionel Dedekind who provided expert guidance in my use of NX Nastran. His assistance greatly increased the efficiency of the work dissertation.

Lastly, thanks to my family and close friends for support and perspective.

## **Abstract**

Composites are used in lightweight structural designs. In this dissertation, a robust carbon fibre reinforced polymer (CFRP) space frame chassis for a lightweight electric tricycle is produced. In large, most composite research is directed toward flat laminates rather than closed sections. This dissertation addresses the complexities of stresses at joints and buckling (local and global). The space frame design consists of two segments of iterations. The second and more important segment is based on optimisation using NX Nastran finite element analysis (FEA). The final design incorporates the use of steel sleeves to address stress concentrations at joints and local buckling. The design and execution of a new test method was developed to validate FEA results. The test method involves applying compressive stress on tubes fabricated using unidirectional (UD) fibre set at  $35^\circ$ , to induce compressive and shear stresses along the primary fibres. In this way, four major failure criteria were compared: Tsai-Wu, Hoffman, Hill and Maximum Strain. The Hoffman and Tsai-Wu criteria were shown to be accurate and conservative. The Hill criteria showed inaccuracy by having incorrectly high strength ratios, while the Maximum Strain criteria had the highest strength ratio, proving to be the least conservative and most inaccurate. This dissertation shows that certain failure criteria may be used confidently in applications such as filament winding and continuous pultrusion methods, which are widely used in producing closed sections.

# Table of Contents

List of Figures .....	iii
List of Tables.....	vi
Nomenclature .....	viii
Acronyms and Contractions .....	ix
1. Introduction .....	1
1.1. Topic Description .....	1
1.2. Background .....	2
1.3. Aims and Objectives.....	2
2. Literature Review .....	3
2.1. Composite Materials.....	3
2.2. Tube Joins.....	6
2.3. Space Frame Chassis .....	8
2.4. Composite FEA .....	10
2.5. Failure Theories and Associated Criteria.....	13
3. Methodology.....	17
3.1. Composite Panels Fabrication and Testing .....	17
3.2. Composite Tubes Fabrication and Testing.....	20
3.3. Tube Finite Element Simulations .....	23
3.4. Design Methodology .....	24
3.5. Finite Element Processes for the Chassis.....	24
3.6. Layup and Sleeve Optimisation.....	25
4. Theoretical Approaches and Considerations .....	27
4.1. Material Selection Considerations .....	27
4.2. Manufacturability.....	29
4.3. Comparison of Members .....	31
4.4. Selecting Optimal Element Sizes .....	34
4.5. Composite Design Considerations .....	37

5.	Testing and Associated FEAs .....	40
5.1.	Coupon Testing for Laminate Properties .....	40
5.2.	Coupon Testing of Cylindrical Members .....	42
5.3.	Failure Criteria Analysed Through FEA.....	42
5.4.	Sensitivity to Material Properties .....	48
6.	Chassis Geometry Design .....	52
6.1.	Bulk Geometry Design and Modifications .....	52
6.2.	Chassis Geometry Optimisation.....	57
7.	Chassis Layup and Sleeve Optimisation .....	71
8.	Discussion.....	86
9.	Conclusions .....	88
10.	References.....	90
	Appendix A .....	94
	Appendix B .....	96

## List of Figures

Figure 2-1: Crimped sleeve and connecting plate (Yang et al. 2016) .....	7
Figure 2-2: Driver and cockpit dimensions (Diamond 2015) .....	10
Figure 2-3: Tube join with thin join region indicated.....	11
Figure 2-4: Example of joint meshing .....	12
Figure 2-5: Detail of example mesh at joint.....	12
Figure 3-1: Tensile panel during infusion.....	19
Figure 3-2: Fabric cut diagram for tube .....	20
Figure 3-3: Tube layup.....	21
Figure 3-4: Tube mid-infusion .....	21
Figure 3-5: Finished tube specimen .....	22
Figure 3-6: Crushed end.....	22
Figure 3-7: Tube compression test setup.....	23
Figure 3-8: Tube test FEA setup .....	24
Figure 4-1: Young's modulus vs density (Ashby 2010).....	28
Figure 4-2: Tensile strength vs density (Ashby 2010) .....	28
Figure 4-3: Staggered seam illustration .....	30
Figure 4-4: Member of changing elliptical cross section .....	31
Figure 4-5: Cross section sketches .....	32
Figure 4-6: Visual of test loading conditions.....	32
Figure 4-7: Element size test part geometry.....	34
Figure 4-8: Test with 6 mm elements .....	35
Figure 4-9: Test with 3 mm elements .....	35
Figure 4-10: Test with 1 mm elements .....	35
Figure 4-11: Test with 6 mm elements and mesh control .....	36
Figure 4-12: Symmetrical laminates (Bailie et al. 1997) .....	37
Figure 5-1: Graph of SR vs E22 .....	49
Figure 5-2: Graph of SR vs G12.....	51



Figure 6-1: Cycling machine schematic.....	52
Figure 6-2: Cycling machine schematic – dimensioned .....	53
Figure 6-3: Chassis version 1 chassis design side view .....	54
Figure 6-4: Chassis version 1 chassis design render.....	54
Figure 6-5: Chassis version 1 design stress analysis result.....	55
Figure 6-6: Chassis version 2 .....	55
Figure 6-7: Chassis version 2 with edits highlighted .....	56
Figure 6-8: Chassis version 2 stress analysis result .....	56
Figure 6-9: Chassis version 3 .....	58
Figure 6-10: Chassis version 3 front join .....	58
Figure 6-11: Chassis version 3 top join.....	59
Figure 6-12: Chassis version 4 .....	59
Figure 6-13: Chassis version 4 front join .....	60
Figure 6-14: Chassis version 4 top join.....	60
Figure 6-15: Chassis version 4 front join meshed .....	61
Figure 6-16: Simulation constraints .....	62
Figure 6-17: Simulation loads.....	63
Figure 6-18: Chassis version 4 displacement plot .....	65
Figure 6-19: Chassis version 4 Hoffman failure index plot .....	66
Figure 6-20: Chassis version 4 ply failure zone close up .....	66
Figure 6-21: Chassis version 4 nodal stress plot close up .....	67
Figure 6-22: Chassis version 4 buckling plot .....	67
Figure 6-23: Chassis version 5 without sleeves.....	69
Figure 6-24: Chassis version 5 .....	69
Figure 7-1: Seat fixture locations relative to human’s approximate mass centre .....	72
Figure 7-2: Chassis version 5 with constraints highlighted .....	74
Figure 7-3: Chassis version 5 displacement plot .....	75
Figure 7-4: Chassis version 5 maximum nodal stress region .....	75
Figure 7-5: Chassis version 5 maximum glue pressure region .....	76
Figure 7-6: Chassis version 5 maximum glue traction region .....	76
Figure 7-7: Chassis version 5 Hoffman strength ratio plot (sleeves hidden for clarity).....	77
Figure 7-8: Chassis version 6 - alterations to chassis version 5 highlighted .....	78
Figure 7-9: Chassis version 6 displacement plot .....	79

Figure 7-10: Chassis version 6 maximum nodal stress region .....	79
Figure 7-11: Chassis version 6 glue pressure extremes .....	80
Figure 7-12: Chassis version 6 maximum glue traction region .....	80
Figure 7-13: Chassis version 6 Hoffman strength ratio plot (sleeves hidden for clarity).....	81
Figure 7-14: Chassis version 7 displacement plot .....	82
Figure 7-15: Chassis version 7 maximum nodal stress region .....	82
Figure 7-16: Chassis version 7 glue pressure extremes .....	83
Figure 7-17: Chassis version 7 glue traction plot .....	83
Figure 7-18: Chassis version 7 Hoffman strength ratio plot (sleeves hidden for clarity).....	84
Figure A1-1: Diagram of mass centre relative to chassis mounting points .....	94

## List of Tables

Table 2-1: Specific modulus and specific strength of typical fibres, composites, and bulk metals (Kaw 2006) .....	4
Table 2-2: Specific modulus parameters $E/\rho$ , $E1/2/\rho$ , and $E1/3/\rho$ for typical materials (Kaw 2006) .....	4
Table 2-3: Properties of some fibres (Nijssen 2015).....	5
Table 2-4: Resin properties (Nijssen 2015) .....	5
Table 2-5: Failure criteria nomenclature .....	14
Table 4-1: Comparison of top fibres based on performance indices.....	29
Table 4-2: Comparison of cross sections results.....	33
Table 5-1: Material properties used in failure criteria - descriptions .....	40
Table 5-2: Laminate test results summary.....	41
Table 5-3: Comparison of laminate test results with Bru et al. (2016).....	41
Table 5-4: Tube test specimen results .....	42
Table 5-5: Results for specimen 1 .....	44
Table 5-6: Results for specimen 2 .....	45
Table 5-7: Results for specimen 3 .....	46
Table 5-8: Failure criteria vs strength ratios .....	47
Table 5-9: FEA results for strength ratios using minimum wall thickness .....	48
Table 5-10: Results from altering E11 .....	49
Table 5-11: Results from altering E22 .....	49
Table 5-12: Results from altering NU12.....	50
Table 5-13: Results from altering G12 .....	50
Table 5-14: Result from including all stiffness values from Bru et al. (2016) .....	51
Table 6-1: CFRP ply properties.....	64
Table 6-2: Spabond LV properties used .....	64
Table 6-3: Summary of geometric optimisations.....	70
Table 7-1: Stainless steel properties from NX.....	72

Table 7-2: Moment loads applied to chassis.....	73
Table 7-3: Chassis version 5 safety factors .....	77
Table 7-4: Chassis version 6 safety factors .....	81
Table 7-5: Chassis version 7 safety factors .....	84

## Nomenclature

$a$	Acceleration
$E$	Elastic modulus
$F$	Failure index
$F_{12}$	Tsai-Wu interaction coefficient
$F_{12}^*$	Normalised interaction term
$G$	Shear modulus
$\nu$	Poisson's ratio
$r$	Radius
$S$	Laminate shear strength
$SR$	Strength ratio
$T_g$	Glass transition temperature
$t$	Time
$v$	Velocity
$v_0$	Initial velocity
$X_c$	Laminate compressive strength parallel to the fibre direction
$X_T$	Laminate tensile strength parallel to the fibre direction
$x$	Distance
$Y_T$	Laminate tensile strength perpendicular to the fibre direction
$Y_c$	Laminate compressive strength perpendicular to the fibre direction
$\sigma_1$	Applied stress parallel to the fibre direction
$\sigma_2$	Applied stress perpendicular to the fibre direction
$\tau_{12}$	Applied shear stress

## **Acronyms and Contractions**

1D	One-dimensional
2D	Two-dimensional
3D	Three-dimensional
CAD	Computer-aided design
CFRP	Carbon fibre reinforced polymer
CV	Coefficient of variance
DUT	Durban University of Technology
GFRP	Glass fibre reinforced polymer
FEA	Finite element analysis
FEM	Finite element model
MWCNT	Multiwall carbon nanotubes
PI	Performance index
SAE	Society of Automotive Engineers
UD	Unidirectional
UV	Ultraviolet

## **1. Introduction**

This dissertation details the design, analysis and optimisation stages of a composite space frame chassis to be used in a lightweight electric tricycle. The focus areas are composite material behaviour, composite failure criteria, buckling, and stresses at joints.

This dissertation begins with a review of current literature, mainly in the focus areas. Next, a theoretical design stage is presented which explores theoretical and practical considerations in a composite space frame. After deciding on a material and member geometry based on a range of factors including manufacturability, experimental testing is presented that eventually validates finite element analysis (FEA) results and Hoffman and Tsai-Wu composite failure criteria in the application of tubes using unidirectional (UD) fibre. Next, with the use of FEA, is the design and optimisation of the chassis (including the addition of steel sleeves at joints) and layup and sleeve optimisation.

After an optimised composite space frame chassis is reached, it is assessed in terms of performance, application, reliability. Also discussed are the test methods and their applicability to other areas, improvements for the chassis based on possible objectives, and further research areas related to this design scenario.

### **1.1. Topic Description**

A composite space frame chassis is required for a lightweight electric tricycle to be manufactured in the future at the University of KwaZulu-Natal. Aluminium space frames have been previously fabricated, but they are heavy in comparison to what can be achieved by using composites. The space frame allows the seating of two people, as the previous space frames have done, and the single wheel, should be positioned at the rear. Front wheel or rear wheel steering may be incorporated in this chassis.

The research in this dissertation is geared toward joint stresses and buckling, as these are known problems in composite structures. The goals of this research are to explore the issue of joint stresses, and to be able to use computational design and optimisation methods with confidence. This research allows better understanding of composite joint behaviour, shows successful methods employed to negate unwanted behaviours, and produces a method of validating computational results.

## **1.2. Background**

Composite materials are useful in applications from aerospace to bicycles. The reason that composite materials are of interest in this dissertation is that they offer high strength-to-mass ratios. Composite materials can be incorporated into many more products if more research is done on them. Comparatively, steel is widely used in engineering due to the abundance of knowledge about how steel reacts under many different conditions.

Analysing very simple geometries made from composite materials can be done analytically but these analyses have been made much simpler and more applicable to complex cases through FEA packages with composite analysis tools. NX Nastran and ANSYS packages can simulate composite laminates that have orthotropic properties, and that have different layup angles. In this report, NX is used. This includes modelling tools for simplification, the finite element modelling (FEM) discretiser, and the NX Nastran solver. NX can model connections as contact or glue elements, however, modelling the joints is more accurately achieved by designing geometry between connecting components and applying the adhesive material to those joints. The reason for such complexity is that the discontinuity of fibres must be accounted for in the software and because joints can be high stress areas, and likely the failure zones. Members in a spaceframe may be in compression. Buckling is always a consideration for slender members in compression, and as such should be duly assessed in structures such as space frames. NX Nastran and ANSYS can both compute buckling studies but NX is used throughout this study.

## **1.3. Aims and Objectives**

The aim of this research was to produce a space frame chassis design for a light vehicle made from composite materials and to validate computational results. The following objectives are defined:

- Research and select suitable composite materials (filler and matrix)
- Research current methods of producing composite parts
- Research how fibre orientation affects strength of the laminate
- Analyse joint stresses and other stress concentrations
- Develop joint geometries and methods of joining parts to handle or minimise stress
- Analyse buckling on the chassis
- Optimise the chassis to avoid buckling and joint failure under reasonable loading
- Optimise fibre orientations to minimise stress
- Validate FEA results and failure criteria by testing failure experimentally



## **2. Literature Review**

Research in composite materials is becoming more abundant. The following literature review presents some of the current research relating to composites and space frames, and the context of this dissertation in relation to that research.

### **2.1. Composite Materials**

A composite material is the term used to describe the combination of two or more materials that remain separate and do not mix together after combining them. In general, 2 materials are used. One material is called the matrix, and implanted in it is the reinforcing material (Kaw 2006). The reinforcing material can be long or short fibres, particles or even flakes. Carbon fibre reinforced polymer (CFRP) is an example in which the carbon (graphite) unidirectional fibres or weave is the reinforcement in a polymer matrix. Concrete is an example in which stones are the discrete reinforcing in the macroscopically continuous cement matrix.

In mechanical engineering applications such as vehicle design, CFRP is used in many vehicles and in many applications. Koenigsegg, for example, produces components such as the intake manifold, the wheel rims and various body panels from CFRP and Kevlar based composites (Shury 2015). In temperature intensive environments, composites are used to reduce the thermal expansion where that of metals is too high (Kaw 2006). The main advantage to using composites is the reduction of mass. Kaw (2006) composed Table 2-1 which shows properties of common reinforcement fibres against common metals. It highlights the reduction of mass that is possible with either similar or even much higher strength.

Table 2-1: Specific modulus and specific strength of typical fibres, composites, and bulk metals (Kaw 2006)

Material Units	Specific Gravity	Young's Modulus (GPa)	Ultimate Strength (MPa)	Specific Modulus (GPa.m <sup>3</sup> /kg)	Specific Strength (MPa.m <sup>3</sup> /kg)
Carbon fibre	1,8	230,00	2067	0,1278	1,148
Aramid fibre	1,4	124,00	1379	0,08857	0,9850
Glass fibre	2,5	85,00	1550	0,0340	0,6200
UD carbon/epoxy	1,6	181,00	1500	0,1131	0,9377
UD glass/epoxy	1,8	38,60	1062	0,02144	0,5900
X carbon /epoxy	1,6	95,98	373,0	0,06000	0,2331
X glass/epoxy	1,8	23,58	88,25	0,01310	0,0490
Quasi-isotropic carbon /epoxy	1,6	69,64	276,48	0,04353	0,1728
Quasi-isotropic glass/epoxy	1,8	18,96	73,08	0,1053	0,0406
Steel	7,8	206,84	648,1	0,02652	0,08309
Aluminium	2,6	68,95	275,8	0,02652	0,1061

UD – unidirectional

X – cross-ply

specific gravity is the ratio of material density to that of water

Kaw (2006) goes on to derive performance indices that optimise mass and deflection in a rod based on failure due to buckling. These are shown respectively in the last two columns of Table 2-2. Maximising  $E^{1/2}/\rho$  minimises mass, and maximising  $E^{1/3}/\rho$  minimises deflection (Kaw 2006). The table highlights composites' large rigidity compared to metals. Note that further analysis using performance indices will be computed during the design stage.

Table 2-2: Specific modulus parameters  $E/\rho$ ,  $E^{1/2}/\rho$ , and  $E^{1/3}/\rho$  for typical materials (Kaw 2006)

Material Units	Specific Gravity	Young's Modulus (GPa)	$E/\rho$ (GPa.m <sup>3</sup> /kg)	$E^{1/2}/\rho$ (GPa <sup>1/2</sup> .m <sup>3</sup> /kg)	$E^{1/3}/\rho$ (GPa <sup>1/3</sup> .m <sup>3</sup> /kg)
Carbon fibre	1,8	230,00	0,12780	266,4	3,404
Aramid fibre	1,4	124,00	0,08857	251,5	3,562
Glass fibre	2,5	85,00	0,03400	116,6	1,759
UD graphite/epoxy	1,6	181,00	0,11310	265,9	3,535
UD glass/epoxy	1,8	38,60	0,02144	109,1	1,878
X carbon/epoxy	1,6	95,98	0,06000	193,6	2,862
X glass/epoxy	1,8	23,58	0,01310	85,31	1,593
Quasi-isotropic carbon/epoxy	1,6	69,64	0,04353	164,9	2,571
Quasi-isotropic glass/epoxy	1,8	18,96	0,01053	76,50	1,481
Steel	7,8	206,84	0,02652	58,3	0,7582
Aluminium	2,6	68,95	0,02662	101,0	1,577

Nijssen (2015) compares some general fibres in Table 2-3 which shows that carbon fibre has much better performance considering its mass, strength and stiffness. Fracture length is the ultimate strength divided by the density and gravitational constant. As such, it is closely proportional to the specific strength (Nijssen 2015).

Table 2-3: Properties of some fibres (Nijssen 2015)

Property	Stiffness (GPa)	Breaking Strength (MPa)	Failure Strain (%)	Density (kg/m <sup>3</sup> )	Fracture Length (km)
E-glass	70-80	2 400	2,6	2 500-2 600	96
Carbon	160-440	2 000-5 300	1-1,5	1 800-2 000	187
Aramid	60-180	3 100-3 600	1,7	1 540	238
Bamboo	15-12	100-200	-	400-800	25

While fibre properties are of high importance, matrix properties must be equally considered. In general, elastic modulus of the fibre will be much higher, causing it to undertake much more stress than the matrix. Table 2-4 shows some common resin properties.

Table 2-4: Resin properties (Nijssen 2015)

Property	Stiffness (GPa)	Ultimate Strength (MPa)	Ultimate Strain (%)	Density (kg/m <sup>3</sup> )	Curing Shrinkage (%)
Polyester	2,4-4,6	40-85	1,2-4,5	1 150-1 250	6-8
Vinylester	3-3,5	50-80	5	1 150-1 250	5-7
Epoxy	3,5	60-80	3-5	1 150-1 200	<2

The filler should be chosen with a lower surface tension than the fibre material such that it can sufficiently wet the fibres in order to achieve adhesion (van Rijswijk 2017). This allows the matrix to carry the loads to the fibres effectively. The matrix material that is generally used for high mechanical strength is epoxy resin. In polymer matrices, one should not use the epoxy near its glass transition temperature ( $T_g$ ), as the softening will reduce its mechanical properties (AMT Composites 2017). This is applicable in the case of a vehicle, as it can reach elevated temperatures when out in the sun. Additionally, the sun produces ultraviolet (UV) rays which degrade materials by severing chemical bonds, but this can be prevented by using a gel coat (van Rijswijk 2017). The gel coat is applied on the finished product or in the mould.

Further, more comprehensive material selection charts have been made available by Ashby (2010) and Shah (2014) which better compare specific composite materials visually. These are used in section 4.1 and are explained in context.

Pre-impregnated (or prepreg) plies are sheets of fibre that have been impregnated with the matrix already, and only require assembly and post-cure. These provide an alternative manufacturing method to conventional wet-layup methods.

Because fibres are orthotropic, the laminates too are orthotropic. Laminates can be made to exhibit strength in one or more directions by altering the orientation angle in the fibre plies it is made up of. This means that the layup angles can be optimised for a specific loading condition such that strength is only exhibited in the directions in which it is needed. NX Nastran has optimisation capabilities which allow it to isolate ply existence and/or ply orientation angle as an optimisation variable to optimise the model for minimum stress, mass or other goals. This optimisation is a key factor in this dissertation.

Light material is sometimes used between plies to increase thickness and therefore bending strength of the overall sandwich panel (van Rijswijk 2017). It is possible to incorporate this into circular sections by using hard foams, but this complicates and limits manufacturing methods.

Laminate properties can be calculated by hand based on constituents, although both NX Nastran and ANSYS either use existing laminate properties, or calculate laminate properties based on volume fractions of constituents.

## **2.2. Tube Joins**

Composite materials are known for their high strength-to-mass ratios, resulting in high strength components taking up less space than the equivalent metal component for example. Stress concentrations occur at joins in all materials. Joins are especially important in composite materials because at those regions, the strength of the material can drop significantly because the adhesive material has lower strength than the laminate. The other major issue is that the stress transfer in the fibres is interrupted, and does not transfer to the fibres in the next member directly.

NX Nastran can simulate joints such as these by defining a region of adhesive material near the join, on one of the tubes being joined. This effectively shows both the discontinuity of fibre, and allows a detailed representation of the joint stresses.

To help distribute the forces at joints, wraps made from twill fabric are sometimes used. This method is very difficult to model computationally. Additionally, this method can be inconsistent depending on the fabrication method. If a wet-layup is performed, the twill weave is distorted, and this distortion is slightly different for each joint and each fabrication. A testing

method that is better suited to this is experimental testing and statistical analysis. Quantitative information for these joining methods are not readily available and are generally kept proprietary by the companies that develop the techniques.

More et al. (2017) conducted a comparison of a steel space frame against an equivalent space frame using properties of carbon fibre using ANSYS. The carbon fibre section of the analysis was inaccurate because firstly the material was treated as isotropic, and secondly it did not consider any discontinuities. These factors are extensively covered in this dissertation.

A part solution to increase strength of the join material is to introduce multiwall carbon nanotubes (MWCNT) into the join material, knowing that this type of combination can produce a synergetic product. Zielecki et al. (2016) experimentally tested the fatigue aspect of three epoxies used in joins and concluded that MWCNT does in fact increase the fatigue life of the joins in question (although no tensile strength values are presented as it is purely a fatigue study). In general, composites resist fatigue better than metals do and this is attributed to the fact that crack propagation in the matrix is continuously slowed by fibres (van Rijswijk 2017). At these “crack arrest zones”, the crack must change direction to go around the fibre.

Yang et al. (2016) sidestep this problem successfully by using crimped metal sleeves (Figure 2-1a) bonded adhesively to the end of glass fibre reinforced polymer (GFRP) tubes, and bolted connections (Figure 2-1b).



Figure 2-1: Crimped sleeve and connecting plate (Yang et al. 2016)

These joints were tested in tension and compression with the variable of interest being bond length between steel and composite. Success of the bond was determined by buckling failure of the GFRP tube, buckling failure of the crimp, or tensile failure of the steel or GFRP tube.

Currently there is much research on flat laminates some of which compare experimental results with FEA results (Chowdhury et al. 2016), but little work has been done on tubular laminates. Some work done on joining tubular laminates includes both experimental and finite

element testing (Hoa & Lee 2015), but they consider only butt joints or lap joints which are perpendicular to the length on the tubes. This is not applicable to space frames, in which the cuts will be complex (multi-axis cuts) and joints will be both edge-to-edge and edge-to-surface. The joint members are also not parallel.

### **2.3. Space Frame Chassis**

This dissertation presents a tricycle structure rather than a conventional high speed or motorised/downhill vehicle. As such, it is not required to abide by the standards associated with such vehicles. That being mentioned, the standards are generally to serve the purpose of safety and stability, so these factors are considered during design.

The considerations of the space frame design are as follows:

- Driver protection in a crash or roll
- Ability to maintain a level of rigidity during loaded conditions (no large displacements)
- Maintaining stability during turning\*
- Driver ergonomics

\*While the chassis is a contributing factor, the suspension plays a larger role in that the ride height and track width can be altered to maintain contact/traction during turns.

Siegler et al. (1999) express that roll bars are required for safety, and include a low centre of mass as an optimisation constraint to even out weight distribution. In a lightweight space frame, it is important to have a low seating position as most of the mass is due to the driver. A lower centre of mass reduces the moment load when turning. Left unchecked, this moment can cause toppling. Another method of avoiding toppling is to widen the track width.

Eurenius et al. (2013) consider torsional stiffness as a high priority in their composite chassis. They see value in this metric as a high torsional stiffness results in better handling, although they note that the best way to increase this lies in the suspension and force distribution to suspension components. The application for this metric is for high-speed and high-performance vehicles, especially those designed to turn at high speeds.

To withstand frontal crash impact, Siegler et al. (1999) employed a sacrificial nose cone in their Formula-style vehicle for the annual Society of Automotive Engineers (SAE) competition. Composites such as CFRP absorb energy by fracturing rather than yielding, so sacrificial members may serve the purpose of dissipating crash energy.

Adali et al. (2003) used analytical techniques to predict and inhibit buckling of composite laminates in which loading conditions were uncertain. Walker et al. (1995) analytically

optimise cylindrical tubes under torsion and compression using CFRP material properties in which the optimisation variable is ply angle. In their study the beam is simply supported. These methods to predict buckling can serve as a qualitative goal in this dissertation because the space frame is under very different loading. For example, Walker et al. (1995) determine that 90° plies inhibit buckling caused by torsion. Because this study is computational, these papers are considered qualitatively, and buckling checks are computed through FEAs.

Regarding FEA, Siegler et al. (1999) conducted extensive non-linear impact analyses using ANSYS on their metal monocoque chassis to optimise the shape. NX Nastran has the capability to run explicit non-linear FEAs, but they require high computational power, and knowledge of damage characteristics of the material. An approximate equivalent non-linear static analysis may be set up using calculated parameters about the system stiffness and mass, provided that the impact time is large in comparison to the system's natural period (Juvinal & Marshek 2012).

Ergonomics addresses the logistical concerns surrounding the driver and vehicle operation. This includes the following:

- Comfortable seating in the vehicle
- Easy operation of the pedals
- Lines of sight from seated position
- Embarking and disembarking the vehicle

It should be reiterated that this dissertation includes the design of the chassis, but not the associated fixtures such as seat fixtures, although mounting points are included in the design (which constrains the load applied by the driver and passenger).

To assist in seating position of the driver, Figure 2-2 is presented, which relates to several types of vehicles.

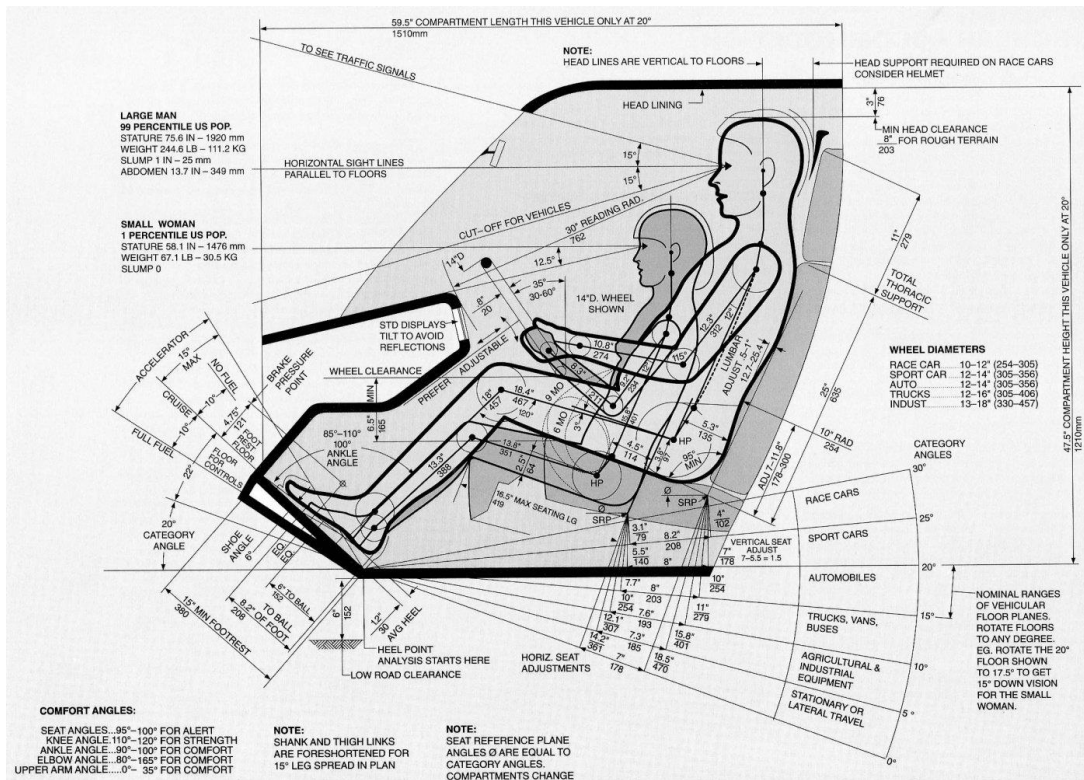


Figure 2-2: Driver and cockpit dimensions (Diamond 2015)

The safety factor of a vehicle is an important consideration because of the nature of the application. It is known that vehicles experience imperfections in road conditions and must perform manoeuvres in an emergency. Crash safety is a critical factor because even if the vehicle is in conditions it was not designed for, effort should be made to reduce harm to the driver and passengers. It must be stated that the safety factor is not included to allow the vehicle to withstand loads outside the scope of the design, but in some cases, may account for design loading. On one side of the spectrum is aircraft. They have low safety factors to allow reduction of mass. For aircraft, the requirement for the ultimate safety factor is 1,5 (Modlin & Zipay 2014). This is based on very well-known materials and loading conditions in various scenarios. For the space frame in this dissertation, recommendations by Juvinal & Marshek (2012) suggest that safety factors can be as small as 1,5 - 2,5 due to material, loading and environment certainty. They further recommend doubling safety factors where ultimate strength is used instead as the allowable limit, and state that impact loading may warrant the use of safety factors between 2 and 4.

## 2.4. Composite FEA

FEA consists of discretising a computationally modelled object or series of computationally modelled objects into one-dimensional (1D), two- dimensional (2D) and/or three-dimensional



(3D) shapes. The use of FEA provides a simpler way to analyse a design for the purpose of optimisation, because changes can easily be made, and the model simulated again. This contrasts with experimental testing, in which a new structure would likely have to be made, and tests carried out. This, apart from being likely costly and taking more time, means that a testing jig may have to be designed and built. For small deformations in static analyses, linear models may be used for computational efficiency. In this dissertation, the Nastran direct sparse solver within NX is used.

The main structure of the chassis consists of composite tubes. This is modelled by NX Nastran using 2D shell structures and specifying the material properties (either for filler and matrix separately, or for each ply), number of plies, and each ply orientation and thickness.

As discussed, the joins are more complex to simulate, but are achieved by using separate computer-aided design (CAD) geometry for each join. This usually entails dividing the cylindrical face of one member by offsetting the curve of the join as shown in Figure 2-3.

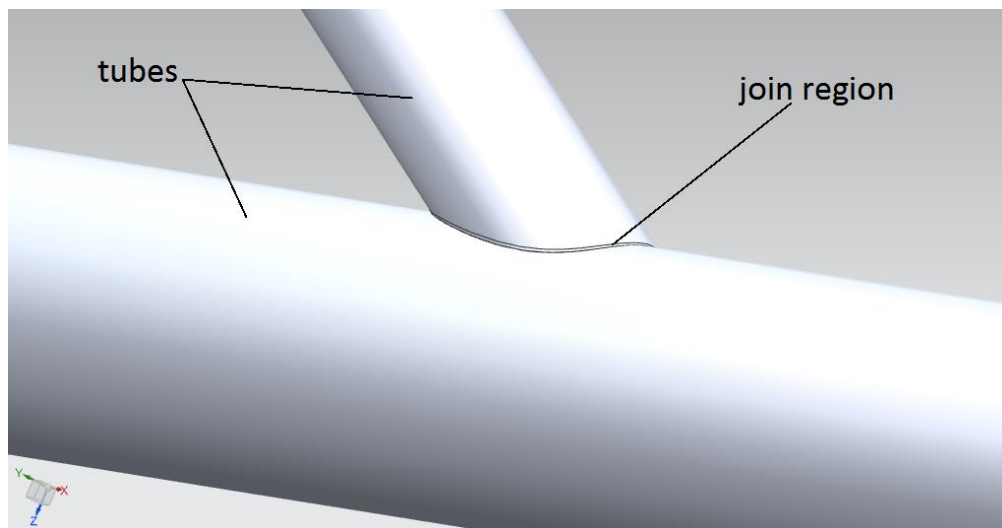


Figure 2-3: Tube join with thin join region indicated

The join region is meshed as a separate entity, but the mesh joins to the tubes. This is illustrated in Figure 2-4.

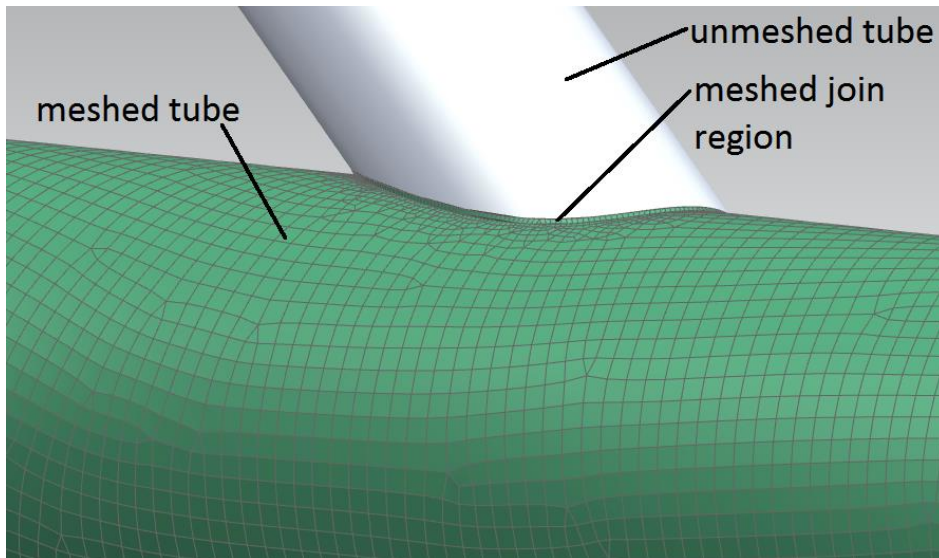


Figure 2-4: Example of joint meshing

Figure 2-5 shows that the mesh of the tube surface has material even inside the hole. This is not always the case, as geometry that is united causes a hole to be present. Care should be taken to obtain the geometry that represents reality.

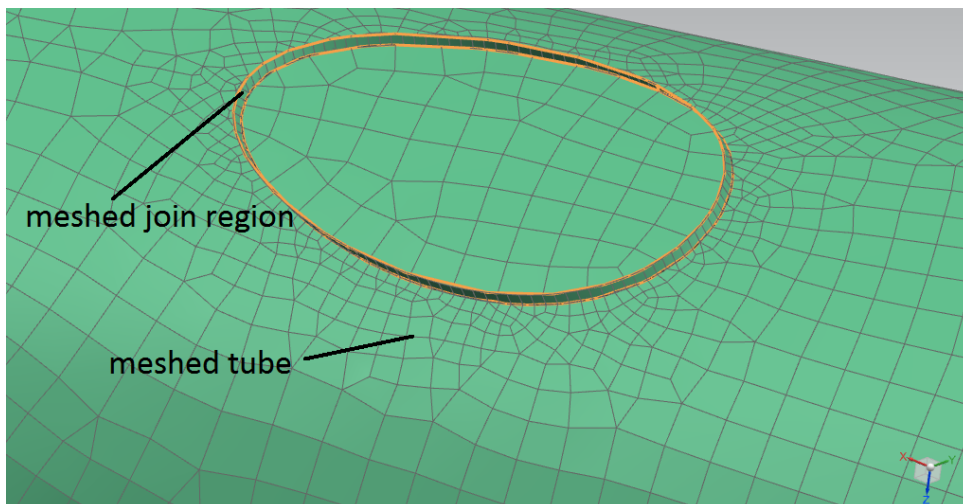


Figure 2-5: Detail of example mesh at joint

In practice, joints can be wrapped in a figure-8 or otherwise to aid in distributing forces through fibre rather than purely the adhesive. Simulating this is incredibly difficult as each wrap is slightly different as they may have different orientations, different levels of stretch and warp, and different amounts of epoxy. Even experimentally testing a joint with wraps would prove challenging to ensure consistency.

Wraps allow better stress distribution in joint regions. This is useful when adhesive material is the failure point. For this reason, they can be added at known areas of high stress (assumed critical areas or results from FEAs), but they should be considered as an extra protection method rather than a measurable stress relieving component until testing can confirm this.

NX allows laminates to be laid up ply-by-ply, with each ply having its own thickness, material and orientation. Reference values for various materials may be obtained from NX, ANSYS or Autodesk Heliux Composite packages.

Buckling is a consideration both for general stability and for crash scenarios. NX can simulate buckling and crashes. One analysis is a pure buckling analysis; the other is a transient nonlinear analysis that can be used to test crashes. A solution is to use the results from the buckling analysis and static analysis separately instead of running a computationally heavy crash analysis.

## **2.5. Failure Theories and Associated Criteria**

Predicting failure of composites is not as simple as it is in metals. The orthotropic nature of composites disallows the stresses to simply be reduced to a single stress that is comparable to the tensile strength of the material as is done in von Mises calculations. Because of this, the micromechanics of composite materials gives rise to various failure criteria, generally consisting of multiple failure strengths in warp and weft directions.

There are many theories and methods to analyse or predict orthotropic laminate failure. Almost all of these methods differ fundamentally (in their approaches) and produce widely varied results. Some show differences of final failure (total fracture and separation) stress of up to 970% as tested by Soden et al. (1998). In addition, many methods neglect the residual stress induced due to curing of the laminate as this effect is highly dependent on more than one variable during curing, including curing time, curing temperature and ambient pressure. Most failure theories use an approach to determine failure of the laminate or individual plies, but interlaminar failure is not assessed because the theories only assess in-plane stress. In NX Nastran, it is possible to predict interlaminar failure by specifying allowable shear stress between plies (dependant mainly on matrix material strength). This value can be obtained through experimental testing. NX Nastran can use various criteria to determine failure, including Puck, Hill, Hoffman, Tsai-Wu, Maximum Stress and Maximum Strain. Unfortunately, the Puck failure criteria requires much experimental work to determine various constants and is therefore not considered in this dissertation.

In NX, the failure criteria tested are Tsai-Wu, Hoffman, Hill and Maximum Strain. In each case, the theory uses a failure index to predict whether failure has occurred or not. A failure index below zero indicates non-failure. The failure index is not necessarily comparable to a safety factor. To address this, a strength ratio is calculated, sometimes as a function of the failure index. The strength ratio is a factor that when multiplied by the loads, causes failure. The following information regarding the processing of the failure criteria by NX and NX Nastran is sourced from the NX Laminate Composite Student Guide by Siemens (2012).

For the following equations relating to the failure theories, the notation is shown in Table 2-5.

Table 2-5: Failure criteria nomenclature

$X_T$	Laminate tensile strength parallel to the fibre direction
$X_C$	Laminate compressive strength parallel to the fibre direction
$Y_T$	Laminate tensile strength perpendicular to the fibre direction
$Y_C$	Laminate compressive strength perpendicular to the fibre direction
$S$	Laminate shear strength
$\sigma_1$	Applied stress parallel to the fibre direction (positive values denote tension)
$\sigma_2$	Applied stress perpendicular to the fibre direction (positive values denote tension)
$\tau_{12}$	Applied shear stress
$F$	Failure index
$SR$	Strength ratio

The Hill failure criterion is described as follows:

$$F = \left(\frac{\sigma_1}{X}\right)^2 - \frac{\sigma_1\sigma_2}{X^2} + \left(\frac{\sigma_2}{Y}\right)^2 + \left(\frac{\tau_{12}}{S}\right)^2$$

With the strength ratio as:

$$SR = \frac{1}{\sqrt{F}}$$

In the Hill failure criterion, the first term uses  $X_C$  if compression is applied, and  $X_T$  if tension is applied. The second term uses  $X_T$  if the applied stresses have the same sign, and  $X_C$  if they have different signs. The third term operates in a similar fashion to the first term.

The Hoffman failure criterion is described as follows:

$$F = \frac{\sigma_1^2}{X_T X_C} - \frac{\sigma_1 \sigma_2}{X_T X_C} + \frac{\sigma_2^2}{Y_T Y_C} - \frac{\sigma_1 (X_T - X_C)}{X_T X_C} - \frac{\sigma_2 (Y_T - Y_C)}{Y_T Y_C} + \left( \frac{\tau_{12}}{S} \right)^2$$

The strength ratio is obtained by multiplying each stress term above by the strength ratio (SR) and setting F equal to one then solving the quadratic equation. The smallest positive root should be considered.

The Tsai-Wu failure criterion is described as follows:

$$F = F_1 \sigma_1 + F_{11} \sigma_1^2 + F_2 \sigma_2 + F_{22} \sigma_2^2 + 2F_{12} \sigma_1 \sigma_2 + F_{66} \tau_{12}^2$$

Where:

$$F_1 = \frac{1}{X_T} - \frac{1}{X_C}$$

$$F_{11} = \frac{1}{X_T X_C}$$

$$F_2 = \frac{1}{Y_T} - \frac{1}{Y_C}$$

$$F_{22} = \frac{1}{Y_T Y_C}$$

$$F_{66} = \frac{1}{S^2}$$

$F_{12}$  is user-defined, but is set as zero if the following equation is not satisfied:

$$F_{11} F_{22} - F_{12}^2 > 0$$

The strength ratio is calculated in the same way as in the Hoffman theory.

The interaction term  $F_{12}$  must be determined experimentally through biaxial testing (Sun et al. 1996). Narayanswami & Adelman (1977) expressed that setting the interaction term as zero provides adequate accuracy for engineering purposes in filamentary composite materials loaded biaxially. Their testing consisted of ten composite combinations and six loading conditions and maximum error in predicted loads was under 10%. Note that setting the interaction term to  $1/X_C X_T$  reduces the Tsai-Wu theory to the Hoffman theory (Sun et al. 1996).

Cui et al. (1991) explored using various values for the normalised interaction term denoted and defined as follows:

$$F_{12}^* = \frac{F_{12}}{\sqrt{F_{11}F_{22}}}$$

Their study focused on delamination, so their final value of 0,7 for the normalised interaction term may not apply to this dissertation. Tsai & Hahn (1980) described the normalised interaction term acting in a similar way to the von Mises criterion in isotropic materials.

### **3. Methodology**

The overall methodology for this dissertation is due to a top-down view. What is required is a design of a composite space frame chassis. A design likely involves iterations and optimisations. To design and optimise this chassis, designs must be analysed. FEA is the chosen method of analysis due to the impracticality of experimentally testing design iterations, the inability to analytically calculate stresses for a large and geometrically complex chassis, and the impracticality of optimising the design and repeating the process. The use of FEA prompts the topic of results validation, possibly through comparative research. If comparative research is unavailable, a method to produce experimental results should be pursued, as is done in this dissertation. The kind of experimental testing should be similar to the conditions that the chassis is under in order to be comparable. For composites, predicting failure is done using failure criteria. This means that testing panels to obtain necessary properties must first be carried out.

The previous paragraph is a step-by-step process in reverse order of how to possibly execute this design. In this dissertation, it is presented this way to an extent, although in many cases, there was work done in perceivably later stages that allowed an initial stage to be done better. An example of this is the simulation of a near-complete design simply to understand the stresses in the composite tubes, then designing testing around that. Van Rijswijk (2017) describes that this approach is far from uncommon because material, design and manufacturing are very closely linked. He uses the term “trinity thinking” to explain this concept.

#### **3.1. Composite Panels Fabrication and Testing**

Testing was completed at the Durban University of Technology (DUT) Composites Technology Station under the supervision of Mr Ebrahim Cassim and Mr Lincoln Govender. Flat panels were fabricated by the author under supervision. 12K 300 GSM UD carbon-fibre cloth manufactured by Gurit (product code R163-040) was laid up and infused with Prime 20LV resin and slow hardener under 1 bar of vacuum. Matrix and filler materials were purchased from AMT Composites in August 2017. Testing adhered to ASTM (previously known as the American Society for Testing and Materials) standards and the report from DUT may be found in Appendix B.

The manufacturing processes for all the flat panels were very similar and were as follows:

- A glass surface was waxed 4 times
- Pre-cut plies of carbon fibre were laid on the glass between two sheets of peel ply
- A mesh was placed over the peel ply almost until the end of the carbon
- Cormat was placed at the vacuum end
- Sealant tape was bordered around the layup
- Resin inlet, vacuum outlet and pressure gauge tubes were positioned along with spiral binder
- The layup was sealed with plastic vacuum bag
- The inlet tube was blocked, and the vacuum end was placed under vacuum until 100 kPa of vacuum was reached
- The outlet tube was blocked, and the system was left for 1 hour to ensure that no leaks were present
- The vacuum was reapplied, and the resin was allowed to infuse
- Procedure for “vacuum-off time” and “de-mould time” were followed from the data sheet for Prime 20LV depending on the ambient temperature
- The system was post cured at 65°C for 7 hours after de-moulding
- The panel was neatened by trimming the edges, ensuring it was square and that 0° lined up with the fibres
- Tabs were adhered onto the panel

Figure 3-1 shows the setup during infusion. Panels were all vacuum-infused to achieve similar fibre volume fractions. The volume fractions of the panels were first calculated before the panel was infused, then they were checked using a matrix digestion test.



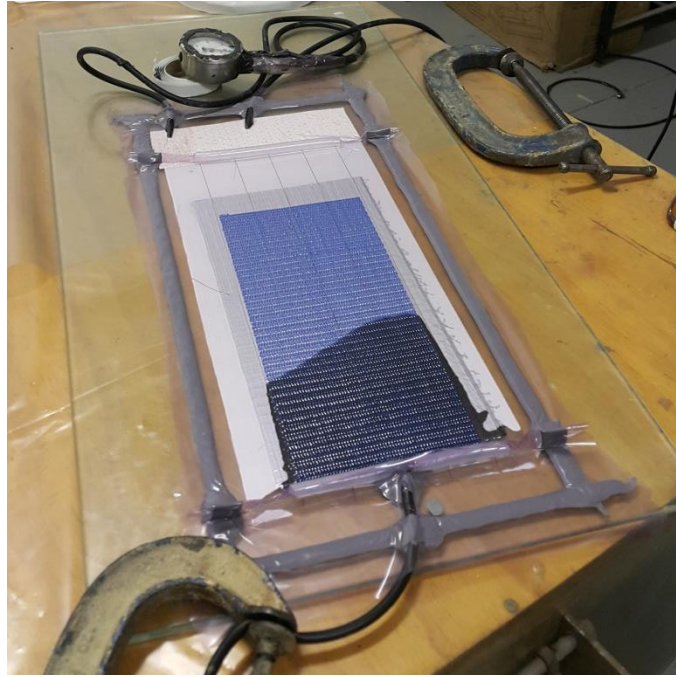


Figure 3-1: Tensile panel during infusion

The tests on the specimens were conducted in accordance with relevant ASTM standards as follows:

- Tensile test and elastic modulus in accordance with ASTM D3039 (0° and 90°) (ASTM International 2014)
- Compressive test in accordance with the Modified D695-15 (0° and 90°) (ASTM International 2015b)
- Shear strength test in accordance with the ASTM D3518 (ASTM International 2013)
- Shear modulus test **guided** by the ASTM D3518 (ASTM International 2013)
- Matrix digestion test in accordance with the ASTM D3171-15 (ASTM International 2015a)

As stated, the shear modulus test was only guided by the ASTM D3518 standard. This is because to measure horizontal shortening during loading, a micrometer was used as there was no usable strain gauge amplifier for that specific job. This means that the  $G_{12}$  value has a measure of uncertainty because the timing of the micrometer reading had to match with the load value or extensometer reading during the test. This was done by the author calling for readings during the test when certain load values were reached, and Mr Govender continuously measuring the specimen and calling out the micrometer value.

The ASTM D3518 standard (In-Plane Shear Response of Polymer Matrix Composite by Tensile Test of a  $\pm 45^\circ$  Laminate) was chosen as the test standard because it is the more likely shear failure mode when compared to shearing of the carbon fibre tows. The ASTM D3518 standard promotes failure dominated by matrix strength as well as friction between fibres.

### 3.2. Composite Tubes Fabrication and Testing

As mentioned, the goal of this test is to validate FEA results because the chassis is only tested computationally. It is impractical to test every member with each possible layup, so a simplified but more universal test is designed.

Early simulations showed that many members in the chassis were under compression or a combination of compression and shear loading. Bending stresses were also present, but their effects were small in comparison to the compressive stresses.

To simulate a member under compression and shear loading, the following test was designed. A tube was fabricated from UD cloth with the fibre angle set at  $35^\circ$ . By testing the specimen in compression, the fibres would experience a combined load of compression and shear due to the angle, thus including more terms in failure criteria expressions and testing the theories more fully. The  $35^\circ$  angle was chosen to induce a certain amount of shear without weakening the tube in the axial direction so much that it failed in the wrong mode. Figure 3-2 shows how the fabric was cut so as not to sever fibres in their primary direction.

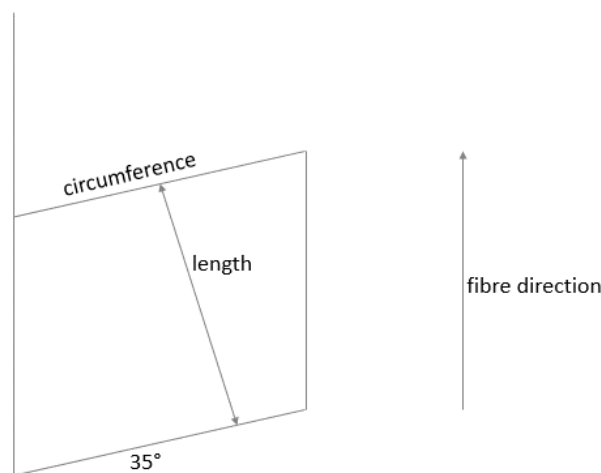


Figure 3-2: Fabric cut diagram for tube

Two layers of fibre were used per tube to avoid buckling. This was determined using approximate properties from Bru et al. (2016) and simulating the test. UD fabric and the same angle were used to eliminate interlaminar shear playing a role, and so that initial failure would

quickly lead to final/ultimate failure. This removes the need for a transient, non-linear damage analysis. The plies were laid up on a polished aluminium mandrel as shown in Figure 3-3.



Figure 3-3: Tube layup

The layup was vacuum infused to maintain the same properties as the flat test specimens so that the properties from those tests may be used in simulating this test. Infusion and cure conditions were identical to previous flat panels. Other consumables were experimented with and used in the infusion to ensure a good tube. Mainly, a blue mesh was incorporated to ensure a uniform vacuum around the tube, and to stop the vacuum bag from being directly against the mandrel, as that would lock the pressure off. Figure 3-4 shows the process of infusing the tube. The dark region of carbon fibre is wet with resin while the lighter portion has yet to be impregnated.

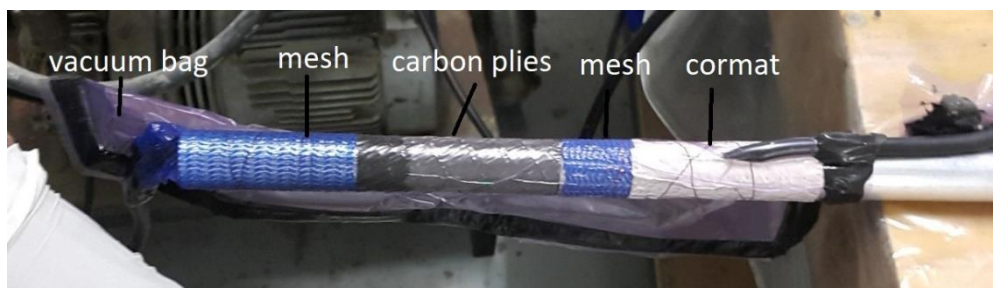


Figure 3-4: Tube mid-infusion

The finished tube is shown in Figure 3-5. The tubes' surfaces were wavy because of the vacuum bag compressing the fibres to a point where they found a place to pleat. Peel ply was tested to improve this, but it was impossible to remove after de-moulding without damaging the tube. This waviness means that the tube thicknesses were inconsistent, and that there were small stress concentrations rather than uniformity throughout.



Figure 3-5: Finished tube specimen

Three tubes were tested in compression. End crushing was first experienced, shown in Figure 3-6.



Figure 3-6: Crushed end

Sandpaper was then used at the top and bottom of each specimen to stop slip and end crushing. In addition, a collar was used at the bottom to ensure a fixed rotation condition at that end. The top did not have a collar. Figure 3-7 shows this setup.

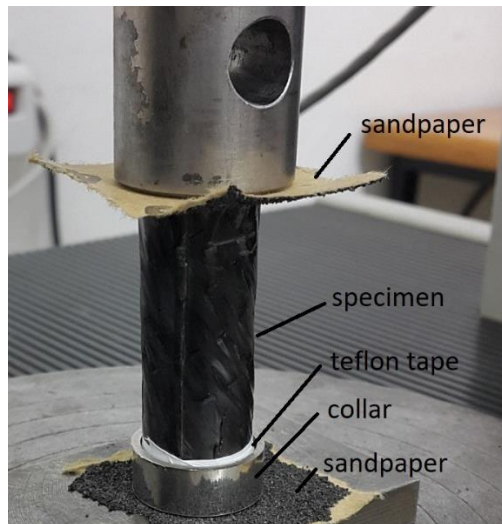


Figure 3-7: Tube compression test setup

### 3.3. Tube Finite Element Simulations

FEAs in NX Nastran were conducted to compare against the experimental data. The FEMs (generated in NX) consisted of 1 mm CQUAD4 elements for accuracy. Each test had the geometry and ply thickness changed to match the experiment. Because the inner diameter was measured, the reference plane was set to “BOTTOM” from the default “MIDDLE”. When the Tsai-Wu failure criteria was selected, the interaction term was unspecified, because it requires testing, but it can still be used with a degree of confidence without it. Also, using the Tsai-Wu theory without any parameters that require additional testing puts it on level pegging with other failure criteria. Some FEAs had different material properties to others, so the body of the report contains material property data. To directly compare the FEA to experimental results, the material properties from flat coupon testing was used in the FEA.

At the lower end where the collar was, the mesh was fixed in translation and rotation. At the top, translation was fixed in the horizontal plane and rotation was only allowed about the local angular coordinate. Figure 3-8 shows the meshed geometry with the loads and constraints active.



Figure 3-8: Tube test FEA setup

The force applied to the top was the failure load from the compressive test, so the results of the FEAs are failure indices and strength ratios.

### 3.4. Design Methodology

In this dissertation, “trinity thinking” (van Rijswijk 2017) was used to design. Manufacturing constraints were explored extensively because CFRP tubes have many manufacturing methods, some of which have stress anomalies that weaken the overall structure (such as hand layup), and because some methods restrict ply angles (such as pre-made tubes from woven fabric).

Considerations such as centre of mass position (Siegler et al. 1999) and safety were used in designing the geometry of the chassis. Geometric optimisation of the chassis was based on analysing FEA results to find stress concentrations or large displacements, then repositioning members to redirect forces. Safety factor recommendations from Juvinal & Marshek (2012) were used to determine a minimum safety factor of 2 for the chassis, and then the chassis was optimised to meet this requirement.

### 3.5. Finite Element Processes for the Chassis

Modelling the structure computationally was done using SolidWorks for its weldments function. Custom weldment profiles were designed for the tubes, adhesive films and sleeves.

NX then handled geometry optimisation, meshing and simulation. The geometry was imported to NX using a parasolid file. The geometry was optimised within the modelling application

where necessary, then meshed. Tubes were meshed using 2D shell meshes on the outer diameters. They were 6-10 mm, CQUAD4 elements for most tubes, but the change in element size to accommodate small features was automatically handled by NX. Mostly, free mapped meshing resulted in good quality meshes. The laminate reference plane was set to "TOP". Sleeve and adhesive meshes were 3D, CTETRA10 elements to enhance mesh quality. They were 8 mm and 6 mm respectively to increase computational efficiency without increasing aspect ratio enough to significantly reduce mesh quality. For the 3D meshes, free mapped meshing resulted in unacceptable skewing because of join regions, so the standard meshing method was used. Laminate layup was handled within the FEM application. Material properties were defined within NX. Some FEAs had different material properties to others, so the body of the report contains material property data.

The simulation function in NX then handled loading conditions, constraints and gluing. The loading and constraints were dependant on each other because dynamic situations, such as turning and braking, were simulated as a static scenario for computational efficiency. Suspension points were constraints, and loads were applied in directions that would simulate braking and turning, despite the true acceleration direction of the vehicle. The gluing function (specifically surface-to-surface gluing) identified two faces and allowed their contact faces to move rigidly with one another. This was used for all adhesive-to-tube and adhesive-to-sleeve connections. The outputs of the glue regions are "glue pressure" which shows the tensile or compressive stress perpendicular to the faces, and "glue traction" which shows the shear stress parallel to the faces.

### **3.6. Layup and Sleeve Optimisation**

Plies were specified to predominantly run parallel to the tubes' lengths (0° plies). This is because the stresses in space frames tend to be mainly tensile or compressive. 0° plies were added to reduce deflection and decrease the likelihood of global buckling. No ply angle optimisation was required due to the high strength of the tubes in comparison to other components that would surely fail first. A possible method for optimisation may include analysing stresses in the 0° plies to observe the ratio of stresses in the fibre direction to stresses perpendicular to the fibre direction (or shear stresses, depending on what contributed to failure index more). A ply in the existing layup may then be rotated to an angle that would attempt to translate the perpendicular stress or shear stress into axial stress along the fibre length of that ply.

First designs showed that joining tubes to each other produced high stresses, so methods from Yang et al. (2016) were employed. Sleeves were used, but instead of crimped ends, the entire composite join was surrounded by a steel sleeve. These sleeves were lengthened and shortened based on the amount of stress they and their associated adhesives were under. Reducing the sleeve length shed mass, while increasing the length reduced stresses in the adhesive and the sleeve. Increasing fillet radii also reduced stress drastically, although impractically large fillet radii may be replaced by gussets if modelled and tested. The steel sleeves are assumed to be cut (and bent if needed) and welded from round tube stock. Where material sizes may be unavailable, larger diameter pipes may be used so long as the minimum wall thickness is maintained. Composite tubes may be sized accordingly.



## 4. Theoretical Approaches and Considerations

Design must begin with considering manufacture and material (van Rijswijk 2017). This section explores material selection based on the application, making use of performance indices. Manufacturability is then explored with focus on possible manufacturing methods that allow accurate modelling and FEA. Member comparisons are then presented in the application of space frames. Mesh sizing is then considered, and optimal meshing methods are determined.

### 4.1. Material Selection Considerations

In Table 2-1, it is seen that the main fibre constituents used in structural applications are carbon fibre, aramid fibre and glass fibre. This is because of their strengths and moduli in relation to their masses.

To minimise mass, Ashby (2010) provides performance indices as follows:

- PI1.  $\text{Max}\{E/\rho\}$  – struts loaded in tension (section area is the free variable), **minimises deflection**
- PI2.  $\text{Max}\{E^{1/2}/\rho\}$  – beams loaded in bending (section area is the free variable), **minimises deflection**
- PI3.  $\text{Max}\{\sigma_u / \rho\}$  – struts loaded in tension (section area is the free variable), **minimises stress**
- PI4.  $\text{Max}\{\sigma_u^{2/3} / \rho\}$  – beams loaded in bending (section area is the free variable), **minimises stress**

In a space frame, members predominantly experience tensile, compressive and bending loads. Two objectives are to minimise deflection because of stability concerns, and to minimise stress because in laminates, stresses in multiple directions can cause failure according to the available failure criteria. Thus, all 4 performance indices are of interest. Figure 4-1 and Figure 4-2 show the material selection charts relevant to these 4 performance indices.

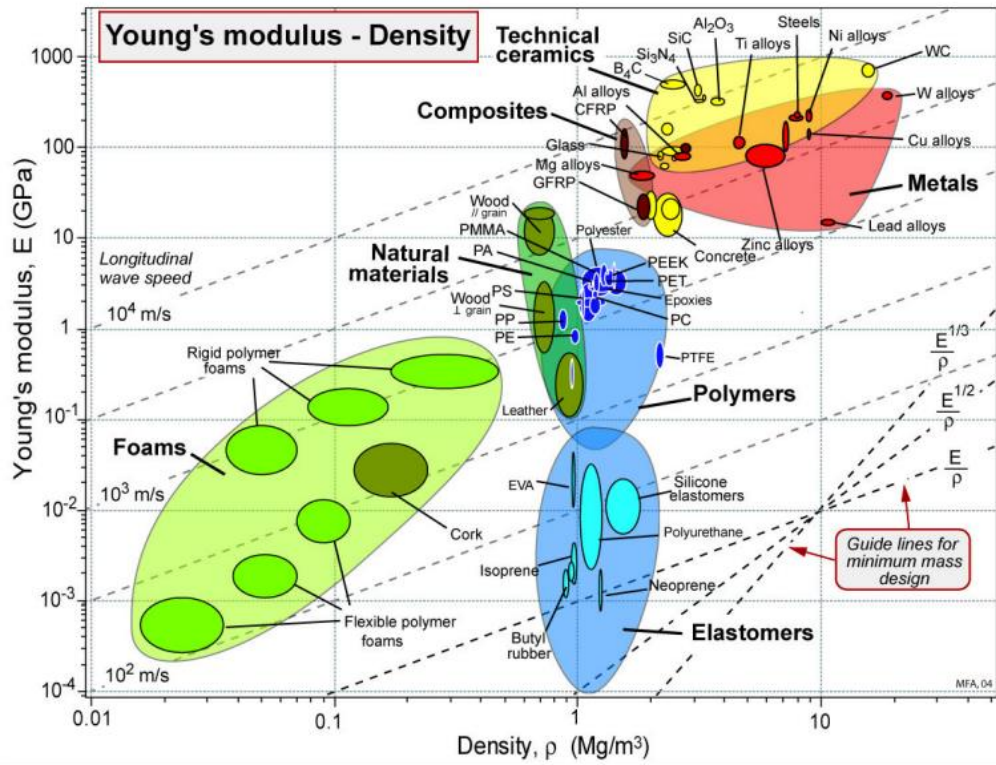


Figure 4-1: Young's modulus vs density (Ashby 2010)

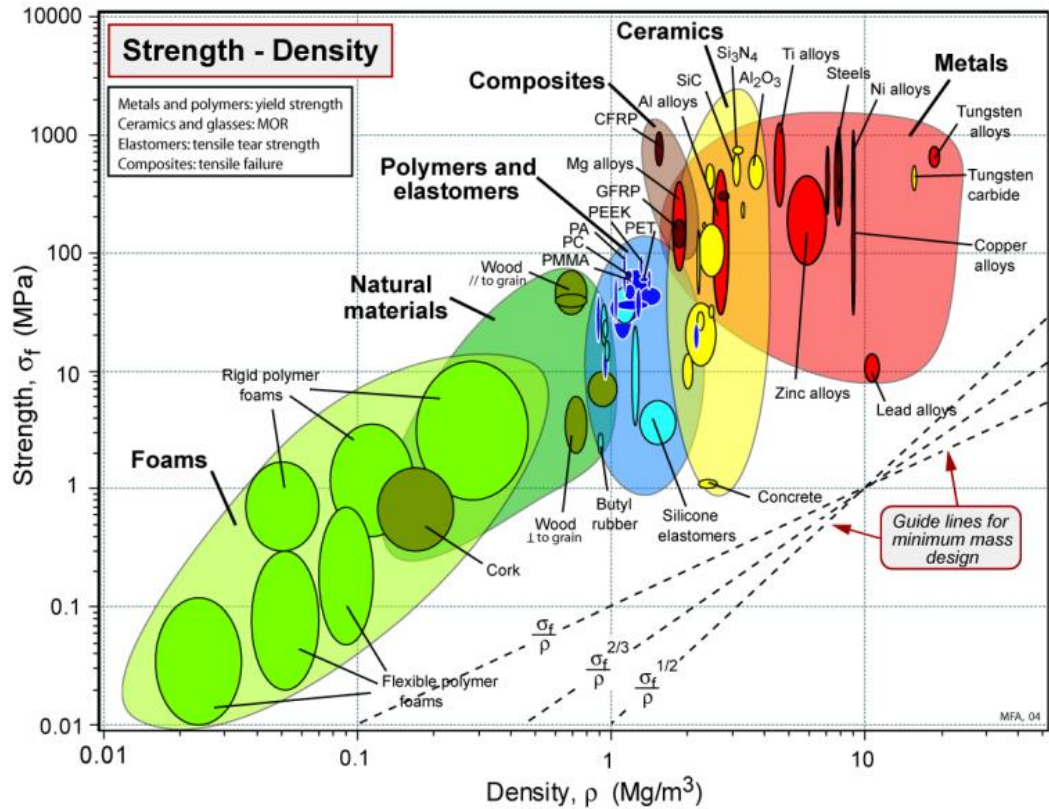


Figure 4-2: Tensile strength vs density (Ashby 2010)

CFRP is higher than GFRP for all 4 categories based on the above charts. These relate directly to laminates rather than the fibre constituents. Considering the fibre constituents, Table 2-2 provides data relating to performance indices 1 and 2 and shows that carbon fibre is the most rigid in a mass optimisation situation. Table 2-1 has data on performance index 3 and allows the calculation of performance index 4. Again, carbon fibre has the highest value. This data is summarised in Table 4-1.

Table 4-1: Comparison of top fibres based on performance indices

	PI1	PI2	PI3	PI4
	$E/\rho$ (GPa.m <sup>3</sup> /kg)	$E^{1/2}/\rho$ (GPa <sup>1/2</sup> .m <sup>3</sup> /kg)	$\sigma_u / \rho$ (MPa.m <sup>3</sup> /kg)	$\sigma_u^{2/3} / \rho$ (MPa <sup>2/3</sup> .m <sup>3</sup> /kg)
Carbon	0,12780	266,4	1,148	0,0901
Aramid	0,08857	251,5	0,9850	0,0885
Glass	0,03400	116,6	0,6200	0,0536

To conclude, carbon fibre is the fibre constituent chosen for this space frame, having the highest values in all 4 performance indices of interest and showing promise when combined with a polymer. This is shown by CFRP having high values than GFRP for all 4 performance indices as well (no comparison is available for aramid fibre combined with a polymer). The matrix selected is an epoxy resin as this is what is widely used with carbon fibre for its high strength and modulus as shown in charts by Nijssen (2015). This is also what is supplied and recommended by composite suppliers in South Africa.

## 4.2. Manufacturability

Space frames in vehicles usually consist of rods or tubes loaded in tension and compression. Therefore, the method of manufacture recommended in this dissertation is pultrusion and filament winding. This is because stress concentrations at seams are avoided, and pultrusion involves running fibre along the length of the section, giving it strength in that direction. By continuously winding fabric, angles of plies can be accurately laid-up. Note that for machine-wound laminates, if the mandrel has a non-circular cross-section, there could be fibre/weave distortion at the corners due to different fibre tension as distance from the mandrel's centre changes.

A lower cost method that may be useful for small batch sizes is the hand layup method. With the use of a rotating mandrel (of any cross section), sections can be continuously wound with unidirectional or cross-ply fabric without discontinuity along the length of the tube. The only weakness is at the overlap line. The fibre steps up, causing non-uniformity and an area at

which the fibre may be less stretched; leading to premature failure dominated by the matrix. Additionally, at the overlap line, fibres would be severed if cross-ply is used, meaning that hoop stresses would be interrupted on the top and bottom layers. Note that automated versions of this process are employed using prepreg material.

An alternative method is to wind UD fabric one layer at a time, and the seam can be staggered for each successive layer. In Figure 4-3, four layers are shown with staggered seams 90° apart. This pattern can then be repeated for each successive layer.

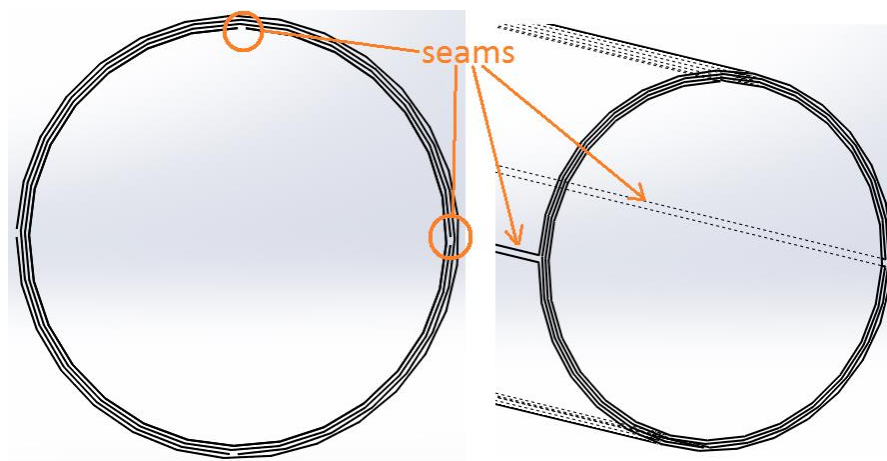


Figure 4-3: Staggered seam illustration

The discontinuity makes an insignificant difference in UD fibre because load bearing fibres are not severed in preparing the plies. This means that so long as the ends are neat and join very closely, the ply, and therefore finished laminate, will show no anomaly at any seam.

Koenigsegg, the car manufacturer, uses prepreg carbon fibre and the hand-layup method for all their carbon fibre parts on panels and wheel rims (von Koenigsegg 2013). They use prepreg material (with pre-determined volume fraction) so that there are no inconsistencies in ply properties that may occur with wet-layup by hand, so that the laminate is more consistent. Prepregs are also used for easier workability.

For consistency between panels and tubes, the impregnation method is vacuum infusion.

The consideration of manufacturing method is significant for the modelling and FEAs that follow. By assuming no discontinuities in the fibre, the remaining critical points in the structure are the joins.

### 4.3. Comparison of Members

In a space frame, a variety of cross-sections are available for members. Here, the cross-sections that are assessed are circular, square and elliptical.

Circular cross sections provide uniform strength properties due to axial symmetry. They are the most mass-produced of the three.

Square cross sections provide a higher moment of area for the same nominal size as circular cross sections, albeit using more material. They provide an opportunity to make the space frame more rigid without making it bulkier. A downfall of this cross section is the stress concentrations at the corners. Introducing fillets reduces this, but also diminishes the advantage over circular cross sections.

Elliptical cross sections, offer the most in terms of strength and lightness. One can provide strength in bending along one axis, while saving material in shortening the other axis. Bicycles make use of this by using an elliptical cross section at one end of a member, then transforming it to another ellipse that is orientated perpendicular to the first. This helps to handle the stresses at both ends of the member. This is shown in Figure 4-4.

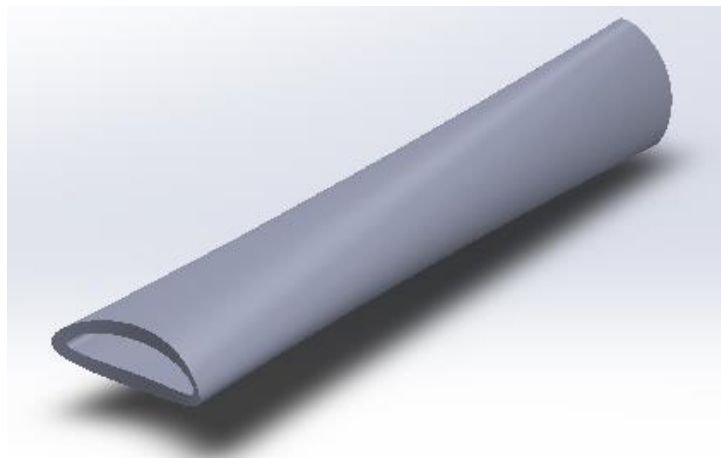


Figure 4-4: Member of changing elliptical cross section

Using NX Nastran, the three cross sections were compared by constructing a 400 mm pipe with the various cross sections as shown in Figure 4-5. Note that the square cross section tested three fillet radii to reduce the possible stress that may be present with a low radius. Each cross section has a nominal size of 60 mm, with the ellipse having the minor diameter as half its major diameter.

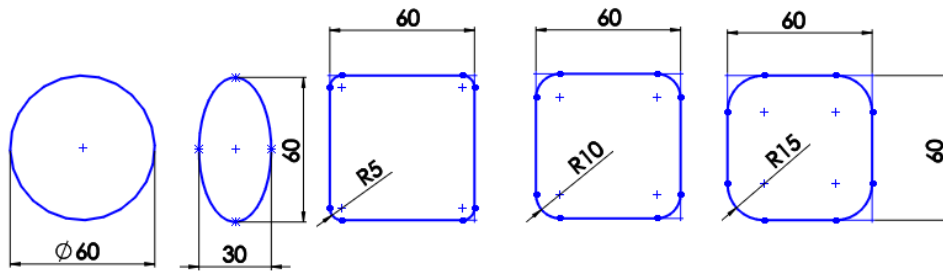


Figure 4-5: Cross section sketches

Two scenarios were tested. The first was for bending, in which one end of the beam was loaded with a 500 N force and the other end was fixed. In the case of the ellipse, the force acted parallel to the major diameter (as this would be the scenario in which the member is used). The second scenario was for torsion, in which one end was loaded with a 25 Nm torque and the other end was fixed. Due to the orthotropic nature of the composite, the torque was applied in the same direction relative to the layup in each case. Figure 4-6 shows the two scenarios. In each case, four layers of AS4 graphite were used with an epoxy matrix in a 60:40 volume ratio (matrix and filler components sourced from Autodesk Heliux Composite and defined separately in NX). The finished thickness used was 1 mm, with the layup being four plies of UD fibre at [45/-45/-45/45] to give a broad view of CFRP behaviour.

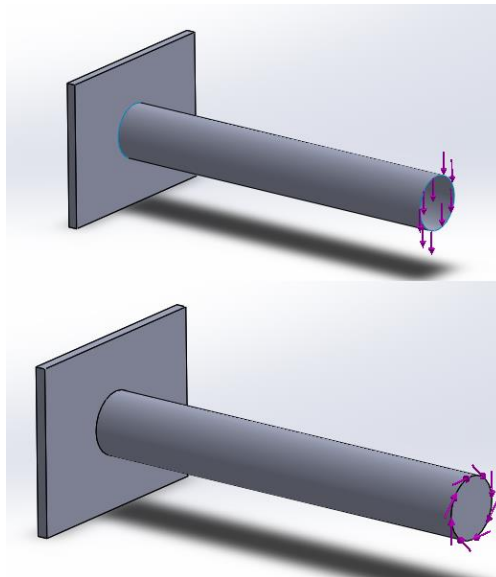


Figure 4-6: Visual of test loading conditions

The results are summarised in Table 4-2. Relative perimeter and stiffness are with reference to the circular cross section as it is the simplest and most symmetrical.

Table 4-2: Comparison of cross sections results

Cross Section	Bending Scenario		Torsion Scenario		Average Perimeter (mm)	Second Moment of Area (x10 <sup>3</sup> mm <sup>4</sup> )	Relative Perimeter	Relative Stiffness
	Maximum Displacement (mm)	Maximum Stress (MPa)	Maximum Displacement (mm)	Maximum Stress (MPa)				
Circular	3,162	60,89	0,01260	58,38	188,5	84,8	1,00	1,00
Elliptical	4,948	91,43	0,06065	71,08	145,4	55,0	0,77	0,65
Square (5 mm) fillet	1,961	66,78	0,02260	170,2	231,4	135,9	1,23	1,60
Square (10 mm) fillet	2,108	55,53	0,01407	42,69	222,8	127,0	1,18	1,50
Square (15 mm) fillet	2,297	54,16	0,01340	44,03	214,2	117,3	1,14	1,38

With comparison to the circle, the ellipse loses significant stiffness and has much higher stress for its 23% material savings. The issue is that the elliptical shape has comparatively little material at its stressed extremities, resulting in a lower second moment of area about the neutral axis. It is therefore an inefficient cross section for this application. It should be noted that it experiences more stress due to the smaller loaded area and stress concentration on the major axis. The square cross sections greatly increase the stiffness, but require more material. The optimal cross section from the three square cross sections is the one with 10 mm fillets, as it experiences only slightly more stress than the larger fillet size, and much less than the smaller fillet size in bending. In torsion, it strikes a balance between increasing its second polar moment of area and reducing the stress concentration caused by the corner. The smaller fillet size causes too much of a stress concentration, and the larger fillet size means that the second polar moment of area is reduced as its shape becomes more circular. For this cross section, 18% more material than the circular cross section results in 59% more stiffness. For so much more stiffness, the stress value is not as low as expected. This is due to the stress concentrations at the corners. Pursuing this cross section would be prudent, but the fillet size would have to be increased to an optimal point that it reduces stress significantly enough to warrant the increased perimeter and manufacturing complexities. An optimised design would be that instead of circular beams, smaller square beams could be used, which may eventually save material.

In this dissertation, the circular cross section is chosen because it has fewer manufacturing complexities and is used more commonly. Also, joining square tubes will likely produce higher stress concentrations than joining circular tubes.

#### 4.4. Selecting Optimal Element Sizes

To determine the range for optimal element size, a series of FEAs were conducted on a test part that consists of two cylinders that are to be meshed as tubes. The large tube has a 90 mm nominal diameter and the intersecting small tube has a 60 mm nominal diameter. These sizes are arbitrary, but the relation to the element sizes is significant. The geometry is shown in Figure 4-7.

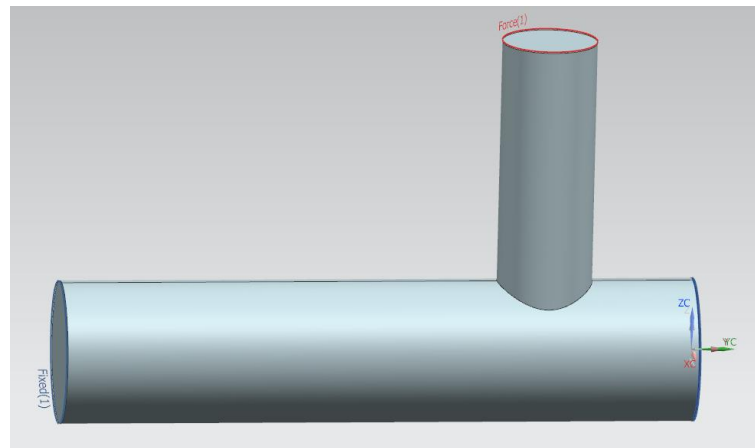


Figure 4-7: Element size test part geometry

The ends of the large tube experience fixed constraints while the top end of the small tube experiences a force in the negative Y direction (coordinate system shown in the figure). The meshes were set up using the orthotropic sample fibre in NX and the epoxy materials, so the results that follow are only quantitatively important when comparing to **each other**. Four plies were set up for symmetry and the results all show the first ply. Figure 4-8 shows the result with 6 mm element sizing.

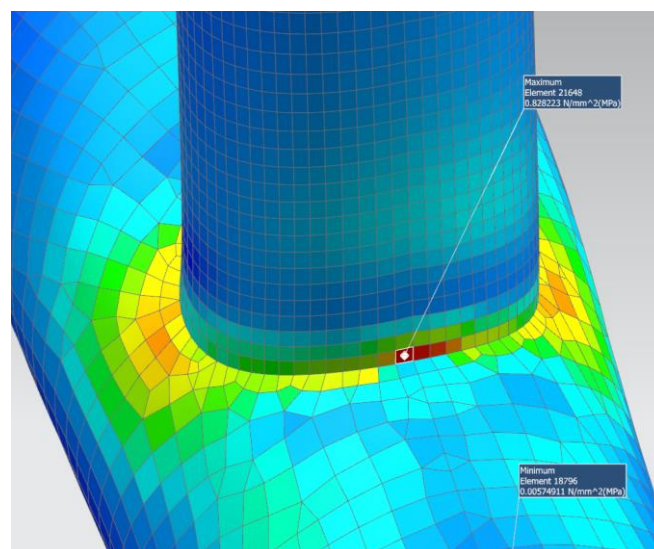




Figure 4-8: Test with 6 mm elements

Figure 4-9 shows the result with 3 mm element sizing. The stress changes by less than 2%.

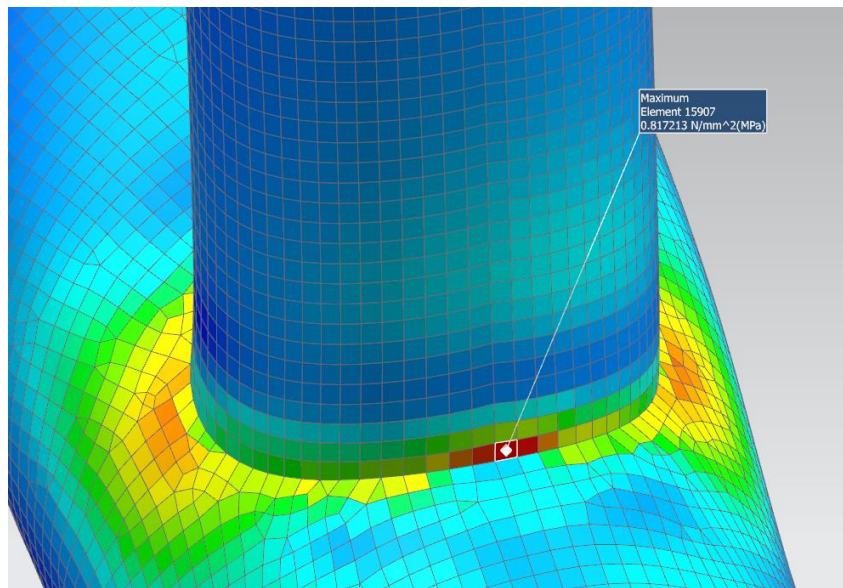


Figure 4-9: Test with 3 mm elements

Figure 4-10 shows the result with 1 mm elements. Mesh control was adopted as automatic mesh generation produced large elements at the join. The difference in stress is 16%. Note also the area of low stress before a band of higher stress that is actually further away from the join.

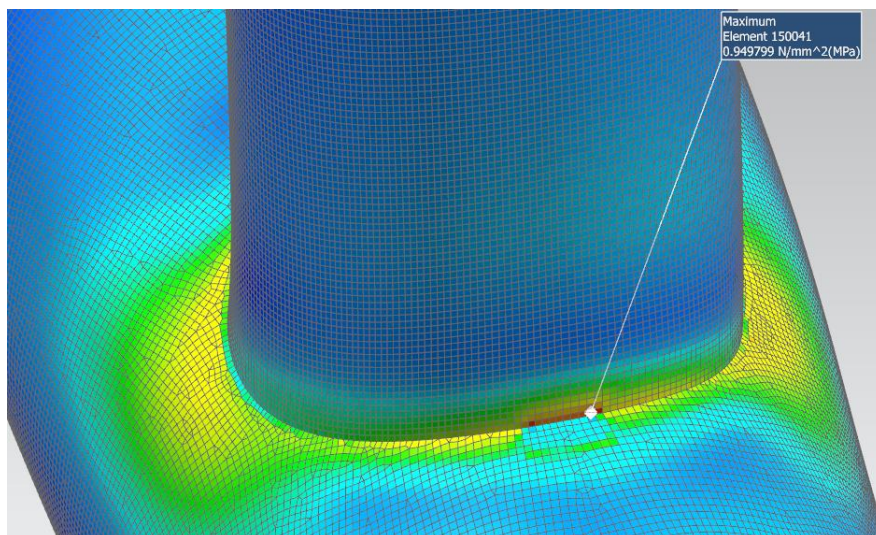


Figure 4-10: Test with 1 mm elements

These results show that using elements 2% the size of the diameter provide significantly more accurate results than using elements 10% the size of the diameter. This implies that elements

10% the size of the diameter do not provide sufficient accuracy. Note also that there may be stress anomalies such as the band of low stress surrounded by higher stress. This may be attributed to the orthotropic nature of the material as well as the fact that the analysis looks only at one ply of the laminate for uniformity.

A final FEA was conducted on the test piece using a 6 mm element size, but with user-enforced mesh control at the joining edge, as was done when using 1 mm elements. Figure 4-11 shows the result.

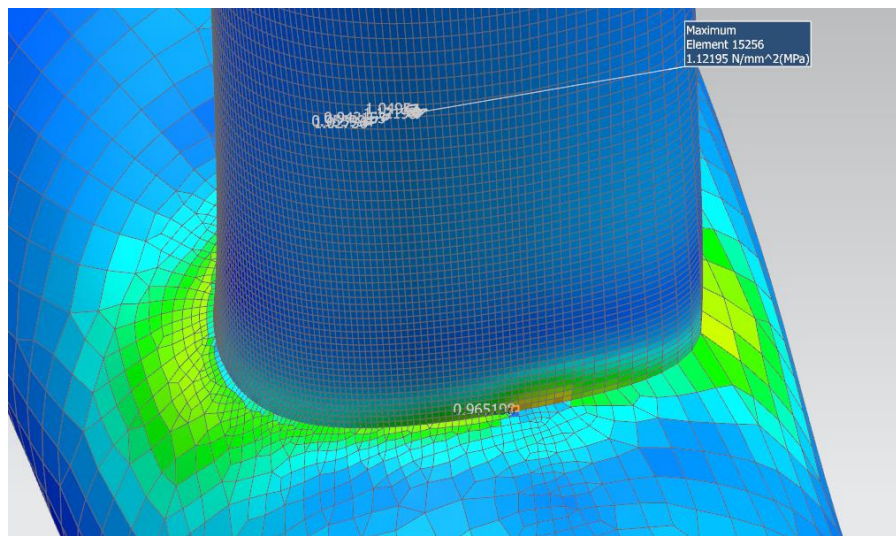


Figure 4-11: Test with 6 mm elements and mesh control

The above figure shows a much more computationally efficient model while preserving the advantages of small elements. This is advantageous at zones where the geometry is complex, or where higher accuracy is required. The maximum stress has increased as shown in the diagram, but that specific element had a bad aspect ratio and it is likely abnormally high due to this. This element is also outside the area of interest and can therefore be ignored for this purpose. The highest stressed element in the area previously analysed is shown on the figure near the area. The difference in stress there compared to the 1 mm test is 1%.

It can therefore be concluded that with sufficient mesh control at the significant edges, smaller element sizes can be incorporated into larger meshes to reduce the inaccuracy of the simulation. The element size at the joints should be in the region of 2% the size of the smaller diameter involved in the join to achieve mesh independence. Element quality should also be considered.

#### 4.5. Composite Design Considerations

If a ply of UD fabric in a laminate is at an angle to the applied stress, it will take the load but cause flexure stress in the laminate. To avoid this, laminates can be designed to be symmetrical about their middle planes (van Rijswijk 2017). This means that the layup pattern from the mid plane to one outer surface is the same as from the mid plane to the other outer surface. An example of a symmetrical callout would be  $[0/30/90]_s$  which is the same as  $[0/30/90/90/30/0]$ . This setup also prevents warping due to thermal changes because forces on one side of the symmetrical plane (or neutral axis) are directly opposed to forces on the other side of the symmetrical plane. This type of warping is common because of cooling during curing (Barbero 2011). In addition, it is suggested that the laminate be balanced, to eliminate the membrane coupling between the in-plane shear and normal stresses (van Rijswijk 2017). This entails matching each ply with another ply orientated in the negative angle of that ply (except for  $0^\circ$  and  $90^\circ$ ). This concept is illustrated in Figure 4-12.

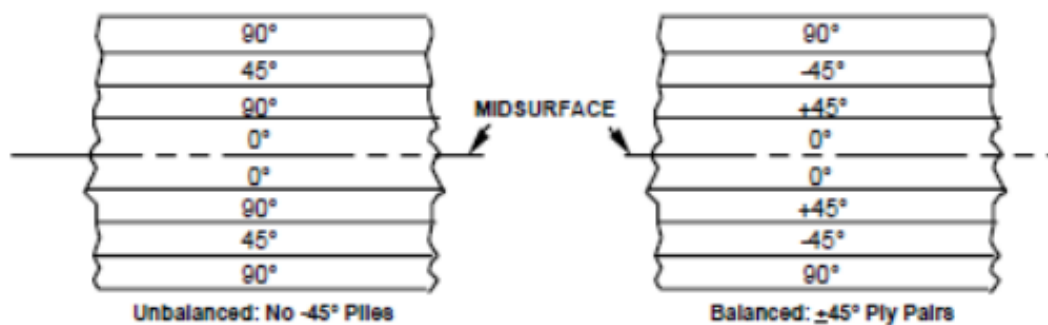


Figure 4-12: Symmetrical laminates (Baillie et al. 1997)

These techniques can be employed in tubular laminates to minimise the warping and flexure effects. It does not eliminate all the stresses due to the different radii of plies inside and outside of a symmetrical surface (note that the symmetrical plane would instead be structured as a cylindrical surface).

A practical design technique is to place the ply that carries the primary load (fibres parallel to the load) on the innermost surface, away from the environment. This is so that if the laminate is scratched or other minor surface damage occurs, the fibres of the most important ply are undamaged (van Rijswijk 2017). A gel coat can be used to minimise this damage, and to protect the laminate from harmful UV rays (van Rijswijk 2017).

While high fibre content is desirable, it is important to note that the more fibre is present (compared to the matrix), the more surface area of fibre must be covered with matrix. This

comes a point at which increasing fibre content becomes detrimental to laminate strength due to ineffective adhesion of matrix material.

In a crash scenario, the driver must remain safe. Vehicles make use of metal crumple zones to absorb this crash energy. While metal plastically deforms to absorb the energy from an impact, composite materials such as CFRP and GFRP absorb this energy by fracturing and delaminating (specifically debonding), and aramid composites tend to buckle to absorb the energy (Thornton & Jeryan 1988). Although the vehicle does not have to adhere to automobile standards, it would be careless to completely neglect crash or low-velocity impact safety.

The following points describe what may be considered when determining the safety factor of the vehicle, partly based on broad recommendations by Juvinall & Marshek (2012):

1. Uncertainties/tolerances in layup procedure: the hand layup method means that small deviations in fibre angles may be present
2. Defects in laminate due to environment: unless the environment is extremely controlled, the laminate will exhibit slight differences in properties to the finite element model (van Rijswijk 2017); this can be due to contaminants or voids weakening the laminate, temperature inconsistencies causing undesired curing effects, or moisture reducing adhesion between fibre and matrix
3. Hardener volume inaccuracies: causes undesired curing effects
4. Residual thermal stresses caused by curing (Soden et al. 1998)
5. Differences in failure criteria (Soden et al. 1998)
6. Human injury as a consequence of structural failure
7. Dynamic loading such as bumps or quick reactions

While the above factors contribute to the safety factor, analyses should always be carried out alongside material property testing to validate FEA results, and to avoid using the safety factor incorrectly. Points 1 to 4 can be eliminated by testing the material used, provided it was manufactured under manufacturing conditions of the chassis. Testing of components can be carried out using the standard workshop procedures developed by the ASTM. Their guidelines include test methods as well as details concerning fabrication of test specimens, from raw materials to manufacturing environment specifications (van Rijswijk 2017). Point 5 can be eliminated by using either the Hoffman or Tsai-Wu criterion as they are both shown to be accurate in this dissertation. Note that point 7 is a design safety factor rather than a safety factor, but is it used in the safety factor calculation because there is no regulation for this specific application.

Considering the above points and further recommendations from Juvinal and Marshek (2012), the safety factor for this vehicle should be approximately 2,5 but not be below 2.

## 5. Testing and Associated FEAs

To validate any FEA results, experimental testing of circular tubes was carried out. This section details FEAs that attempt to mimic experimental tests. By doing this, the FEAs can be directly compared to the experiments. Furthermore, failure criteria can be compared against each other by analysing the experimental and FEA results.

Firstly, flat panels were tested to attain all properties of a single UD ply that are required to compute a failure index. In this way, layups may include a ply-by-ply analysis which applies to any continuous fibre layup including strategically cut fabric in a hand-layup, pultrusion and filament winding. These tests do not use any cross-ply fabric, so conclusions may not be extended to them. After these tests, a test was designed to induce axial loading and shear loading with respect to the fibre direction so that failure criteria could be tested under compound loading. These tests were then compared to FEAs simulating the experiments to validate results and compare the failure criteria against each other.

### 5.1. Coupon Testing for Laminate Properties

In order to use the failure criteria to predict failure, certain material properties must be known. These are described in Table 5-1.

Table 5-1: Material properties used in failure criteria - descriptions

$X_T$	Laminate tensile strength parallel to the fibre direction
$X_C$	Laminate compressive strength parallel to the fibre direction
$Y_T$	Laminate tensile strength perpendicular to the fibre direction
$Y_C$	Laminate compressive strength perpendicular to the fibre direction
$S$	Laminate shear strength
$E_{11}$	Young's modulus parallel to the fibre direction
$E_{22}$	Young's modulus perpendicular to the fibre direction
$G_{12}$	In-plane shear modulus
$\nu_{12}$	In-plane Poisson's ratio

Laminate shear strength is not described in the NX student guide (Siemens 2012) as any particular direction except that it differs from interlaminar shear. Therefore, it is taken here as the in-plane shear strength, as this corresponds to the in-plane shear modulus.

The results of the flat specimen tests at DUT are summarised in Table 5-2. Matrix digestion tests showed that flat panels and tubes had an average fibre volume fraction of about 58%. Variation in this volume fraction from panel to panel causes error when all values are used together. Note that the coefficient of variance is abbreviated to CV.

Table 5-2: Laminate test results summary

Test Variable	Mean (MPa)	CV (%)
X <sub>T</sub>	1 989,4	2,1
X <sub>C</sub>	790,35	7,3
Y <sub>T</sub>	29,462	13,1
Y <sub>C</sub>	117,25	7,3
S	83,958	0,7
G12	2 814,5	5,5
E11	108 890	6,3
E22	6 521,0	1,5

Table 5-3 is presented to compare the obtained results with results obtained by Bru et al. (2016), who used similar UD with a fibre volume fraction in the region of 60%.

Table 5-3: Comparison of laminate test results with Bru et al. (2016)

Test Variable	Test by Narsai		Test by Bru et al. (2016)	
	Mean (MPa)	CV (%)	Mean (MPa)	CV (%)
X <sub>T</sub>	1 989,4	2,1	1 787	9
X <sub>C</sub>	790,35	7,3	631	9
Y <sub>T</sub>	29,462	13,1	29,2	3
Y <sub>C</sub>	117,25	7,3	130	9
S	83,958	0,7	77,8	3
G12	2 814,5	5,5	4 400	7
E11	108 890	6,3	140 000	6
E22	6 521,0	1,5	9 000	10
NU12	-	-	0,28	17

Strength values were very close, but modulus values show significant differences. The results for all except G12 are consistent and carried out to standards. It is possible that this disagreement in G12 is due to scissoring in shear tests and the utilisation of a non-standard method to obtain the in-plane shear modulus.

## 5.2. Coupon Testing of Cylindrical Members

Coupon testing of the fabricated tubes produced results that are compiled in Table 5-4. The collar length was 9,57 mm. Further information regarding the setup may be found in section 3.2.

Table 5-4: Tube test specimen results

Specimen	Length (mm)	Inner Diameter (mm)	Average Wall Thickness (mm)	Failure Load (N)
1	58,39	19,50	0,72	3 449,1
2	55,26	18,42	0,61	2 680,9
3	56,60	19,79	0,68	3 405,5

It is intuitive that the failure load should increase as the specimen's cross-sectional area increases. Thus, it is seen that failure load increases with average wall thickness. The failure load should also increase with inner diameter, but the failure load is a function of both the wall thickness and inner diameter combined. Failure was seen as a crack that propagated along the 35° of the fibres, but sometimes propagated across the fibres before continuing along the 35° angle.

## 5.3. Failure Criteria Analysed Through FEA

The measurements and failure loads from the tubes in section 5.2 were used to run FEAs to compare the following failure criteria: Tsai-Wu, Hoffman, Hill and Maximum Strain. Note that the Tsai-Wu interaction term was left unspecified, as would be the case in an environment without much data. For each failure criterion, a corresponding FEA was run with the output being the strength ratio rather than the failure index. This is because the strength ratio is a factor that can be multiplied by the loads to obtain failure. This means that in the results, a value of less than one predicts failure and a value larger than one can be viewed in a comparable manner to a safety factor. It also provides a term that is comparable across the failure criteria.



For these simulations, failure index results of slightly less than one are expected for two reasons. The first is that the waviness on the surfaces of the tubes may cause stress concentrations that could lead to premature failure. The second reason is that the average wall thickness is the value used in the simulation. This is to match the amount of fibre in the real tube, but the failure regions on the tubes are in the areas that are thinner than the average wall thicknesses.

The simulations make use of boundary conditions that attempt to mimic the experimental conditions. At the lower end where the collar was, the mesh was fixed in translation and rotation. At the top, translation was fixed in the horizontal plane and rotation was only allowed about the local theta coordinate.

The results are displayed in a table for each specimen. Failure indices and strength ratios are both shown. Strength ratios can be compared across failure theories, failure indices cannot. The results of the FEAs for specimen 1, 2 and 3 are shown in Table 5-5, Table 5-6 and

Table 5-7 respectively. The failure index plots illustrated are the worst loaded ply. The strength ratio plots show the worst loaded elements regardless of ply location.

Table 5-5: Results for specimen 1

Failure Criterion	F	SR	Images
Tsai-Wu	0,821	1,164	
Hoffman	0,822	1,163	
Hill	0,643	1,247	
Maximum Strain	0,763	1,311	

Table 5-6: Results for specimen 2

Failure Criterion	F	SR	Images
Tsai-Wu	0,783	1,207	
Hoffman	0,784	1,207	
Hill	0,611	1,279	
Maximum Strain	0,742	1,347	

Table 5-7: Results for specimen 3

Failure Criterion	F	SR	Images
Tsai-Wu	0,851	1,132	
Hoffman	0,852	1,131	
Hill	0,681	1,212	
Maximum Strain	0,783	1,278	

Table 5-8 shows a comparison of failure criteria using strength ratios for each specimen. The lower the strength ratio, the closer to failure the specimen is (as predicted by the relevant theory). This means that the lower the strength ratio, the more conservative the failure criterion is.

Table 5-8: Failure criteria vs strength ratios

	<b>Tsai-Wu</b>	<b>Hoffman</b>	<b>Hill</b>	<b>Maximum Strain</b>
<b>Specimen 1</b>	1,164	1,163	1,247	1,311
<b>Specimen 2</b>	1,207	1,207	1,279	1,347
<b>Specimen 3</b>	1,132	1,131	1,212	1,278
<b>Average</b>	1,168	1,167	1,246	1,312
<b>CV (%)</b>	3,2	3,3	2,7	2,6

The most conservative criterion is seen to be Hoffman. The variation in results between the theories is similar, indicating that they are all equally sensitive to the loading conditions. The fact that the specimens failed at the loads used for the FEAs means that the strength ratios can be used as an error estimate of the theory. This means that the Hoffman theory had a 16,7% error, if the simulation accurately modelled the real test.

The FEA had two possibly significant flaws. Firstly, average wall thickness was used to determine the layup, whereas the failure zones were in the thinner areas. Secondly, the value of  $G_{12} = 2\,814,5$  MPa was found to be much lower in comparison to the literature. Bru et al. (2016) obtained a value of 4 400 MPa. Murakami & Matsuo (2015) obtained a value of approximately 5 000 MPa for lower fibre volume fraction carbon fibre in thermoplastic. A data sheet used by ACP Composites (2014) presents a value of 5 000 MPa.

Using the minimum thicknesses, as well as a value for  $G_{12}$  of 4 400 MPa, further FEAs for all three specimens were conducted. The results in Table 5-9 show that tube failure is predicted most accurately by the Hoffman criterion. The strength ratio is close to 1, and the “error” percentage has dropped to 2,2%. This provides validation for using tested material properties except for  $G_{12}$ , which is set to 4 400 MPa. It is however recommended that further testing be done with uniform tubes to eliminate uncertainty due to the waviness on the tube surface.

Table 5-9: FEA results for strength ratios using minimum wall thickness

	Tsai-Wu	Hoffman	Hill	Maximum Strain	Minimum Wall Thickness (mm)
<b>Specimen 1</b>	1,012	0,998	1,183	1,218	0,53
<b>Specimen 2</b>	1,052	1,041	1,221	1,427	0,45
<b>Specimen 3</b>	1,040	1,026	1,216	1,431	0,53
<b>Average</b>	1,035	1,022	1,207	1,359	-
<b>CV (%)</b>	2,0	2,1	1,7	9,0	-

These results show that the Hoffman failure criterion is the most accurate and most conservative criterion for the tested tubes. It will therefore be used in the design of the space frame chassis, as will the value of G12 equal to 4 400 MPa. The Hoffman criterion is very closely followed by the Tsai-Wu failure criterion, which is very nearly as conservative and accurate. Because the Tsai-Wu interaction coefficient is not defined, it is possible that that criterion could be more conservative and/or more accurate. This would require more testing of specimens to determine the coefficient, and further testing of more uniform tubes of known properties.

#### 5.4. Sensitivity to Material Properties

Firstly, FEAs were carried out to assess the errors that may be present due to errors in the tested material properties. This was done by altering certain material properties individually in the same FEA process as the FEAs done in section 5.3. Specimen 3's dimensions (as per Table 5-4) were used as a reference, and the Hoffman failure criterion was used. The values that showed significant differences to the results from Bru et al. (2016) were tested:

- E – elastic modulus (E11 and E22 only)
- NU – Poisson's Ratio (NU12 only)
- G – shear modulus (G12 only)

All other properties were held constant while the properties of interest were tested. The reference values are the values from Table 5-2 and are highlighted in each table. The strength ratio presented is the Hoffman strength ratio. The observed result was the lowest strength ratio of all elements across both plies.

Table 5-10, Table 5-11, Table 5-12 and Table 5-13 show the results of multiple FEAs. Figure 5-1 and Figure 5-2 are included where the variations in SR are not very small. The property being

altered is in grey for each section. Altering E11 yields almost no variation in SR, as seen in Table 5-10. This is likely because it is already very large in comparison to other stiffness values, so making E11 stiffer does not increase its loading very much.

Table 5-10: Results from altering E11

E11(MPa)	E22 (MPa)	NU12	G12 (MPa)	SR	Variation in E11 (%)	Variation in SR (%)
85 000	6 521	0,28	2 814,5	1,125	-21,9	-0,5
100 000	6 521	0,28	2 814,5	1,132	-8,2	0,1
108 890	6 521	0,28	2 814,5	1,131	0,0	0,0
115 000	6 521	0,28	2 814,5	1,131	5,6	0,0
125 000	6 521	0,28	2 814,5	1,133	14,8	0,2
140 000	6 521	0,28	2 814,5	1,138	28,6	0,6
160 000	6 521	0,28	2 814,5	1,143	46,9	1,1

Table 5-11 shows that while there is a change in SR when E22 is varied, it requires a large percentage of variation of E22. Making E22 stiffer reduces the strength ratio because load is shifted from the 11 direction to the 22 direction, but ultimate strength in that direction remained constant, thus leveraging terms containing  $Y_C$  in the Hoffman failure criterion expression.

Table 5-11: Results from altering E22

E11 (MPa)	E22 (MPa)	NU12	G12 (MPa)	SR	Variation in E22 (%)	Variation in SR (%)
108 890	5 000	0,28	2 814,5	1,252	-23,3	10,7
108 890	5 800	0,28	2 814,5	1,150	-11,1	1,7
108 890	6 521	0,28	2 814,5	1,131	0,0	0,0
108 890	7 300	0,28	2 814,5	1,083	11,9	-4,2
108 890	8 100	0,28	2 814,5	1,041	24,2	-8,0
108 890	9 000	0,28	2 814,5	0,995	38,0	-12,0
108 890	10 000	0,28	2 814,5	0,949	53,4	-16,1

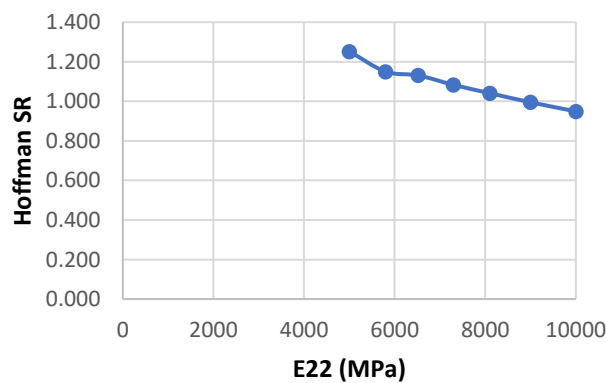


Figure 5-1: Graph of SR vs E22

Changes in NU12 had very little effect on SR, as seen in Table 5-12. This helps warrant the use of NU12 = 0,28 from Bru et al. (2016) in the simulations in this dissertation.

Table 5-12: Results from altering NU12

E11 (MPa)	E22 (MPa)	NU12	G12 (MPa)	SR	Variation in NU12 (%)	Variation in SR (%)
108 890	6 521	0,15	2 814,5	1,119	-46,4	-1,1
108 890	6 521	0,2	2 814,5	1,124	-28,6	-0,6
108 890	6 521	0,25	2 814,5	1,128	-10,7	-0,3
108 890	6 521	0,28	2 814,5	1,131	0,0	0,0
108 890	6 521	0,3	2 814,5	1,133	7,1	0,2
108 890	6 521	0,35	2 814,5	1,137	25,0	0,5
108 890	6 521	0,5	2 814,5	1,150	78,6	1,7

Table 5-13 shows that as with E22, significant changes in SR require large changes in G12. Increases in G12 lead to an increased strength ratio. This could mean that an increasing G12 to around 4 400 MPa or 5 000 MPa (as Bru et al. (2016) as well as Murakami & Matsuo (2015) have respectively found) would allow more accurate predictions of failure. It is curious that increasing G12 produces a higher SR, because that seems to suggest that shear stress is preferred. A possible explanation for this is that by increasing G12, the tube to stay more upright, redirecting stress into the 11 direction rather than the 22 direction. This means that stress is absorbed in the stronger of the two directions.

Table 5-13: Results from altering G12

E11 (MPa)	E22 (MPa)	NU12	G12 (MPa)	SR	Variation in G12 (%)	Variation in SR (%)
108 890	6 521	0,28	2 000	0,986	-28,9	-12,8
108 890	6 521	0,28	2 500	1,079	-11,2	-4,6
108 890	6 521	0,28	2 814,5	1,131	0,0	0,0
108 890	6 521	0,28	3 000	1,159	6,6	2,5
108 890	6 521	0,28	3 500	1,228	24,4	8,6
108 890	6 521	0,28	4 000	1,283	42,1	13,4
108 890	6 521	0,28	5 000	1,361	77,7	20,3



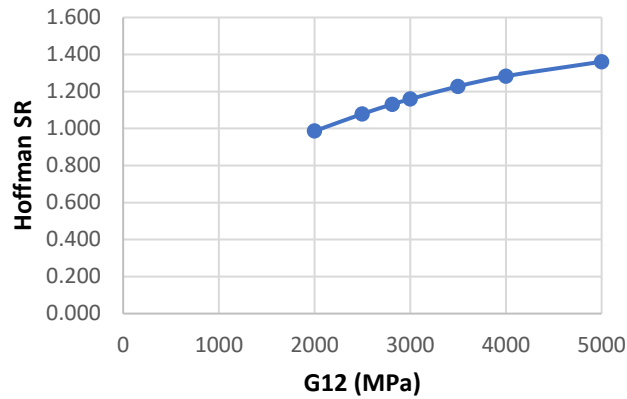


Figure 5-2: Graph of SR vs G12

Finally, a simulation was run in which E11, E22 and G12 were changed to the values from Bru et al. (2016) to see what combined effect it had. The results are presented in Table 5-14. The result shows a 5% increase in SR, meaning that that it is even further from predicting failure.

Table 5-14: Result from including all stiffness values from Bru et al. (2016)

E11 (MPa)	E22 (MPa)	NU12	G12 (MPa)	SR	Variation in SR (%)
140 000	9 000	0,28	4 400	1,188	5,0

To summarise:

- Small errors in E11, E22, G12 and NU12 are not critical and will yield sufficient accuracy
- E11 and NU12 may be estimated grossly with sufficient accuracy
- E22 and G12 should be found within 10% of its true value to yield sufficient accuracy
- An increase in G12 leads to an increase in strength according to the Hoffman failure criterion
- 4 400 MPa will be used for G12 for the chassis design as it is accepted in the literature and using this value in FEAs agrees with experimental results in this dissertation

## 6. Chassis Geometry Design

To begin with, a bulk design of the geometry of the chassis must be created. This chassis design incorporates driver ergonomics and specifies connection locations of the suspension.

This section includes design iterations 1 to 5 of the chassis that implement changes in the chassis members. The design method begins by using existing machinery along with ergonomic principles to shape a cockpit area, and building a basic frame around it as chassis version 1. The chassis is improved on – generating chassis version 2 – through basic simulations that determine high and low stress areas; then it is changed drastically to chassis version 3 by defining different member sections according to the stresses transferred. Chassis version 4 arises through the changing of member connections to reduce joint stresses and local buckling. Finally, chassis version 5 is born through optimising joints and members further, as well as including steel sleeves adhered to the tubes at joints.

### 6.1. Bulk Geometry Design and Modifications

The first design of the space frame or cockpit was based on position and size of the driver, wheel/suspension connections and pedal mounting points. The chassis allows a seat to be installed ergonomically, but the mounting positions and distances must facilitate this. A cycling exercise machine was measured to assist in the initial chassis design because it relates very well to the scenario presented in this dissertation. A 2D schematic of the cycling machine was drawn up and is shown in Figure 6-1, with labels in Figure 6-2 (length values are in mm).

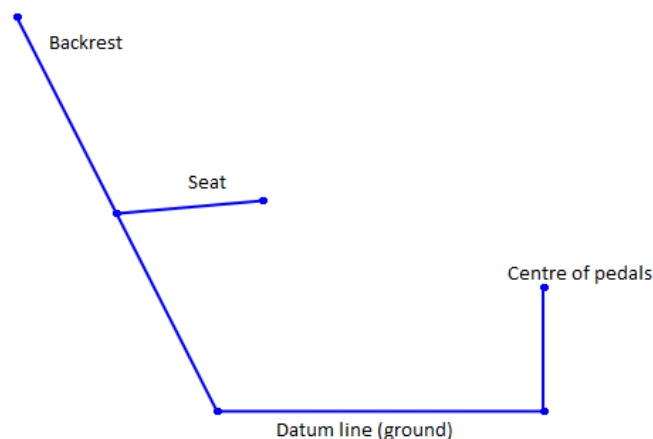


Figure 6-1: Cycling machine schematic

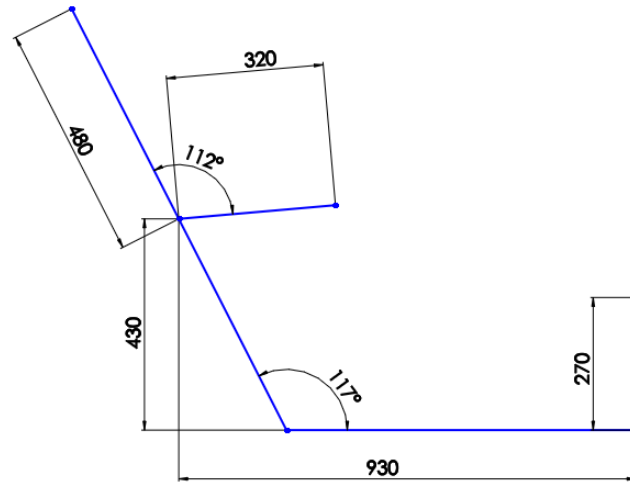


Figure 6-2: Cycling machine schematic – dimensioned

The distance between the pedals' centre and the seat corner is shown as 930 mm which is the maximum value when the seat is adjusted to its maximum position. The minimum position corresponds to a distance of 750 mm.

The following initial designs were modelled and analysed on SolidWorks for quick and simple frame analysis. To complete a full structural and joint analysis on these initial designs would be a waste of design time (joints would have to be much more accurately represented) and analysis time (gluing of meshes, using gap elements to represent adhesive joints, computational solving time). The aim of the initial design was simply to find high loading areas and structural stress concentrations and minimise them by adding additional framework or altering member positions. It also served to locate large displacement and rectify it by stiffening the chassis through the addition of strategic members.

The designed chassis contains tubular members and the material used is plain carbon steel, simply for its rigidity property. The rigidity of a thick steel section (which was used) would represent the rigidity of a thin composite laminate (albeit inaccurately in a quantitative sense). Variables such as pipe size and material were maintained through the initial tests. Figure 6-3 and Figure 6-4 show the initial design of the chassis, also called chassis version 1.

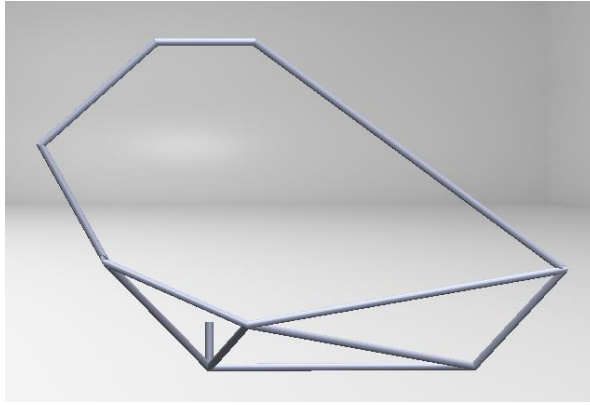


Figure 6-3: Chassis version 1 chassis design side view

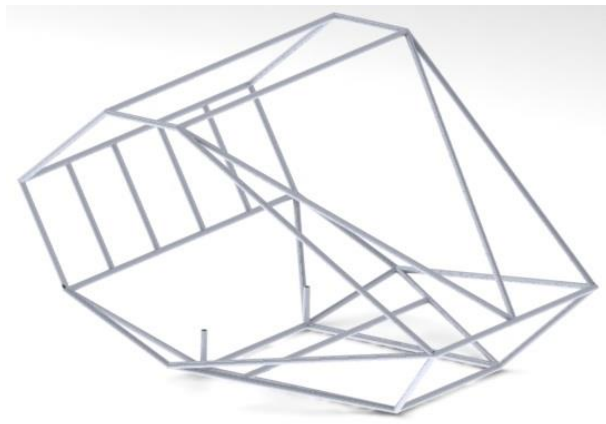


Figure 6-4: Chassis version 1 chassis design render

A stress analysis was conducted to find the weak points in the chassis. Loads included two 1200 N loads to represent the driver and passenger (including associated seating and steering fixtures and a small battery), and an acceleration of 3 times gravity, in line with the horizon to represent an extreme turn at high speed. This load was unreasonably high to account for the omission of realistic moment loads caused by the driver and passenger. Fixture points were the approximate positions at which the suspension should connect, and were found in the front and the back of the frame. The loads, fixtures and analysis results are illustrated in Figure 6-5.

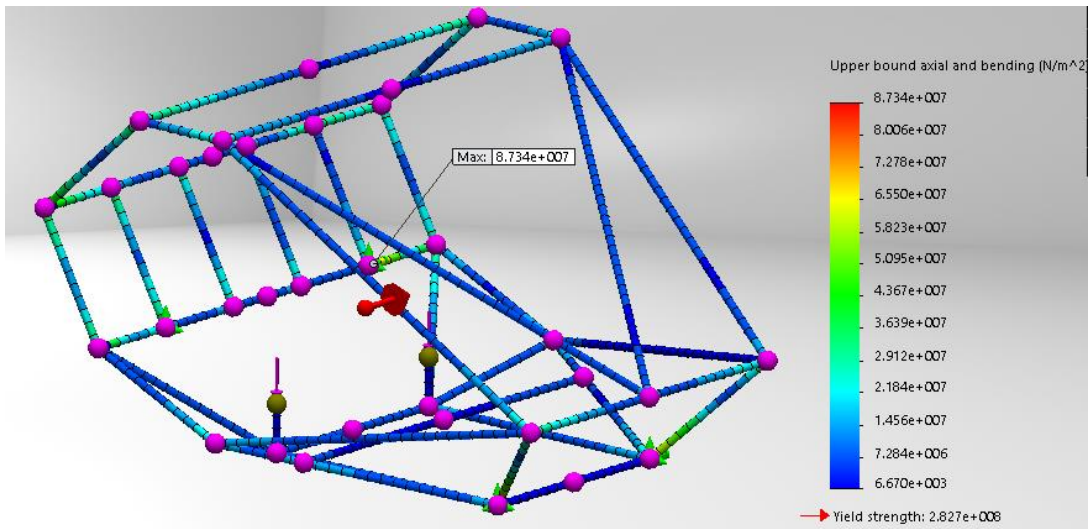


Figure 6-5: Chassis version 1 design stress analysis result

The result shows that maximum stress occurs at the rear suspension mounting points, with high stress also occurring at the front suspension mounting points, among other areas. The result also shows that there is very little stress in some members, which means they should be removed or altered to optimise material usage. Care should be taken when removing members, because even while stress can increase to an allowable value, torsional stiffness can be significantly lost (Siegler et al. 1999).

Version 2 looked to reduce the major stress areas at the joints and reinforce long members with struts. The front panel through which the driver would look, had a long strut for rigidity, but was under little stress. It was therefore replaced by smaller struts at the corners. Figure 6-6 shows the updated side view, Figure 6-7 shows a 3D view of the chassis with the new and altered members highlighted.

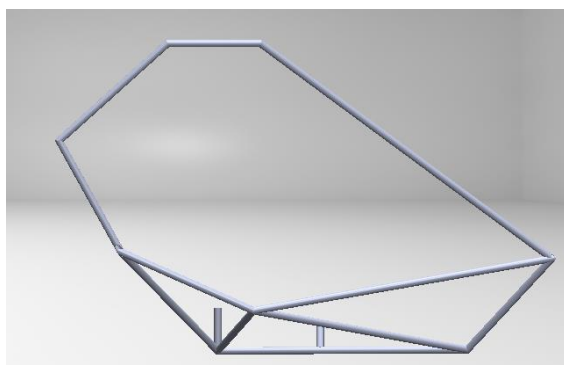


Figure 6-6: Chassis version 2

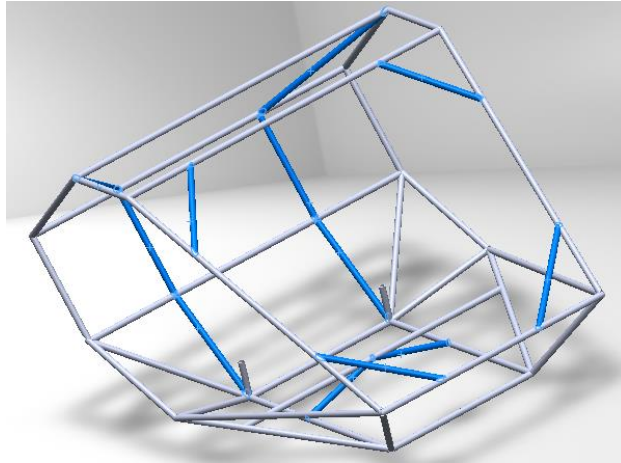


Figure 6-7: Chassis version 2 with edits highlighted

Figure 6-8 shows the result of the stress analysis. The maximum stress is reduced in this version. Importantly, the colour is more distributed, showing that the members are distributing the stress away from the higher stress areas more effectively than in version 1. There are still many areas of low stress, but in some cases these members are necessary for rigidity or for strength in situations such as a roll or various impacts (including front and side impacts).

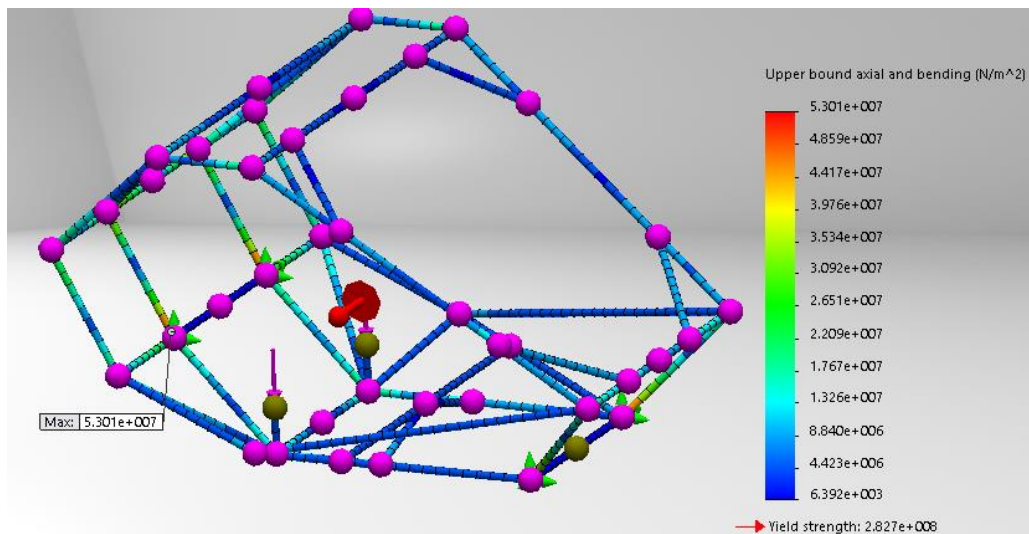


Figure 6-8: Chassis version 2 stress analysis result

A primary concern discovered in this design stage is that joints were extremely complex. They had many members connecting to more than one member and sections were cut more than once to be able to unite with the other members. This was due to the use of members with the same diameter and having too many members joining at a single node. A solution that is implemented in future design concepts is to have larger diameters for outer members that act

as the roll cage, and smaller diameter members for struts and other internal members. The varied sizes will allow simpler connections at nodes. Another solution that is implemented is to reduce the number of members connecting at a single node by offsetting certain connections. The associated risk with the latter solution is that members would then be subject to additional stress due to additional bending moments. This is a secondary concern however, as these should be small increases and joints will likely still be the failure points.

## **6.2. Chassis Geometry Optimisation**

The next step in the design process includes more relevant design with regard to the composite material, and the joints. The initial designs were improved by considering more practical aspects such as impact, roll, and force distribution in the structure and the joints. These considerations result in a design with curved outer members to aid impact or roll scenarios, as well as differently sized members to reduce high stresses and to simplify joints. The joints become less complex as strut contact points are moved a small distance from main frame joints.

The structure is designed with a “main frame” which is a set of larger sections on the outer structure of the vehicle. The outer structure should act as a roll cage and take all primary loads including forces from the suspension. The inner frame contains smaller members because the assumption is that they will not be under the most stress in a scenario which is a crash scenario. Section 4.5 mentions that crash impact energy is absorbed through fracture and delamination however. This means that it may be desirable to additionally have smaller members designed to fail in a crash to absorb the energy while the outer frame remains intact and able to transfer loads. Figure 6-9 shows the updated design, called version 3.

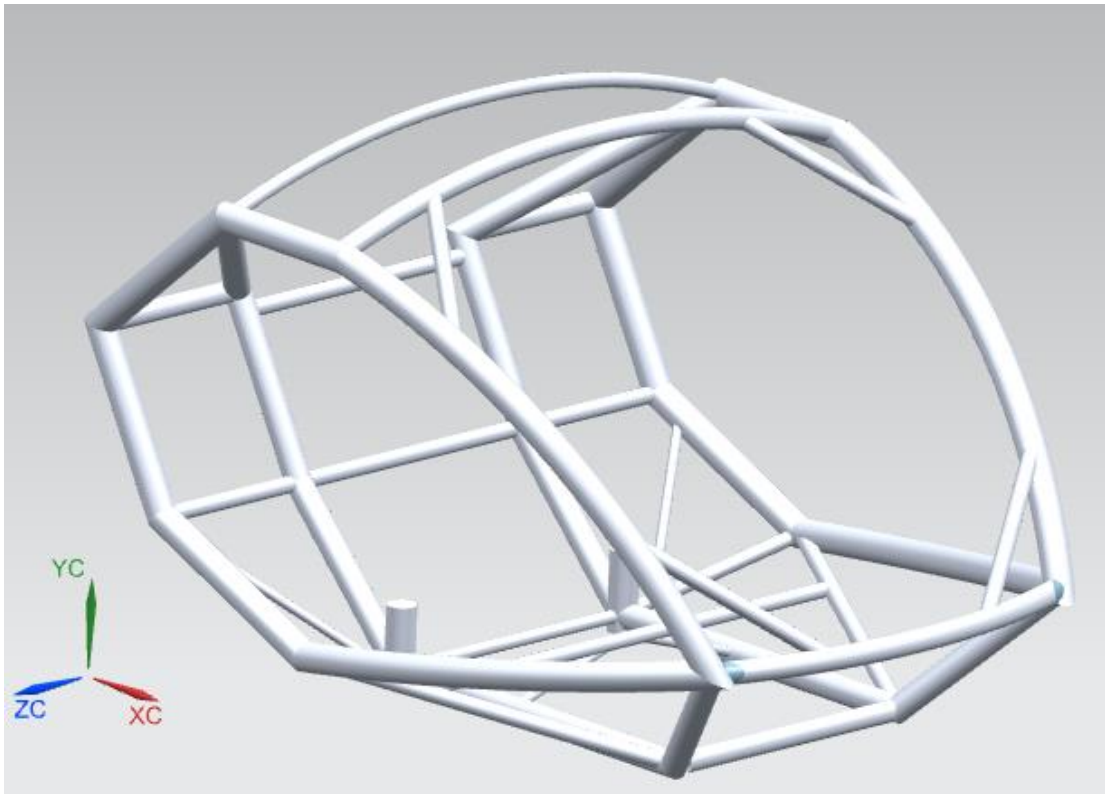


Figure 6-9: Chassis version 3

While this version of the chassis is much more relevant and applicable, it has issues with the joints. Some joints are too complex, even to model. Too many members connect at a node, and the result is impractical cuts that may cause awkward distribution of load into the fibres non-uniformly. Figure 6-10 and Figure 6-11 show two such joints.

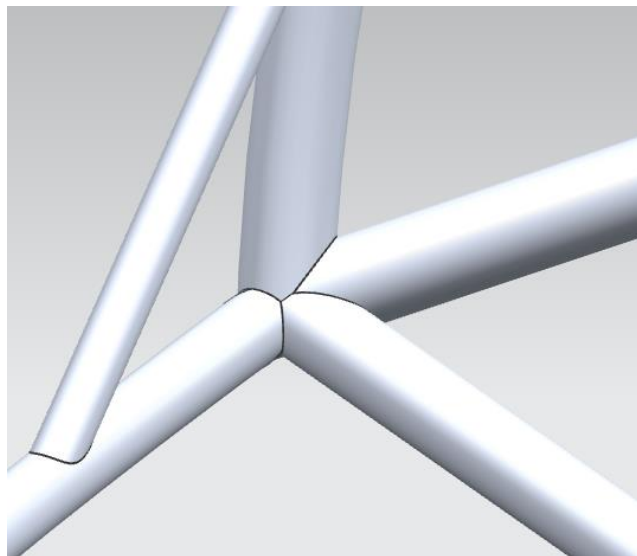


Figure 6-10: Chassis version 3 front joint



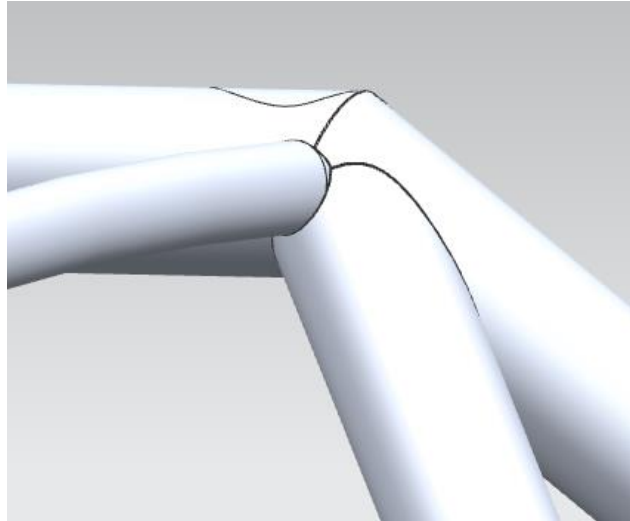


Figure 6-11: Chassis version 3 top join

Pre-processing of frame version 3 proved difficult, as the complex joins even stressed the software and caused various errors in the modelling application of NX. The opportunity was taken to redesign the relevant joins and resize some members. Figure 6-12 shows version 4 of the chassis. Another major difference between versions 3 and 4 is that in version 4, the main frame includes the inner beams at the rear, and not the outer beams. The size difference is an indication of this.

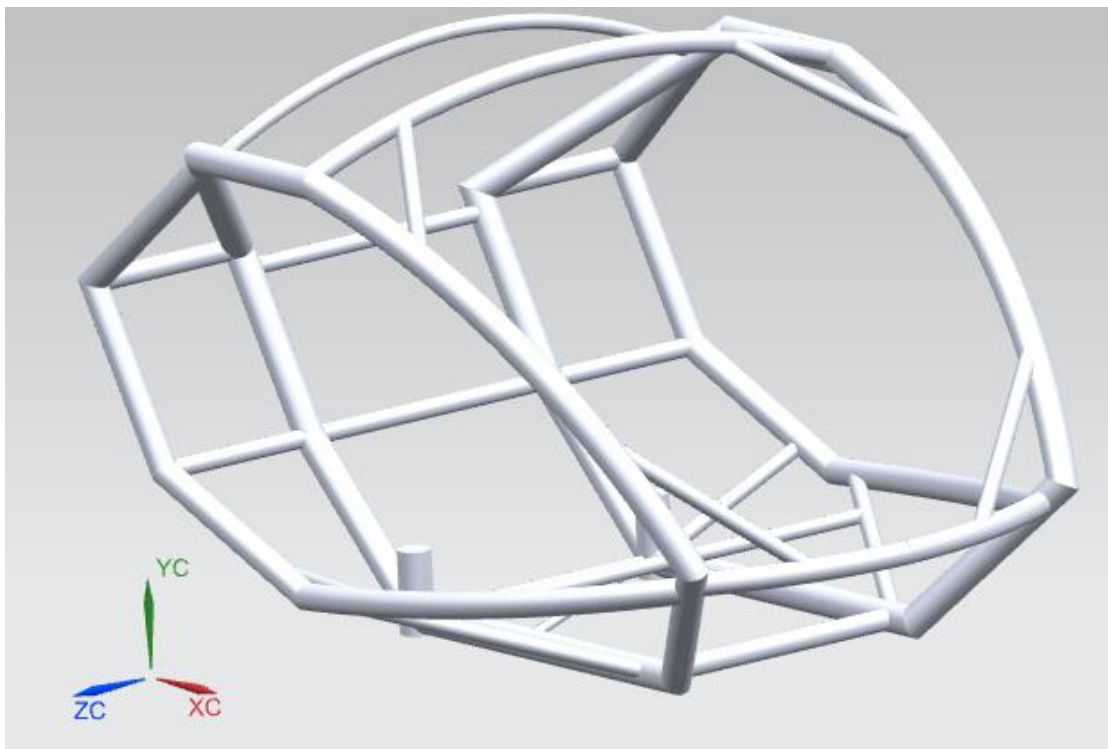


Figure 6-12: Chassis version 4

The main joints that were altered are the front and top joints as shown in version 3. The redesigns are shown in Figure 6-13 and Figure 6-14.

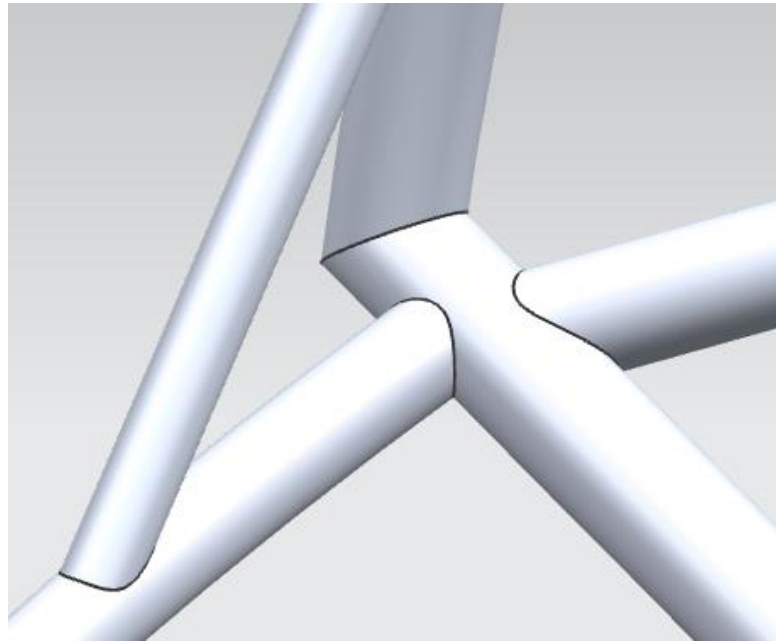


Figure 6-13: Chassis version 4 front joint

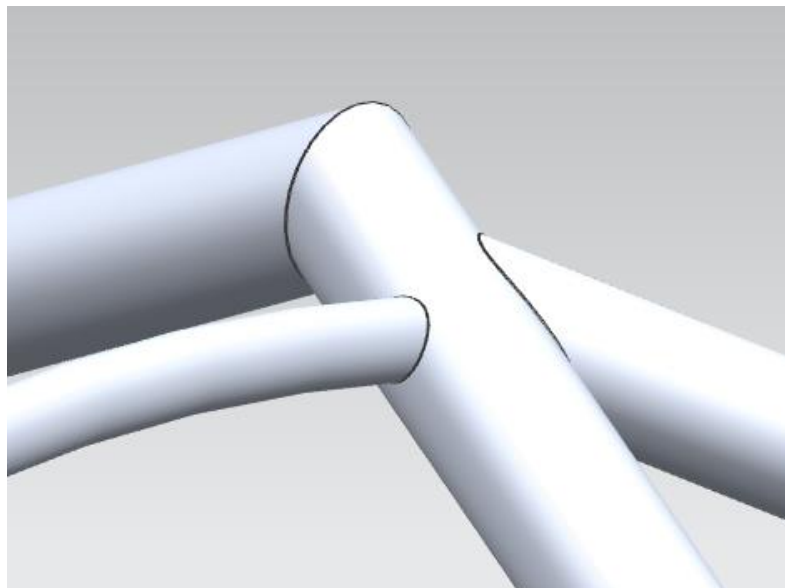


Figure 6-14: Chassis version 4 top joint

Previously, pre-processing proved to be a large issue. Elements in meshes generated there were generated using automatic mesh generation and failed quality checks, even after manual adjustments. It was concluded that along with complex joints, the 1 mm element size was too small in comparison to the base element size and caused these meshing errors. To rectify this, the glue regions that are 1 mm offset were meshed with a size of 3 mm. This introduced an

aspect ratio of 3, which passed element geometry checks. This allowed the members to mesh much more easily around the glue regions. Members had various base element sizes ranging from 6 mm to 14 mm. Large base element sizes should not cause concern as mesh size changed according to curvature of geometry and connection to adjacent meshed (namely the glue region meshes). Figure 6-15 shows the front join meshes (which gives a good indication of the mesh structure for most joins).

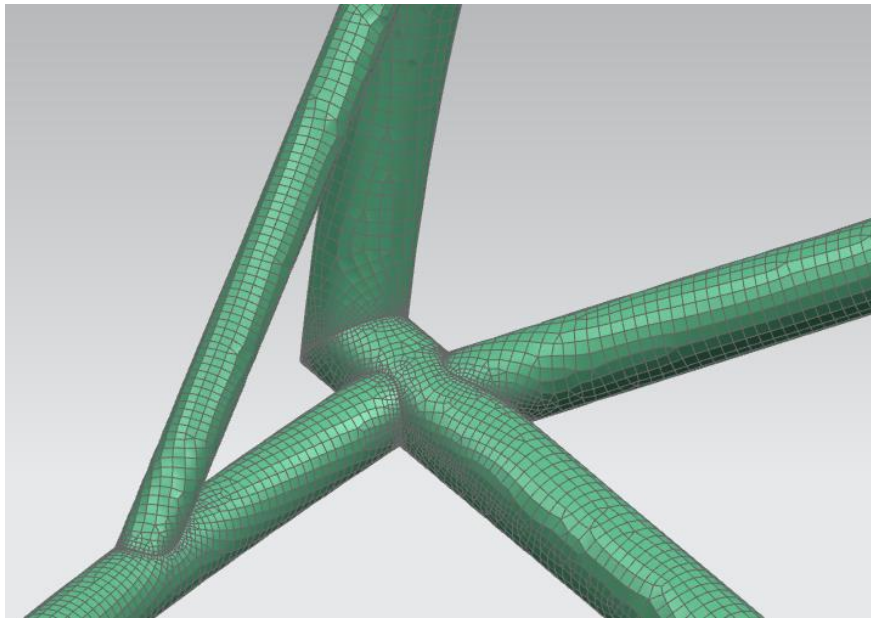


Figure 6-15: Chassis version 4 front join meshed

The simulations chosen are a linear static (SOL 101) and a linear buckling (SOL 105). Linear models are used because the materials are expected to be used within their linear-elastic regions, and deformations are to be small. Non-linear buckling is not explored due to its required computational power. Instead judgment is used along with high buckling factors. The static simulation can allow preliminary fibre orientation optimisation and ply additions to reduce the failure index or increase strength ratio as desired, but it is used here to first optimise the geometry. The buckling simulation analyses the loading of the structure and calculates the factors that may be applied to the loads to induce buckling in various modes. For the simulations, two main loads are considered: braking and turning. For the worst-case scenario simulating an emergency, these will be loaded together in a static simulation with fixed constraints at the suspension points. Note that this is not the general operating condition of the vehicle, but it should be able to sustain these loads without harming the driver or passenger.

“Which” Test Lab conducted tests on braking distances for light road vehicles as reported by Skinner (2012). The best tested vehicle in that category was the 2012 VW Polo, which stopped from 62 miles per hour in 34,2 m. Calculation A1-1 in Appendix 1 shows the average braking acceleration that acts uniformly during braking to be  $11,2 \text{ m/s}^2$ .

Tests conducted on a 2014 Toyota Corolla (Huffman 2013) and a 2014 Ford Fiesta ST (Frankel 2013) by Edmunds, produced values of 0,78 and 0,91 times gravitational acceleration respectively. Using the value for the Toyota Corolla seems more reasonable than the Ford Fiesta ST as the Corolla is less geared towards high speed or performance, which is more applicable to this application. This means that the acceleration due to turning can be taken as  $7,65 \text{ m/s}^2$  if the gravitational constant is taken as  $9,81 \text{ m/s}^2$ .

The values of  $11,2 \text{ m/s}^2$  and  $7,65 \text{ m/s}^2$  will be included with the gravity load of  $9,81 \text{ m/s}^2$ . The situation includes the passenger and driver weighing 98,5 kg each (rounded up to 100 kg) as per the 95<sup>th</sup> percentile of American males according to the National Aeronautics and Space Administration (2008). Loads also include seating and steering/peddling fixtures assumed to have a maximum mass of 20 kg (based on available bicycle equipment). The acceleration loads will be included on the frame as a gravitational load with three Cartesian components.

Constraints are fixed constraints where the suspension points are assumed to be, shown in Figure 6-16.

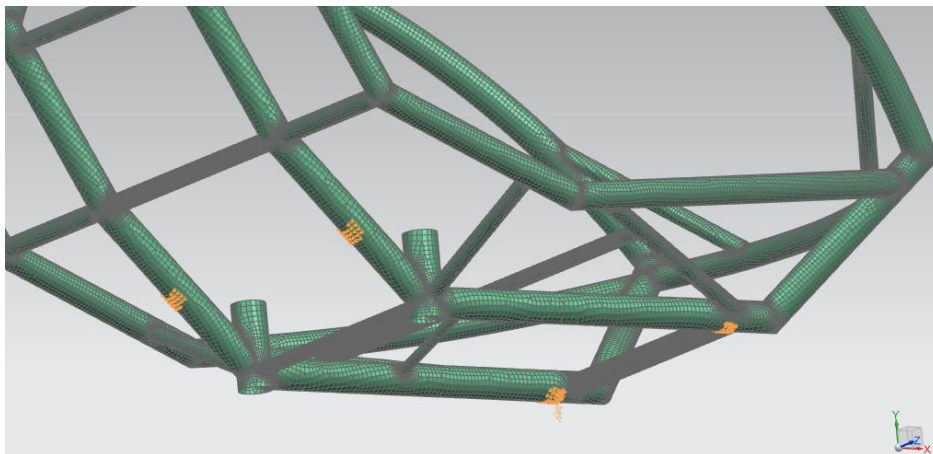


Figure 6-16: Simulation constraints

The loads are based on the braking and acceleration values of  $11,2 \text{ m/s}^2$  and  $7,65 \text{ m/s}^2$  respectively, as well as gravity at  $9,81 \text{ m/s}^2$ . The two humans, a small battery and fixtures of total mass 240 kg are included at the mounting areas of where the seats should be. Figure 6-17 illustrates the specified loads. The braking load is in blue, the turning load is in yellow, and the

gravitational load is in white. All moment loads are omitted for this simulation. They are included when the design is closer to completion, when load and fixture areas are more clearly defined.

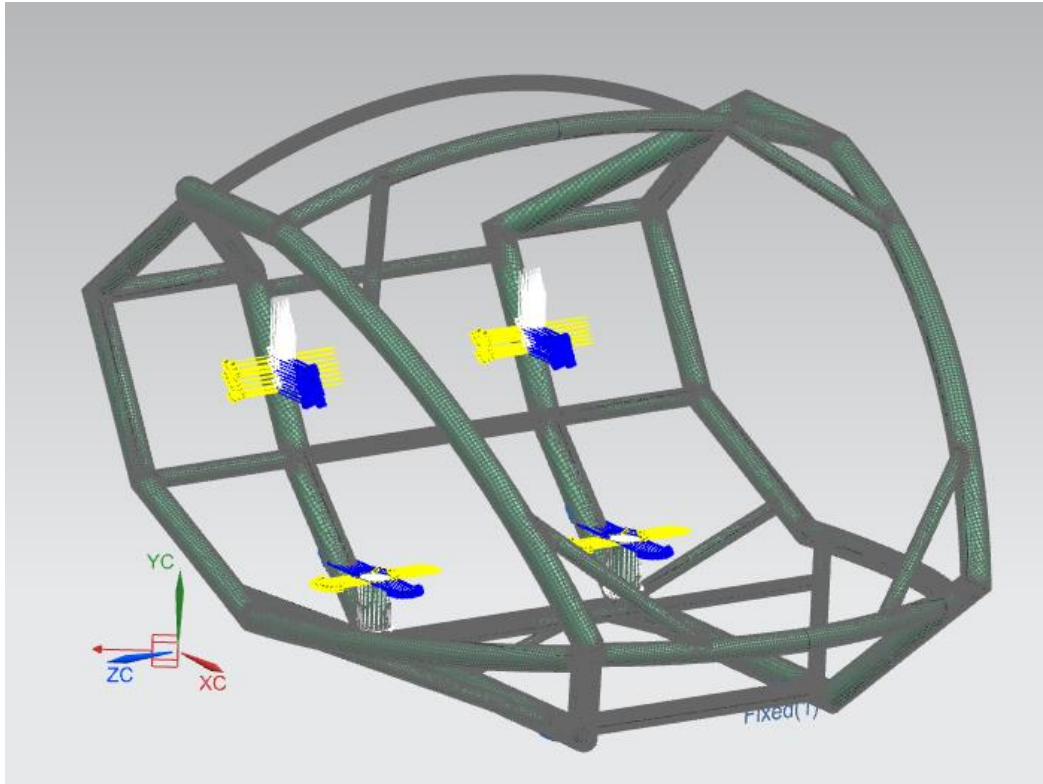


Figure 6-17: Simulation loads

The laminate properties used for this preliminary simulation are found in Table 6-1. The layup for most of the frame was  $[0/0/0]$ . A layup of  $[-45/45/0/45/-45]$  was used for the two large-diameter, vertical tubes on which the loads are placed, in anticipation of high directional stresses. Ply thickness was set to 0,3 mm based on testing from DUT. The Hoffman failure criterion was selected, and bonding strength set to 70 MPa based on information from DUT for similar CFRP laminates.

Table 6-1: CFRP ply properties

Property	Value
X <sub>r</sub> (MPa)	1 989,4
X <sub>c</sub> (MPa)	790,35
Y <sub>r</sub> (MPa)	29,462
Y <sub>c</sub> (MPa)	117,25
S (MPa)	83,958
G <sub>12</sub> (MPa)	4 400
E <sub>11</sub> (MPa)	108 890
E <sub>22</sub> (MPa)	6 521,0
NU <sub>12</sub>	0,28
Ply Thickness (mm)	0,3

The tubes are bonded to each other using Spabond 340LV adhesive system (Spabond 340LV resin and Spabond slow hardener). The properties used for the simulation are shown in Table 6-2. They are obtained from the product data sheet (Gurit 2017), apart from the Poisson's ratio, which was assumed based on the value provided for epoxy in NX.

Table 6-2: Spabond LV properties used

Property	Value
Cured density (g/cm <sup>3</sup> )	1,17
Tensile Modulus (GPa)	2,58
Tensile Strength (MPa)	49
Lap Shear on Steel (MPa)	37
Poisson's Ratio <sup>a</sup>	0,37

<sup>a</sup> Value sourced from NX, not from Spabond data sheet

A static analysis and buckling analysis were completed. The displacement result is shown in Figure 6-18. Moderate displacement is experienced, so stability is not a concern, but an attempt will be made to minimise this.

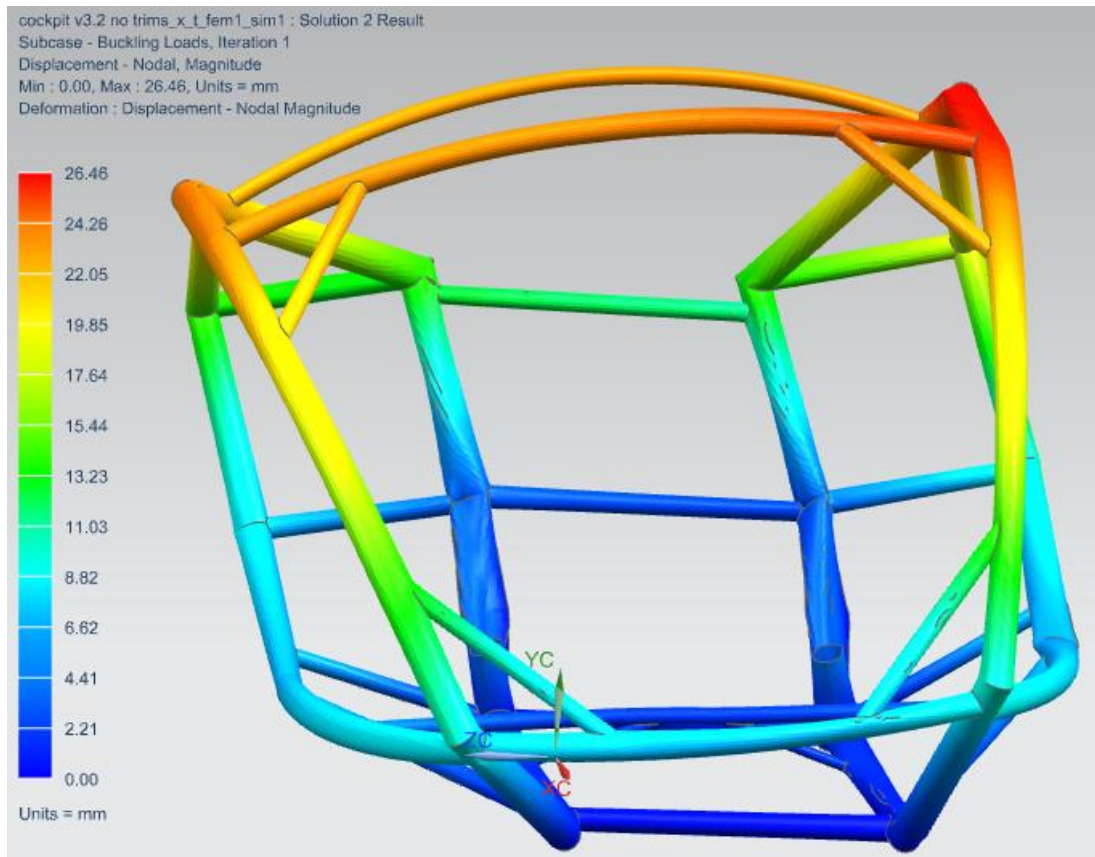


Figure 6-18: Chassis version 4 displacement plot

Figure 6-19 shows the full plot of the Hoffman failure index. Figure 6-20 shows a zone of ply failure with the ply failure index as the plot variable. It is seen that the index goes to just above 4,4 at the joint, but very close by, further into the tube, it drops down to under 0,008. This indicates that the joint is a significant stress concentration, and it is not necessarily the whole structure that is under that load. A check using the strength ratio uncovered that all zones of failure were at joint regions. At those regions, strength ratios dropped to as low as 0,33.

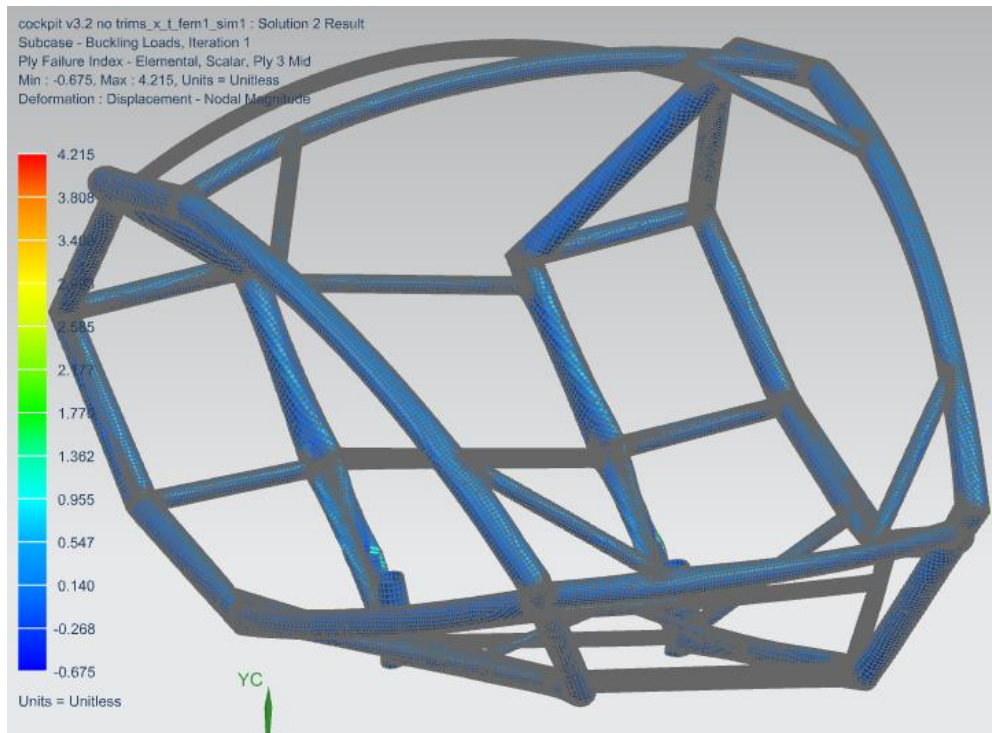


Figure 6-19: Chassis version 4 Hoffman failure index plot

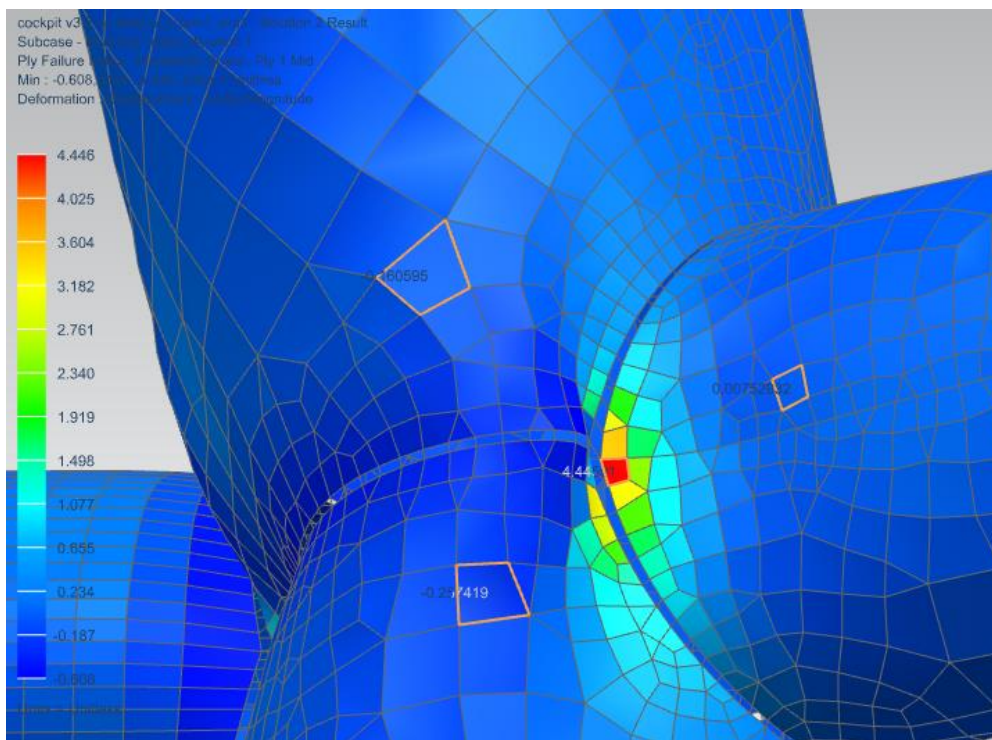


Figure 6-20: Chassis version 4 ply failure zone close up

The nodal stress plot shown in Figure 6-21 reiterates the problem of the joint being a stress concentration. The plot shows stresses of over 436 MPa, which has no chance of being sustained by any adhesive for this application.



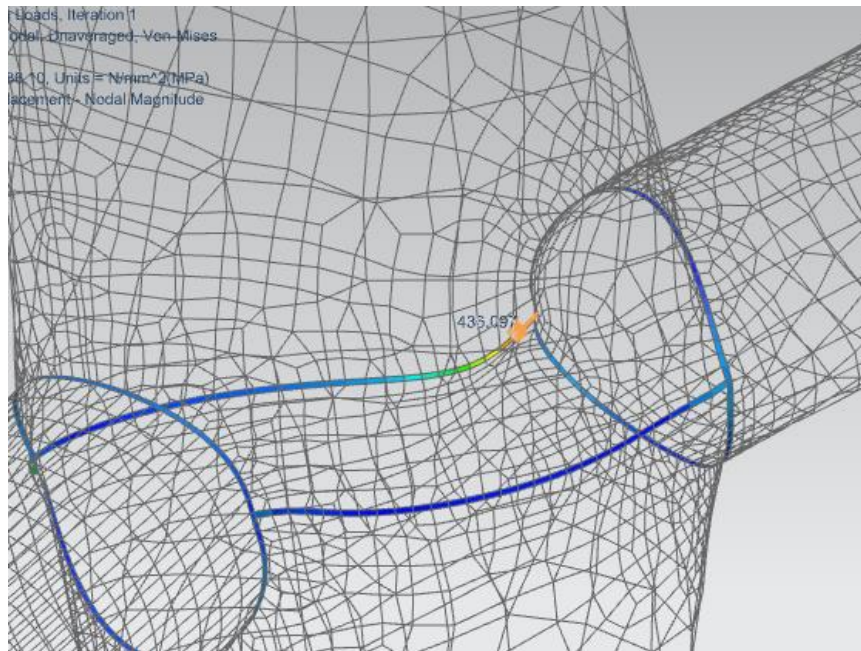


Figure 6-21: Chassis version 4 nodal stress plot close up

Another issue as mentioned is local buckling. Again, the issue is at the join regions. Illustrated in Figure 6-22, the image shows local buckling of the laminate. The first buckling factor was around 2,6 which means that for the structure to buckle, the loads must be multiplied by 2,6 of what they are. All ten buckling modes (the first ten eigenvalues) computed did not show global buckling.

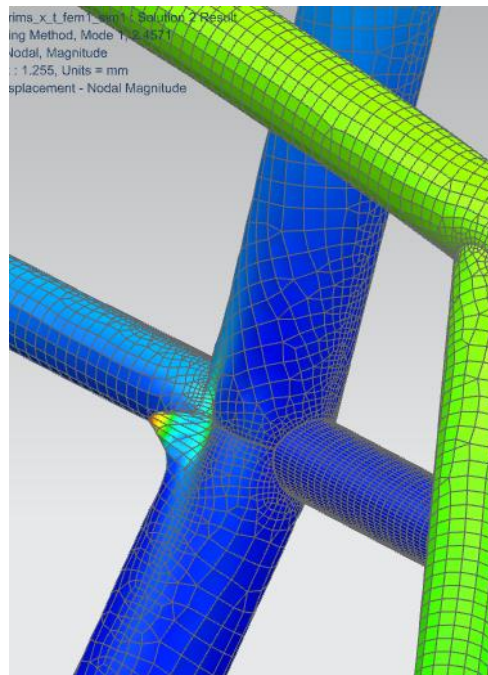


Figure 6-22: Chassis version 4 buckling plot

The results show that the joints would fail first, due to the stress on the adhesive material at the glue regions, and ply failure at the joints. It is also likely that buckling may occur if all loads are included, or the vehicle undergoes slight impact. Thickening the structure is a possibility, but in order to reduce the stress to 10 times less than the 436 MPa shown, it would require an impractical number of plies, especially considering that the plies are mostly unstressed. Stresses at the joints must be reduced, and they must be less susceptible to buckling. Directional stress was not prominent in the two large-diameter, vertical tubes, and so the layup was changed to match the rest of the structure. At this stage the structure has a mass of around 12 kg. For aluminium 6082-T6 to sustain the loads in the simulation with a safety factor of 2, the structure would have a mass of approximately 65 kg.

This prompted chassis version 5 which incorporates the use of steel sleeves and structural adhesive at the joints. The function of these sleeves is to reduce stress on the laminate at the joints and avoid local buckling. This method eliminates the join regions used previously. The adhesive now bonds the laminate to the sleeve only.

In practicality, it is more difficult to join tubes without sleeves as there is more room for dimensional error, and nothing to hold the structure during the curing and post-curing processes. The downside of using sleeves is that they are now a separate set of components that need to be manufactured, and they add significant mass.

Chassis version 5 included the following design changes:

- The alteration of members to increase torsional stiffness through triangulation
- The addition of steel reinforcing sleeves to avoid local buckling and reduce joint stress
- The restructuring of joints to further reduce joint complexity
- Minor sizing adjustments

Figure 6-23 shows version 5 of the chassis design without sleeves to highlight the geometric alterations. Figure 6-24 shows the same chassis but with sleeves on joints included.

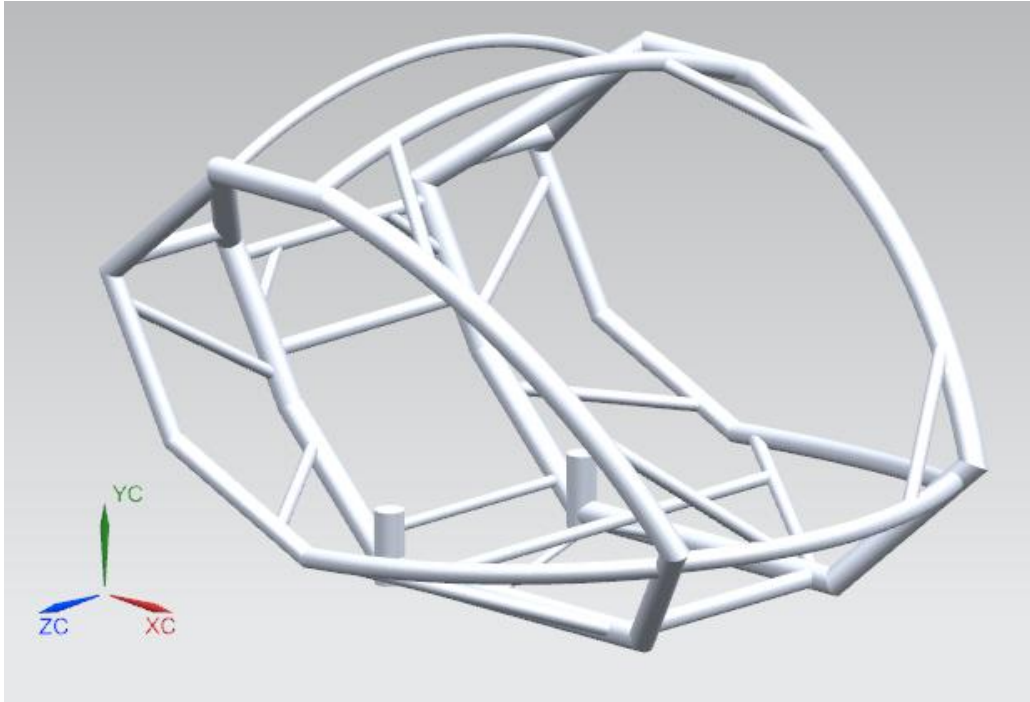


Figure 6-23: Chassis version 5 without sleeves

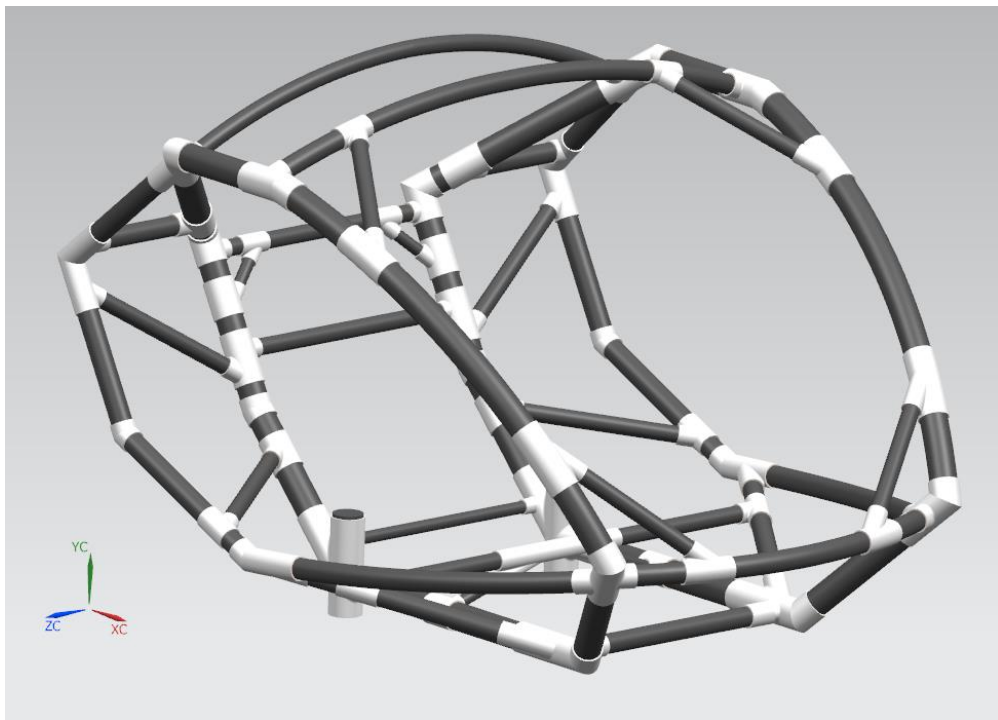
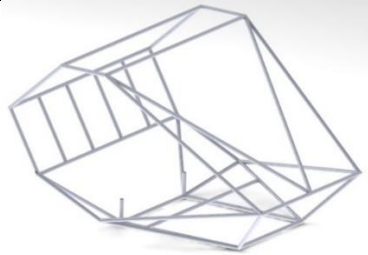
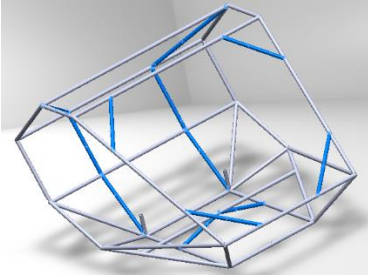
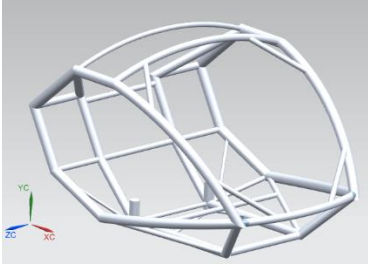
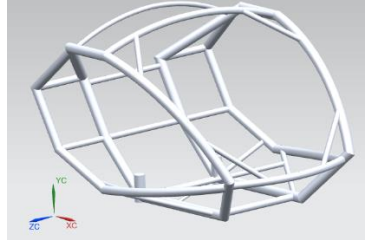
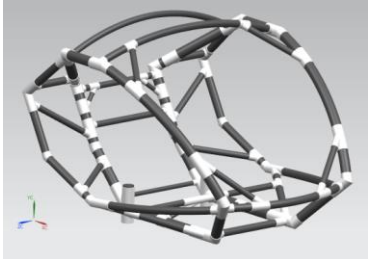


Figure 6-24: Chassis version 5

The FEAs of chassis version 5 and onward are discussed in section 7 as it involves focused optimisation sleeves. To summarise the design changes in this section, Table 6-3 is provided.

Table 6-3: Summary of geometric optimisations

Chassis Version	Chassis Image	Design Points/Changes
1		<ul style="list-style-type: none"> <li>• Baseline design</li> <li>• Material used is steel (rigid isotropic)</li> </ul>
2		<ul style="list-style-type: none"> <li>• Added struts</li> <li>• Removed low-stressed members</li> <li>• Replaced front members for better vision</li> </ul>
3		<ul style="list-style-type: none"> <li>• Designed for composite (orthotropic)</li> <li>• Side bumpers, front bumper and top roll-bar redesigned for crash effectiveness</li> </ul>
4		<ul style="list-style-type: none"> <li>• Joints simplified by relocation of members</li> <li>• Main frame path directed inward</li> </ul>
5		<ul style="list-style-type: none"> <li>• Some straight members changed to diagonal members</li> <li>• Triangulating members added to increase torsional stiffness</li> <li>• Further simplification of joints by relocation of members</li> <li>• Sleeves added</li> </ul>

## 7. Chassis Layup and Sleeve Optimisation

For version 5 of the chassis, steel sleeves were introduced at the joint regions to avoid buckling and reduce high stresses. Inclusion of the sleeves increases the mass of the chassis finally to 92 kg in chassis version 7 – the final design. The sleeves are to be adhered to the CFRP tubes using Spabond 340LV adhesive system as was done in previous simulations. Material properties used for Spabond and CFRP plies for these simulations may be found in Table 6-1 and Table 6-2 respectively.

The adhesive layer is to be 2 mm thick to help distribute the local stresses. Practically, getting a 2 mm thick consistent layer may be difficult, but a possible method is to slide the CFRP tube into a sleeve with sufficient adhesive, then place 2 mm wire between the sleeve and tube. This value was chosen because Adams & Adams (2002) suggest that the use of adhesive thickness of 1,3 mm shows higher strength of the composite when compared to thinner specimens. Additionally, FEAs were performed that corroborated this, although effects were small.

The material chosen for the sleeves was chosen to be stainless steel for its corrosion resistance and because the lap shear test result for Spabond applies to steel, not necessarily aluminium. Aluminium is not considered because its lower elastic modulus may result in inadequate distribution of applied loads. The CFRP tubes may instead take much more load and the SR may drop substantially. Furthermore, lap shear values for Spabond are for steel, so use with aluminium should be tested first. Adhesives used for aluminium, such as Crestabond, have inferior strength and lap shear properties to those used for steel. This is significant because Yang et al. (2016) did observe pull-out failure under tensile loading. This means that quantitative data is required for confident use of aluminium and a relevant adhesive. If lap shear data is found for aluminium and CFRP, aluminium should be tested as a sleeve material for viability as it will greatly reduce mass compared to steel. Stainless steel sleeves should be tested with specimens that have the surfaces roughened prior to bonding to ensure that the hard oxide layer on the stainless-steel surface does not impede bonding. If it does, all stainless-steel contact surfaces should be roughened shortly before applying adhesive. The stainless steel should have a high chromium content to resist corrosion effectively, but options in NX were limited. In NX, the material specified is AISI\_SS\_304-Annealed. Its major properties are listed in Table 7-1.

Table 7-1: Stainless steel properties from NX

Property	Value
Density (g/cm <sup>3</sup> )	7,9
Tensile Modulus (GPa)	190
Tensile Strength (MPa)	572
Yield Strength (MPa)	276
Poisson's Ratio	0,3

The loads were refined by adding the moments caused by the driver and passenger on the seat fixtures. Reed (2006) researched the position of the centre of mass above a seated surface for various individuals. For heavier individuals, the median is approximately 250 mm above the surface. The seat fixture points (where the loads are applied) are shown in Figure 7-1 along with the approximate location of the mass centre of a human being (represented by a red cross).

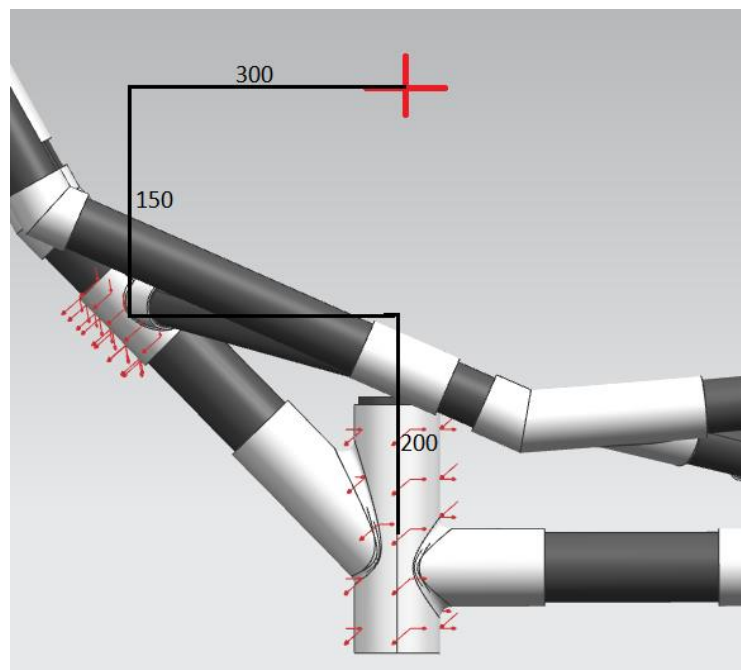


Figure 7-1: Seat fixture locations relative to human's approximate mass centre

The fixtures and battery are assumed to be light enough or close enough to fixture points that their applied moments are small.

The same braking, turning and gravitational accelerations are used as before. The moment loads are calculated by assuming that the human being is split into two 50 kg bodies; one

supported by the top, one supported by the bottom. The values for the moments are determined using the above distances and previously mentioned calculations. Table 7-2 shows the values of the loads applied. Calculations are based on the diagram illustrated in Figure A1-1, found in Appendix 1. Calculation A1-2, Calculation A1-3 and Calculation A1-4 are for the top support which is denoted A (Appendix A). Calculation A1-5, Calculation A1-6 and Calculation A1-7 are for the bottom support which is denoted B (Appendix A). Note that the forces and moments are applied in directions that simulate the dynamic scenario statically.

Table 7-2: Moment loads applied to chassis

TOP	$M_x$	57,4 Nm
	$M_y$	-115 Nm
	$M_z$	-63,2 Nm
BOTTOM	$M_x$	134 Nm
	$M_y$	0,00 Nm
	$M_z$	-196 Nm

The constraints were also refined. The front right suspension point was fixed in translation and free in rotation. The fixed condition in all directions is because a dynamic situation is being modelled statically, so this suspension point is assumed to have full grip to the road while other suspension points are assumed to be free in that plane. The other five suspension points were only fixed vertically, as it is not the job of the suspension to restrain the vehicle any further than that, and translation towards other suspension points is a realistic scenario. Figure 7-2 shows the locations of all suspension points. The fixed suspension is blue, the others are orange.

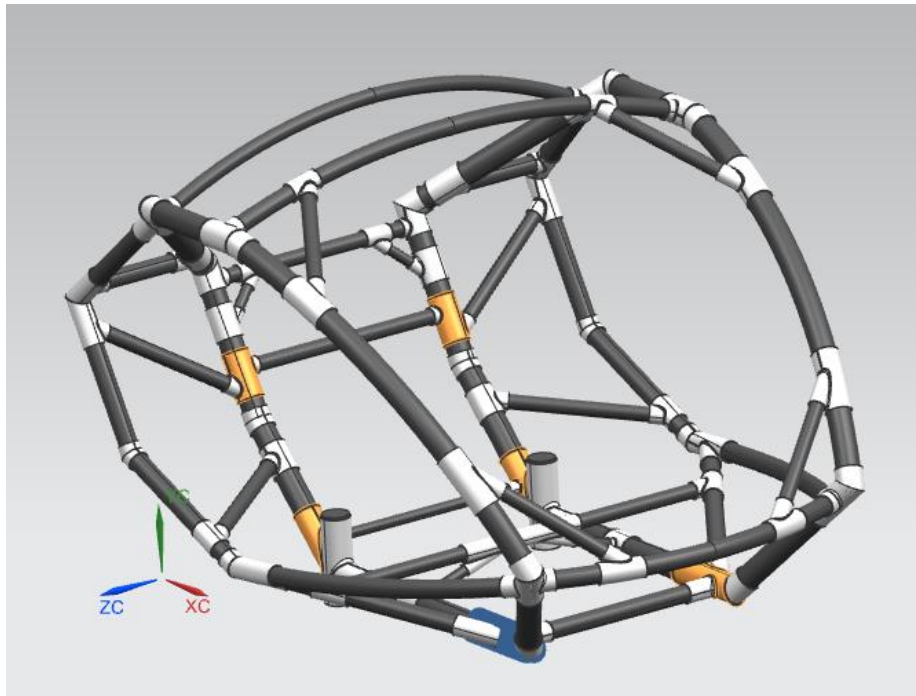


Figure 7-2: Chassis version 5 with constraints highlighted

The adhesive was joined to the tubes and sleeves by using NX's surface-to-surface gluing function. The results of this then output to "glue pressure" which can be compared to ultimate strength, and "glue traction" which can be compared to lap shear strength.

The layup for this simulation was four plies of UD all running the length of the tubes ( $0^\circ$ ). This is because they will have to handle tension or compression because it is a space frame, so this layup is a good starting point to handle the main stresses and minimise displacement.

The displacement plot is shown in Figure 7-3. The maximum displacement is under 6 mm which is small. The reasons for the reduced displacement compared to the previous version are as follows in order of importance:

- Some members have changed from being horizontal to being diagonal to increase torsional stiffness through triangulation.
- The fixture points have been modified such that the furthest fixtures are further from each other, reducing the strain.
- Two additional fixtures are added.
- Four plies of CFRP are used instead of three.
- The sleeves add stiffness at the joints, specifically reducing rotation.



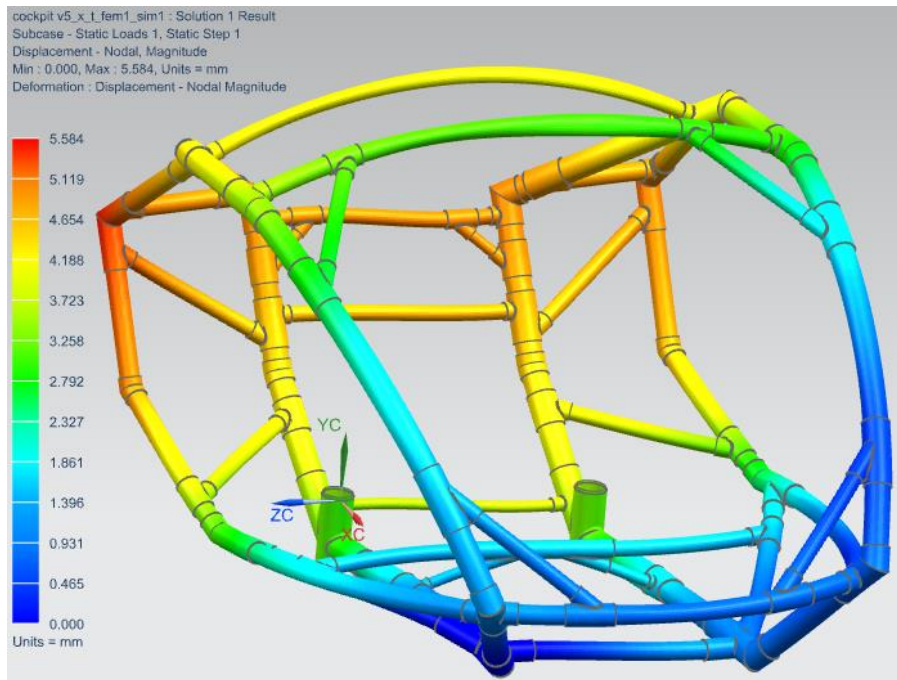


Figure 7-3: Chassis version 5 displacement plot

Figure 7-4 shows a stress plot at a region at the bottom of the chassis where the stress is highest. The stress distribution is uneven. Surrounding regions are unstressed, while the fillet is highly stressed. This indicates a stress concentration that can be optimised.

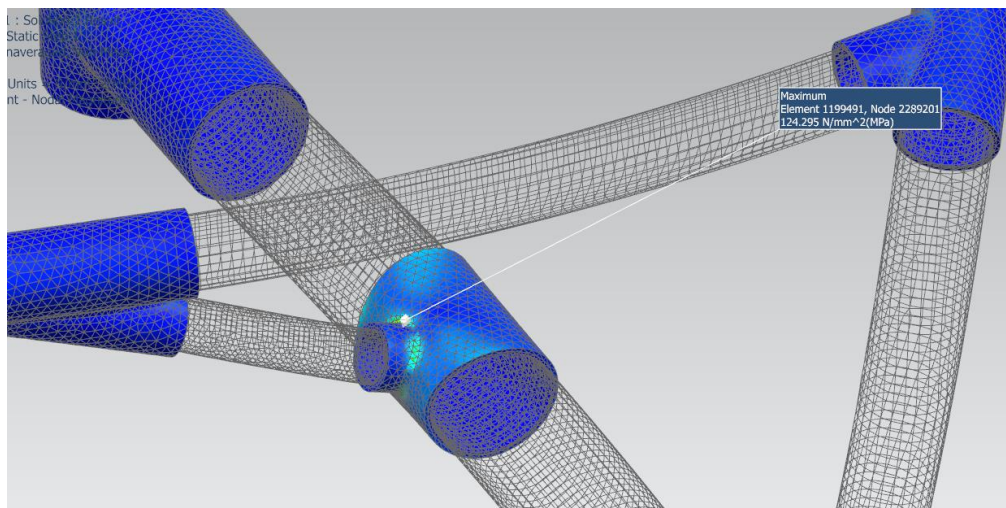


Figure 7-4: Chassis version 5 maximum nodal stress region

Figure 7-5 and Figure 7-6 illustrate the maximum glue pressure and traction respectively. They are both at the same joint. This means that apart from the sleeve requiring better stress distribution, the glue region itself is insufficient in size.

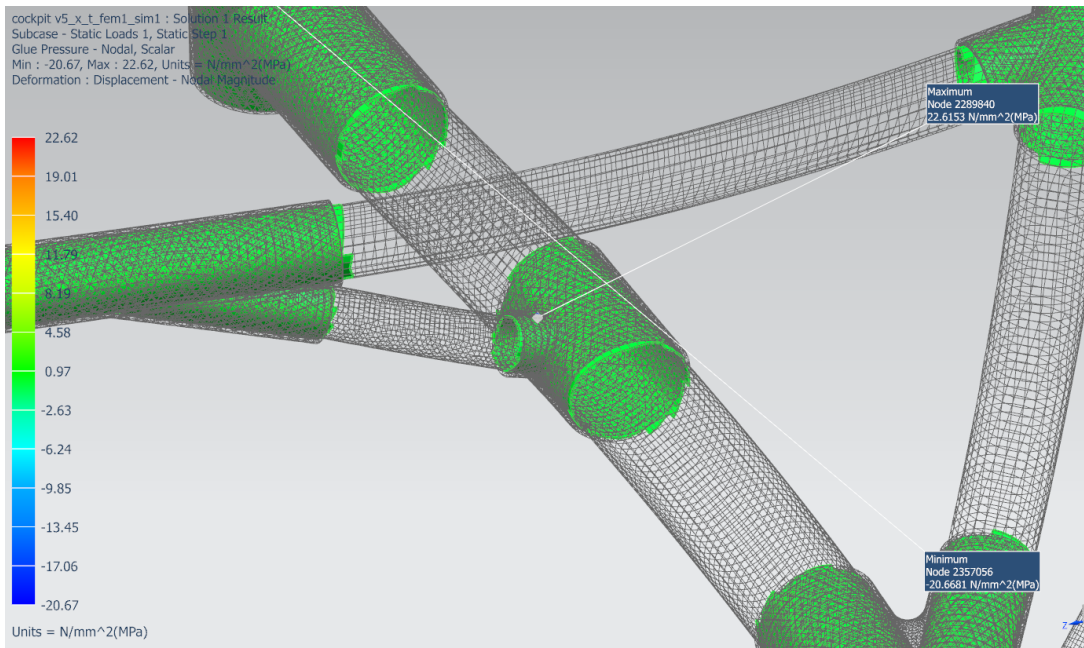


Figure 7-5: Chassis version 5 maximum glue pressure region

Note that the glue traction value exceeds the allowable limit of 37 MPa.

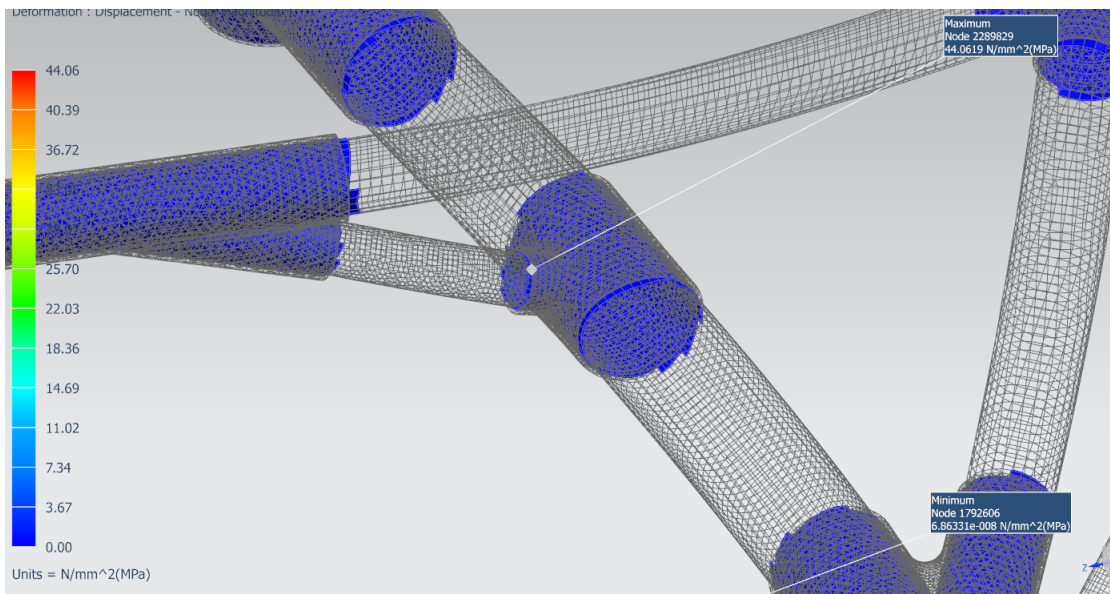


Figure 7-6: Chassis version 5 maximum glue traction region

Plotting the Hoffman failure index becomes meaningless when values are not near 1 because of how unrepresentative it is of a safety factor. Instead, a strength ratio plot is shown. Figure 7-7 shows this plot for chassis version 5. The scale on the plot is manually limited to 50 to illustrate the higher stressed regions better, although the true maximum is over 100 000. It is seen that there is a large strength ratio, meaning that plies are not stressed very much in

comparison to their ultimate strengths. Ply reduction is a possibility if it does not result in large deformation.

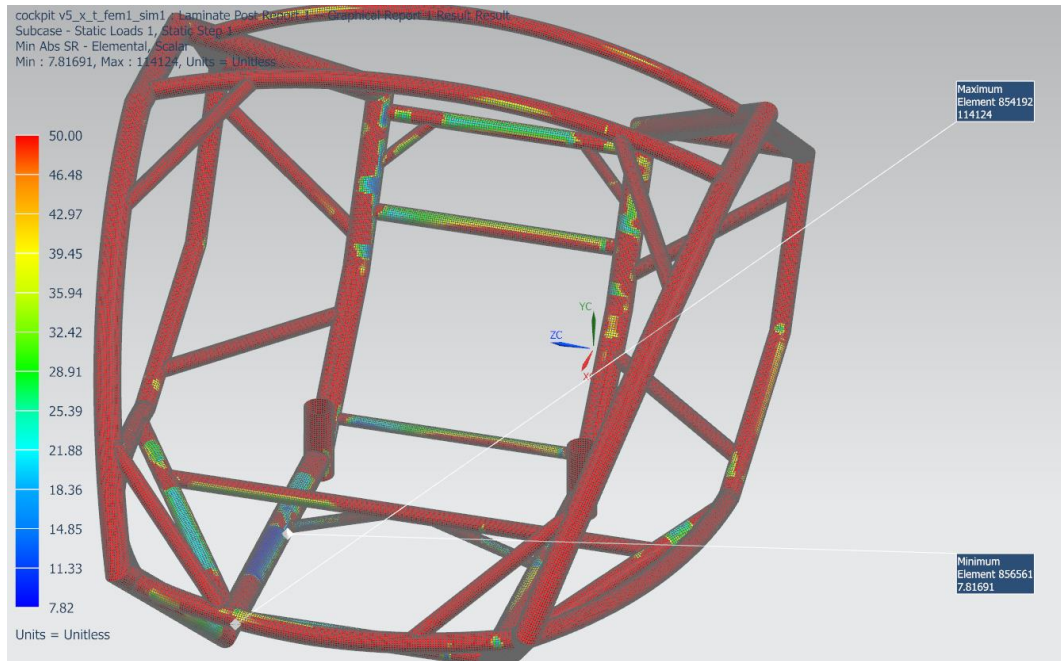


Figure 7-7: Chassis version 5 Hoffman strength ratio plot (sleeves hidden for clarity)

To summarise the results, Table 7-3 is presented. It shows the safety factors of each section to compare equal values.

Table 7-3: Chassis version 5 safety factors

Stress zone	Failure Stress (MPa)	Maximum Stress Experienced (MPa)	Safety Factor
Sleeves	276 <sup>a</sup>	124,30	2,2
Adhesive (pressure)	49 <sup>b</sup>	22,62	2,2
Adhesive (traction)	37 <sup>b</sup>	44,06	0,8
Tubes	-	-	7,8 <sup>c</sup>

<sup>a</sup> Yield stress is used

<sup>b</sup> Ultimate stress is used for lack of yield limit

<sup>c</sup> Strength ratio is presented, which is analogous to safety factor

Because the safety factor of this chassis should be approximately 2,5 and a minimum of 2, the safety factor for the sleeves is slightly low, and the glue material has a value of less than one in shear, indicating failure. Conversely, the tubes have a large safety factor. This may be seen as

unnecessarily large, but until damage analyses are done, high safety factors are preferred for CFRP if cost permits, because of tensile failure being catastrophic in nature. That being said, the goal is to optimise the design.

To reduce lap shear, high stressed adhesive zones were extended along with the sleeves. To reduce stress on the sleeves, some fillet radii were increased. The tops and bottoms of the seat posts experienced relatively low stress, so they were shortened to allow a lower mass centre. The previous images are the extremes; but optimisation was based on considering all high stress areas. The layup was reduced to 3 layers because the minimum strength ratio was high, and displacement was small, possibly small enough to allow this ply reduction.

Even though bulk geometry is largely the same, to avoid confusion, the next iteration will be named chassis version 6. Figure 7-8 shows chassis version 6 with the alterations in sleeve lengths and fillet radii highlighted.

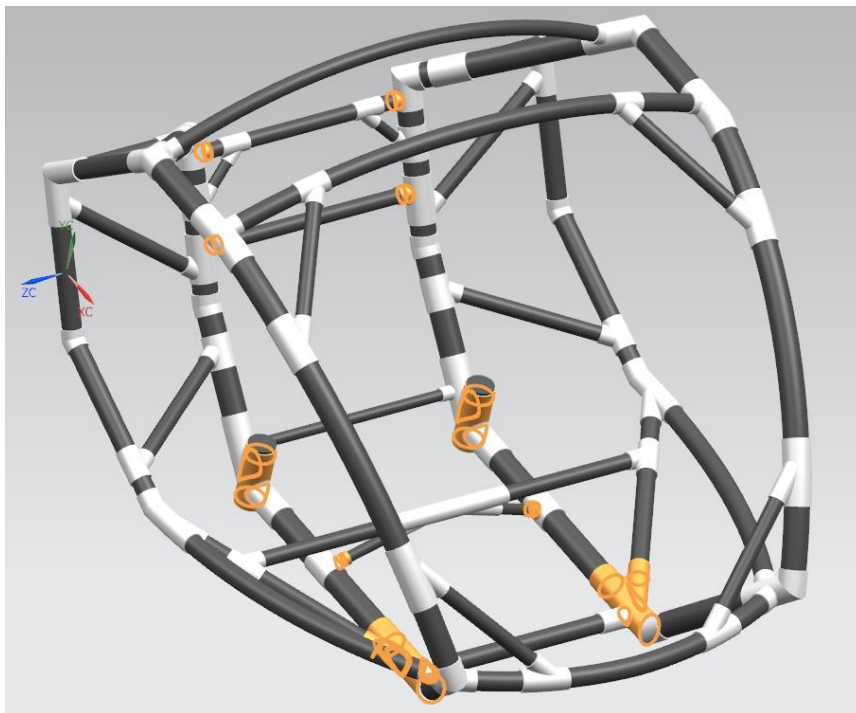


Figure 7-8: Chassis version 6 - alterations to chassis version 5 highlighted

The displacement plot is shown in Figure 7-9. The maximum displacement is 6,6 mm which is still small.

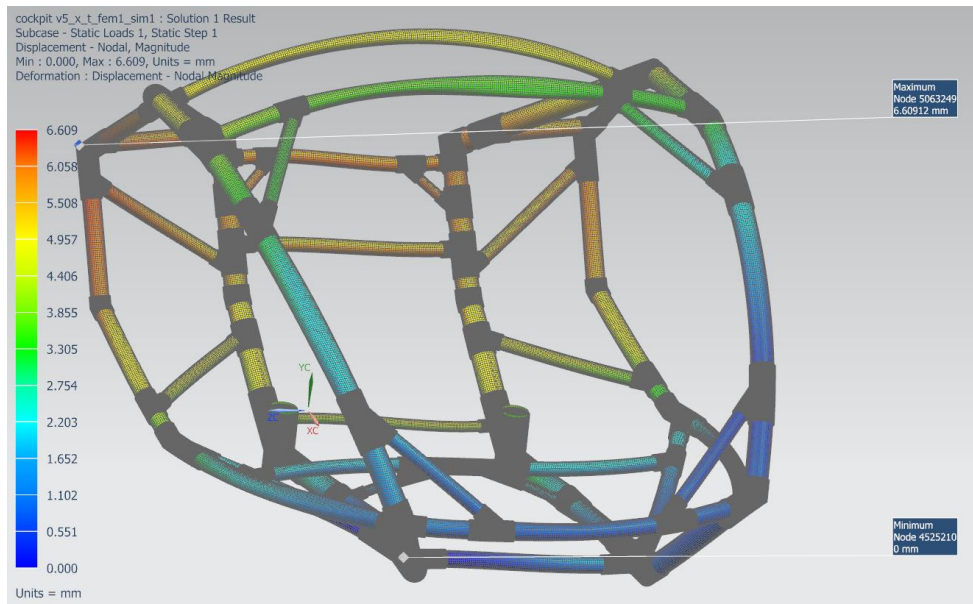


Figure 7-9: Chassis version 6 displacement plot

Figure 7-10 shows the highest stressed region. While most of the structure is still unstressed, the distribution is better than version 5, and the maximum value has dropped.

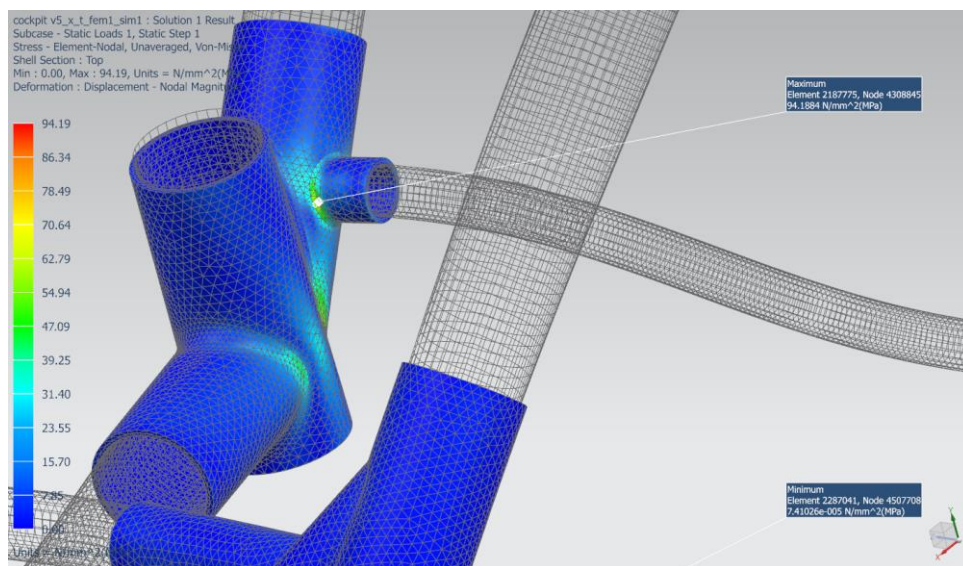


Figure 7-10: Chassis version 6 maximum nodal stress region

Figure 7-11 shows the glue regions worst stressed in pressure. The maximum absolute pressure is compressive, but compressive strengths of brittle materials are significantly higher than tensile strengths (Gere & Goodno 2009). The positive limit is significantly lower, and the region has changed. This shows successful optimisation of the glue region from version 5 to version 6.

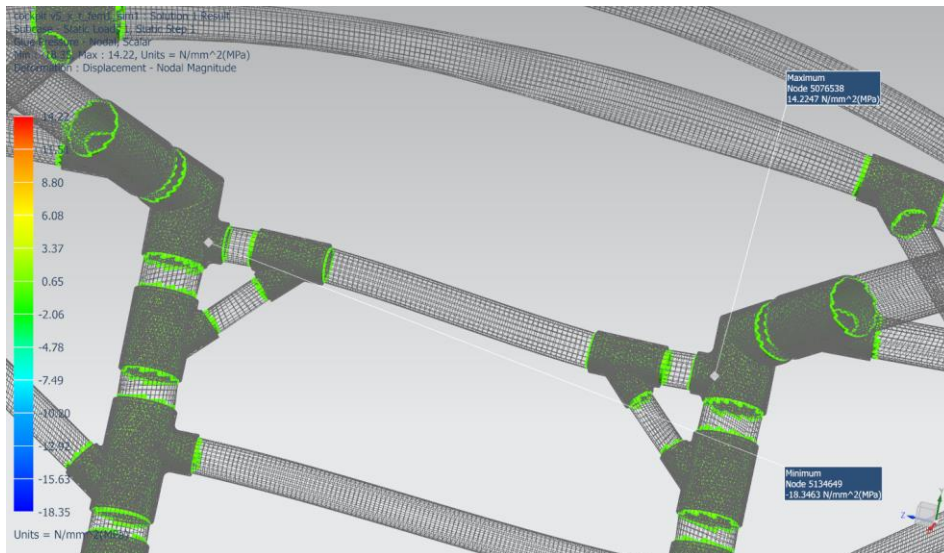


Figure 7-11: Chassis version 6 glue pressure extremes

Figure 7-12 shows the maximum glue traction which has dropped to less than half of what it was in version 5. This reiterates the success in optimisation for the glue region.

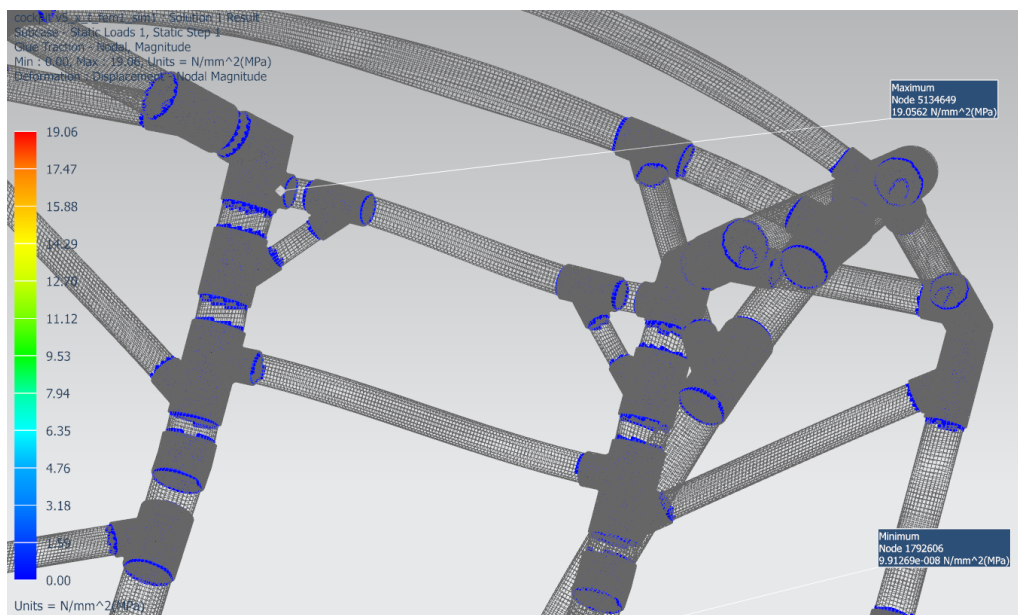


Figure 7-12: Chassis version 6 maximum glue traction region

Figure 7-13 shows a plot of the Hoffman failure index for chassis version 6. It has dropped significantly, but remains high with respect to the goal safety factor. Further ply reduction is possible, but buckling would become a concern, especially considering low-speed impact loading, which would be perpendicular to members' lengths.

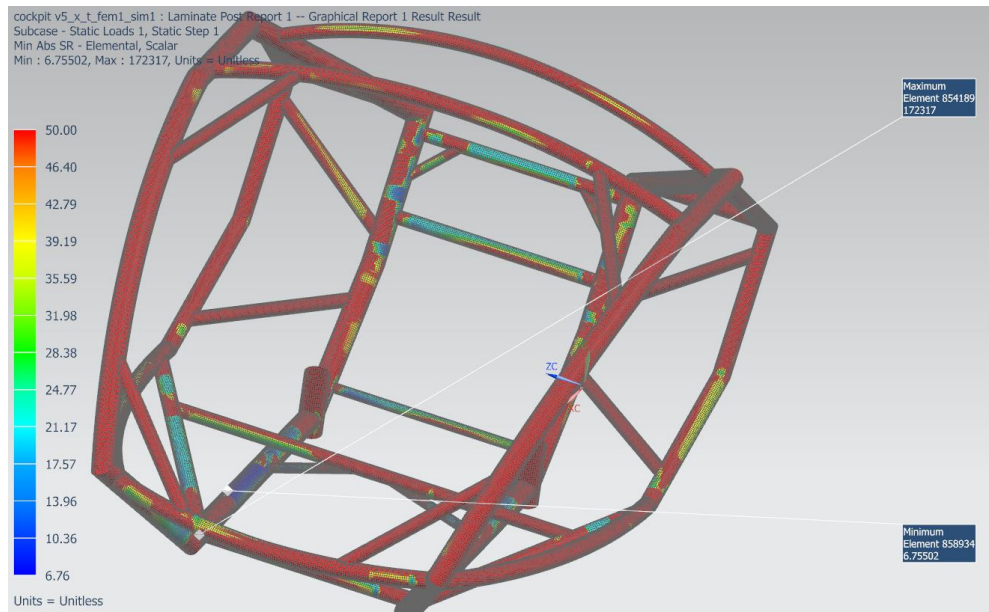


Figure 7-13: Chassis version 6 Hoffman strength ratio plot (sleeves hidden for clarity)

Table 7-4 shows how the safety factors of chassis version 6 have changed in comparison to its predecessor. Note that for normal stress on the adhesive (pressure), the compression stress value is used and compared to the tensile strength value. This is a conservative estimate due to lack of compressive strength data. In reality, the compressive strength would be much higher than the tensile strength value used (Gere & Goodno 2009).

Table 7-4: Chassis version 6 safety factors

Stress Zone	Failure Stress (MPa)	Maximum Stress Experienced (MPa)	Safety Factor	Change in Safety Factor from Previous Version (%)
Sleeves	276 <sup>a</sup>	94,19	2,9	32
Adhesive (pressure)	49 <sup>b</sup>	-18,35	2,7	23
Adhesive (traction)	37 <sup>b</sup>	19,06	1,9	126
Tubes	-	-	6,8 <sup>c</sup>	-13

<sup>a</sup> Yield stress is used

<sup>b</sup> Ultimate stress is used for lack of yield limit

<sup>c</sup> Hoffman strength ratio is presented, which is analogous to safety factor

Chassis version 6 has better safety factors than version 5, but adhesive traction is still slightly below the minimum value of 2. The next design iteration will address this. Note that the results of chassis version 5 did prompt the optimisation of this failure region (the upper region in

Figure 7-8), but the extension of the sleeve was insufficient. Mass of the chassis is increased to 92 kg due to the addition of sleeves. The CFRP components total a mass of just under 12 kg.

The displacement plot is shown in Figure 7-14. The maximum displacement is still 6,6 mm.

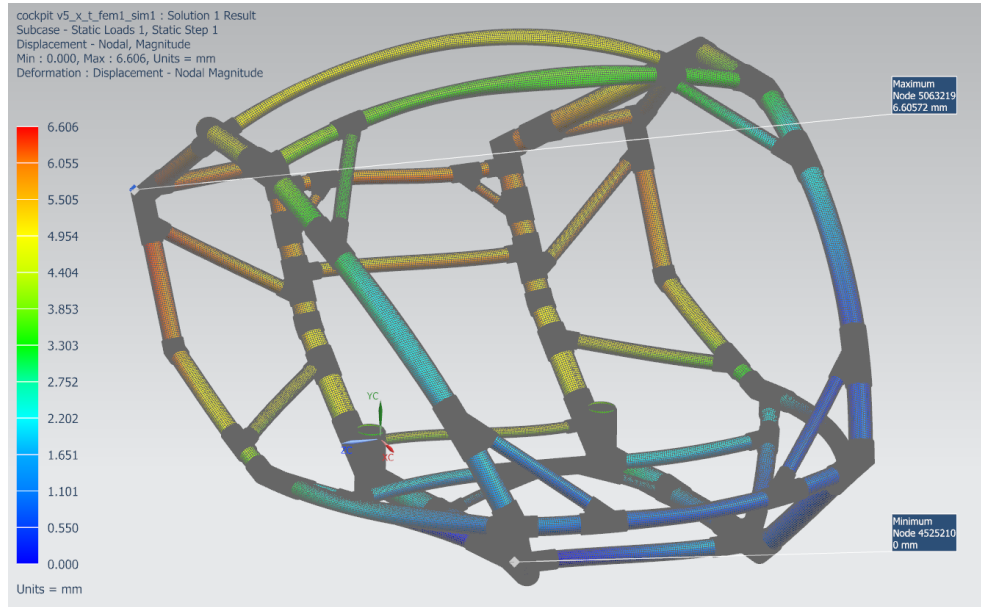


Figure 7-14: Chassis version 7 displacement plot

Figure 7-15 shows the maximum stress in the sleeves.

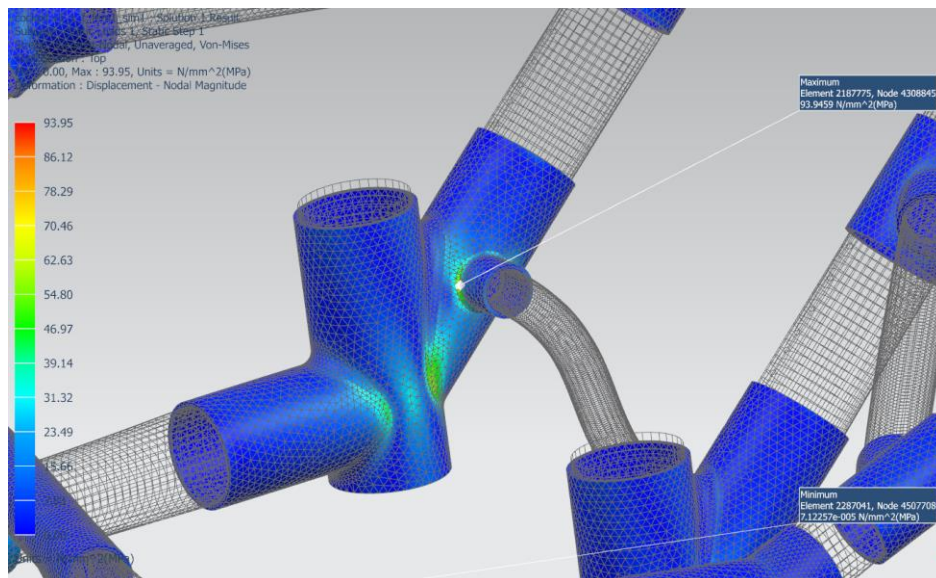


Figure 7-15: Chassis version 7 maximum nodal stress region



Figure 7-16 shows that the region for the maximum positive glue pressure has changed, and its value has dropped. It also shows that the minimum value is lower in magnitude.

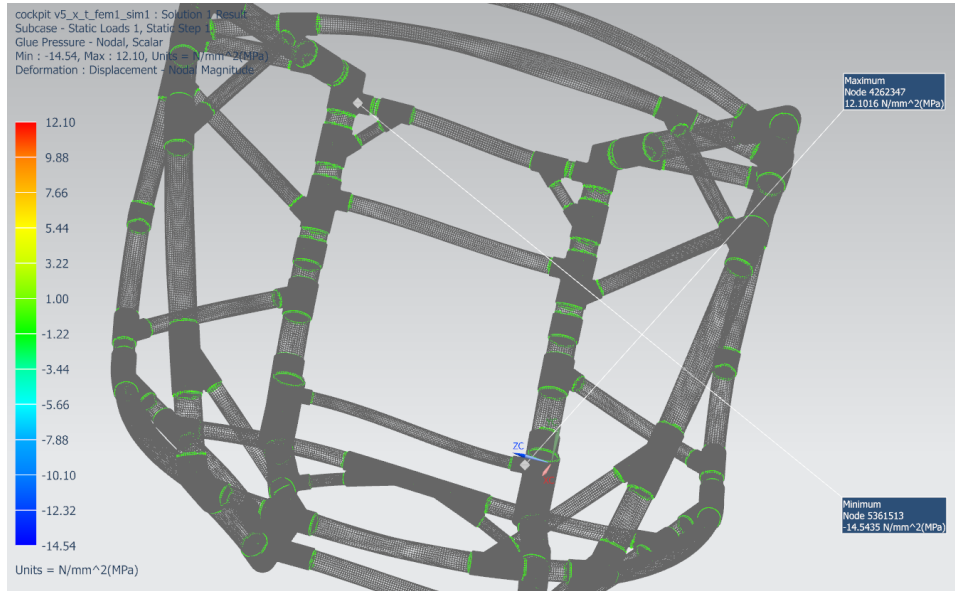


Figure 7-16: Chassis version 7 glue pressure extremes

Figure 7-17 shows that the region of maximum glue traction has moved, and its value has dropped.

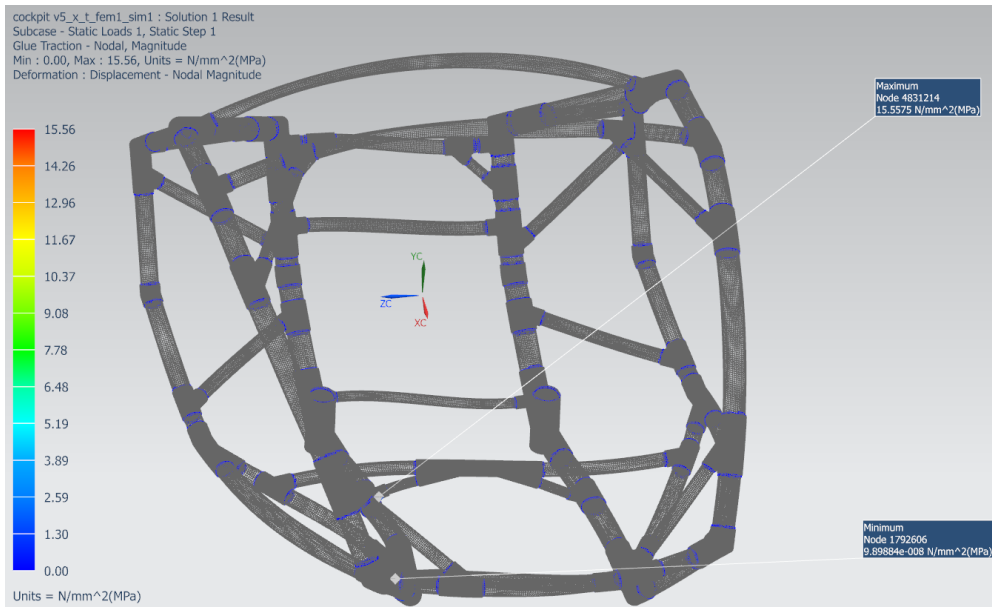


Figure 7-17: Chassis version 7 glue traction plot

Figure 7-18 shows that the minimum strength ratio is almost the same. Some highly stressed locations that are enclosed by the sleeves may be explained by the low modulus of the adhesive material allowing tube deflection during stress transfer.

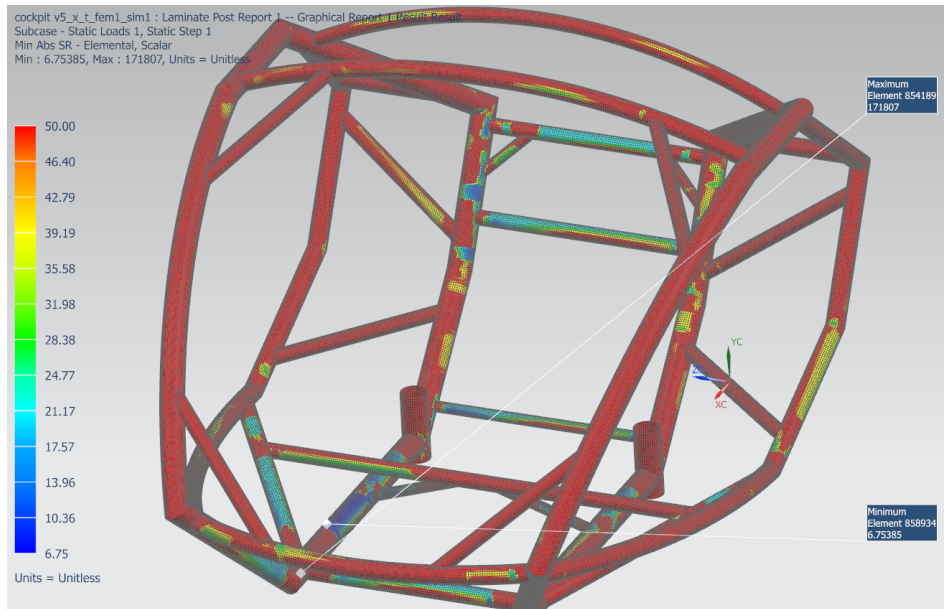


Figure 7-18: Chassis version 7 Hoffman strength ratio plot (sleeves hidden for clarity)

Table 7-5 shows how the safety factors of chassis version 7 have changed in comparison to its predecessor. Again, for normal stress on the adhesive, the compression stress value is used and compared to the tensile strength value.

Table 7-5: Chassis version 7 safety factors

Stress Zone	Failure Stress (MPa)	Maximum Stress Experienced (MPa)	Safety Factor	Change in Safety Factor from Previous Version (%)
Sleeves	276 <sup>a</sup>	93,95	2,9	0
Adhesive (pressure)	49 <sup>b</sup>	-14,54	3,3	22
Adhesive (traction)	37 <sup>b</sup>	15,56	2,4	26
Tubes	-	-	6,8 <sup>c</sup>	0

<sup>a</sup> Yield stress is used

<sup>b</sup> Ultimate stress is used for lack of yield limit

<sup>c</sup> Hoffman strength ratio is presented, which is analogous to safety factor

The adhesive stress has been lowered sufficiently. The lowest safety factor is now 2,4 which is higher than the decided minimum of 2 and close enough to 2,5. This shows successful design and optimisation to handle stress.

As mentioned, the mass of the structure is approximately 92 kg. Based on the maximum stress of the sleeves, an equivalent aluminium frame is calculated to have a mass of about 77 kg to have the same overall safety factor of 2,4. Similarly, an equivalent steel frame would have a mass of around 220 kg.

In chassis version 4, buckling was assessed, and the simulation returned a buckling factor of 2,6. In that scenario, moment loads were omitted, but for that layup, buckling was only seen to be a possibility at joins, and global buckling was not seen to be an issue. Since then, struts have been repositioned to deliver loading more axially and reduce moments, and sleeves have been added. The thickness at the join regions have thus increased from 0,9 mm to 5,9 mm. The better load transfer coupled with the increase in thickness (and increase in outside diameter) instils confidence that local buckling is not an issue. Especially considering that the sleeve material at the outer diameter is significantly stiffer than the tube material. Global buckling is not seen to be a likely possibility for this layup, especially considering the reduction of bending moments within members. The tube thickness should not be reduced further however, because it may become susceptible to kink easily in a low-speed collision.

An FEA was conducted to assess a pure braking scenario. Loading conditions were changed to only include loads due to gravity and braking. Also, the left-front constraint that was previously allowed to move freely except in the z-direction was changed to match the other fixed translation constraint. This means that the FEA considers all braking load is by the front two wheels and no braking by the rear wheel. This makes sense because it is more logical to have brakes on each of the front wheels rather than one brake system on the rear wheel. This FEA showed a minimum safety factor of 10,4 and the failure region shifted from the lower adhesive connection to the sleeves at the seat post. This implies that there is no single area that is the weakest component. Certain areas are stronger under different, known loading conditions, which is an indication that the structure is, at least, partly optimised.

## 8. Discussion

This dissertation detailed the design, analysis and optimisation stages of a composite space frame chassis. The focus areas were mainly composite material behaviour, composite failure criteria, buckling, and stresses at joints.

Suitable composite material constituents were selected using material property charts and performance indices relating to stresses found in a space frame. The matrix was selected based on the availability rather than the optimum matrix that may exist. This links to the method of manufacture which was chosen to be vacuum infusion for its price and consistency, although prepreg material would be best.

Fibre orientation was only briefly explored in preliminary FEAs because it was not necessary in optimisation stages. Using UD plies does improve the mass of the tubes because the load is in the direction of the fibres.

The research problem, aside from the chassis geometry design, is how to validate failure results provided by FEA software. For this reason, a test was designed to compare a real-world scenario to the computational version of it. This also served to compare failure theories.

The results of the tube testing in comparison to the FEA predictions show a very close agreement for the Hoffman and Tsai-Wu failure criteria. An uncertainty in testing is the matter of waviness on the tubes' surfaces. The FEA results are convincing using tube's smallest diameter, but further testing should be carried out using more uniform tubes to replicate the conclusions drawn in this dissertation. The test method should be broadened to include testing cross-ply weaves or UD plies at different angles to each other. This serves to test NX Nastran's ability to accurately simulate the stress transfer within and between plies, and predict failure correctly using the strength and stiffness values of a single ply. For ASTM testing, strain gauges are recommended.

The Hoffman and Tsai-Wu failure criteria showed good correlation with adjusted FEA simulations, thus confirming their ability to accurately predict failure in the application of UD laminate tubes. The Hill and Maximum Strain criteria should not be used as they were inaccurate, erring on the side of danger. This expands on work done by Soden et al. (1998) by showing not only the difference in failure predictions, but also which are most accurate. Computational results were shown not to be exceptionally sensitive to mechanical material

properties so long as moduli are measured with reasonable accuracy. This allows more confident design in the absence of accurate properties.

Through continuous optimisation, the finished chassis design is robust. It has a minimum safety factor of 2,4 in a high stressed loading condition. In a pure braking scenario, the safety factor rises to 10,4. The worst-case scenario was defined as the maximum braking acceleration by a small on-road vehicle, coupled with the maximum turning acceleration by a medium sized on-road vehicle. The scenario included both occupants of 100 kg mass in the chassis, which is slightly conservative. FEA results showed a low displacement value of 6,6 mm which implies successful handling of emergency conditions. While loading scenarios were analysed, they should be considered once more when the suspension components are included. Specifically, toppling during turning should be assessed, so that chassis height and track width can be designed accordingly. Note also that no crash analyses were conducted on this vehicle as this requires a much deeper understanding of composite failure that would need to be validated through additional testing.

Chassis optimisation was mainly focused on the joint regions. This is because other stress concentrations were mitigated by redesigning members and join geometries. No laminate optimisation was required in this chassis, so no information is presented on the strength of laminates as a function of ply orientation. Design iterations involved simplifying joints to reduce stress concentrations, and eventually the incorporation of sleeves to reduce local stresses and the likelihood of local buckling. Global buckling is an unlikely scenario based on buckling a simulation. Local buckling is also unlikely based on the same buckling simulation and the use of sleeves, which distribute stress and increase the second moment of area. The sleeves were based on the sleeves tested by Yang et al. (2016), but involved bonded metal sleeves rather than crimped ends and bolted joints. Optimisation of adhesive stresses was done by adjusting sleeve length. Lengthening sleeves reduced local shear stresses by increasing the shear area. Increasing fillet radii allowed the forces within the sleeves to flow better from one direction to another, thus reducing the maximum stress. The sleeves distributed stress well due to large fillet radii (sometimes in the region of 10-15 mm), but it may be more practical to use smaller fillet radii and include ribs as part of the sleeves that would be attached by welding. This method would have to be tested (likely computationally) before implementation, but the already high safety factor of the sleeves indicates a high probability of success.

## 9. Conclusions

Suitable materials were selected through analysis of performance indices in related applications. Manufacturing methods of composites were considered and accounted for during the design stage. A possible method to optimise ply angles was hypothesised but not implemented because the design did not require it.

In the design stage, joint stresses proved to be the focus due to the high stresses and buckling. Joint stresses were minimised by the alteration of member positions and the implementation and optimisation of steel sleeves. Buckling was analysed through FEA and seen to be unlikely. The sleeves proved to minimise the stresses and reduce the likelihood of buckling, albeit at the cost of added mass.

A robust design for a composite space frame chassis is produced. The total mass of the chassis is under 92 kg, and it has a minimum safety factor of 2,4. Result validation was successfully completed through experimental methods, and some failure criteria such as Hoffman and Tsai-Wu were shown to be more accurate than others, such as Maximum Strain and Hill. A test method is produced involving the testing of tubes with a 35° fibre angle, that validates FEA results and the Hoffman and Tsai-Wu failure criteria.

A method of comparing failure criteria was produced in this dissertation. The design of a 35° UD layup tube test allowed compressive loading of a test specimen to induce complex loading within the specimen. This test validated FEA results from NX Nastran and instilled confidence in the pure computational design of the chassis. This dissertation has shown that by knowing the properties of each ply (some with more accuracy than others) in the laminate, one can accurately design composite structures using UD plies and analyse them computationally using NX Nastran. Although UD fabric was infused with resin, these results hold for methods such as filament winding and continuous pultrusion as well. The key is obtaining properties of one ply or the properties of the matrix and fibre separately. No conclusions may be made concerning the behaviour of cross-ply fabric as they were not tested. A similar test method to the one designed in this dissertation may solve this.

A possibility for further optimisations is to replace steel joints under low load for aluminium ones and change the relevant adhesive zones. Changing even half of the joints to aluminium would result in a mass saving of around 30 kg. Note that this increases manufacturing complexity and reintroduces the possibility of local buckling. Despite its softness compared to steel, solutions using aluminium sleeves must be implemented if testing proves that an

adhesive material has adequate lap shear strength. Using small CFRP plies at joint regions (wraps) may solve the problem of joint stresses, but is difficult to model and simulate, especially where optimisation is concerned. Due to this difficulty, a study on this join method should be carried out experimentally rather than computationally. Using steel as the sleeve material is advantageous because although its ultimate stress is lower than that of UD CFRP, its higher stiffness impedes buckling better than CFRP wraps would. The density of steel is undesirable and is a major factor for the total chassis mass of 92 kg.

Future optimisation of this design may include changing tube diameters, and crash testing. Altering tube diameters provides another way to balance the required strength with the required stiffness. Note that reducing tube diameters would reduce adhesive area and increase stress concentrations on the sleeve, so care should be taken when attempting to optimise purely for mass or cost. Crash testing is not greatly important for this application, but in similar vehicles that are used in higher-speed applications, a crash becomes more dangerous. In those applications, the use of sacrificial members is recommended because CFRP dissipates energy through fracture.

Because fatigue was not assessed, it is suggested that the adhesive be strength tested with MWCNT and implemented if results are satisfactory and in line with any fatigue objectives. Because the adhesive material has the lowest safety factor of the three materials in this chassis, increasing fatigue life by introducing MWCNT is advantageous.

## 10. References

- ACP Composites, 2014. *Mechanical Properties of Carbon Fiber Composite Materials*. [ONLINE] Available at: <https://www.acpsales.com/upload/Mechanical-Properties-of-Carbon-Fiber-Composite-Materials.pdf>. [Accessed 25 October 2017].
- Adali, S, Lene, F, Duvaut, G, Chiaruttini, V, 2003. Optimization of Laminated Composites Subject to Uncertain Buckling Loads. *Composite Structures*, 62 (2003), 261-269.
- Adams, DO, Adams, DF, 2002. *Tabbing Guide for Composite Test Specimens*. US Department of Transportation, Federal Aviation Administration, Washington DC.
- AMT Composites, 2017. *High Tg Epoxy Systems*. [ONLINE] Available at: <http://www.amtcomposites.co.za/products/epoxy-polyester-systems/high-tg-epoxy-systems>. [Accessed 24 May 2017].
- Ashby, M, 2010. *University of Cambridge College of Engineering and Science Resource Booklet: Material and Process Charts*. University of Cambridge (Engineering Department), United Kingdom.
- ASTM International 2013. *ASTM D3518 / D3518M-13, Standard Test Method for In-Plane Shear Response of Polymer Matrix Composite Materials by Tensile Test of a  $\pm 45^\circ$  Laminate*. West Conshohocken, PA.
- ASTM International 2014. *ASTM D3039 / D3039M-14, Standard Test Method for Tensile Properties of Polymer Matrix Composite Materials*. West Conshohocken, PA.
- ASTM International 2015a. *ASTM D3171-15, Standard Test Method for Constituent Content of Composite Materials*. West Conshohocken, PA.
- ASTM International 2015b. *ASTM D695-15, Standard Test Method for Compressive Properties of Rigid Plastics*. West Conshohocken, PA.
- Bailie, JA, Ley, RP, Pasricha, A, 1997. *A Summary and Review of Composite Laminate Design Guidelines*. Task 22 NASA Contract NAS1-19347. Military aircraft Systems Division.
- Barbero, EJ, 2011. *Introduction to Composite Material Design*. 2<sup>nd</sup> ed. eBook: CRC Press.
- Bru, T, Hellström, P, Gutkin, R, Ramantani, D, Petersno, G, 2016. Characterisation of the Mechanical and Fracture Properties of a Uni-Weave Carbon Fibre/Epoxy Non-Crimp Fabric Composite. *Data in Brief*, 6 (2016), 680-695.



- Chowdhury, NM, Wang, J, Chiu, WK, Chang, P, 2016. Experimental and Finite Element Studies of Thin Bonded and Hybrid Carbon Fibre Double Lap Joints Used in Aircraft Structures. *Composites Part B*, 85 (2016), 233-242.
- Cui, WC, Wisnom, MR, Jones, M, 1991, A Comparison of Failure Criteria to Predict Delamination of Unidirectional Glass/Epoxy Specimens Waisted Through the Thickness. *Composites*, 23 (3), 158-166.
- Diamond, EJ, 2015. *Ergonomics and Anthropometrics*. [ONLINE]. Available at: <https://emilyjdiamond.wordpress.com/2015/10/18/ergonomics-and-anthropometrics-2/>. [Accessed 4 April 2017].
- Eurenius, CA, Danielsson, N, Khokar, A, Krane, E, Olofsson, M, Wass, J, 2013. *Analysis of Composite Chassis*. Bachelor Thesis. Göteborg, Sweden: Chalmers University of Technology.
- Frankel, A, 2013. *2014 Ford Fiesta ST First Drive*. Edmunds. [ONLINE] Available at: <https://www.edmunds.com/ford/fiesta/2014/road-test/>. [Accessed 17 October 2017].
- Gere, JM, Goodno, BJ, 2009. *Mechanics of Materials*. 7th ed. Toronto, Canada: Cengage Learning.
- Gurit, 2017. *Spabond 340LV HT*. [ONLINE] Available at: <https://www.amtcomposites.co.za/sites/default/files/media/data-sheets/spabond-340lv-htpdf.pdf>. [Accessed 24 October 2017].
- Hoa, SV, Lee, S, 2015. *Development of Techniques for The Joining of Composite Tubes*. Montreal, Quebec: Concordia Centre for Composites, Department of Mechanical Engineering, Concordia University.
- Huffman, JP, 2013. *2014 Toyota Corolla First Drive*. Edmunds. [ONLINE] Available at: <https://www.edmunds.com/toyota/corolla/2014/road-test/>. [Accessed 17 October 2017].
- Juvinall, RC, Marshek, KM, 2012. *Machine Component Design*. 5th ed. Singapore: John Wiley & Sons, Inc..
- Kaw, AK, 2006. *Mechanics of Composite Materials*. 2<sup>nd</sup> ed. Florida: Taylor & Francis Group.
- More, A, Chavan, C, Patil, N, Ravi, K, 2017. Design, Analysis and Optimization of Space Frame Chassis. *International Journal of Engineering and Technology (IJET)*, 9 (2), 1411-1422.

Murakami, T, Matsuo, T, 2015. In-Plane Shear Properties of Carbon Fiber Reinforced Thermoplastic Composites by Using V-Notched Specimen and Digital Image Correlation. *20th International Conference on Composite Materials*. Copenhagen, 19-24th July 2015.

Modlin, CT, Zipay, JJ, 2014. *The 1.5 & 1.4 Ultimate Factors of Safety for Aircraft & Spacecraft – History, Definition and Applications*. [ONLINE] Available at: <https://ntrs.nasa.gov/archive/nasa/casi.ntrs.nasa.gov/20140011147.pdf>. [Accessed 27 October 2017].

Narayanaswami, R, Adelman, HM, 1977. Evaluation of the Tensor Polynomial and Hoffman Strength Theories for Composite Materials. *Journal of Composite Materials*, 11(1977), 366-377.

National Aeronautics and Space Administration, 2008. *Man Systems Integration Standards: Volume 1 Section 3*. [ONLINE] Available at: <https://msis.jsc.nasa.gov/sections/section03.htm>. [Accessed 30 May 2017].

Nijssen, RPL, 2015. *Composite Materials An Introduction*. 1<sup>st</sup> ed. In Holland: University of Applied Sciences.

Reed, MP, 2006. *Whole-Body Center of Mass Location In Seated Postures*. Final Report. Michigan, United States of America: University of Michigan.

Shah, DU, 2014. Natural Fibre Composites: Comprehensive Ashby-Type Materials Selection Charts. *Materials and Design*. [ONLINE] Available at: <http://dx.doi.org/10.1016/j.matdes.2014.05.002> [Accessed 24 May 2017].

Shury, J, 2015. *Koenigsegg's Latest Carbon Fibre Mega Car Is King of Geneva*. Composites Today. [ONLINE] Available at: <https://www.compositestoday.com/2015/03/koenigseggs-latest-carbon-fibre-mega-car-is-king-of-geneva/>. [Accessed 22 March 2017].

Siegler, BP, Butler, L, Deakin, AJ, Barton, DC, 1999. The Application of Finite Element Analysis to Composite Racing Car Chassis Design. *Sports Engineering (1999) 2*, 245-252. School of Mechanical Engineering, The University of Leeds, Leeds.

Siemens, 2012. *NX Laminate Composites – Student Guide*. Publication number mt15029-s-nx85: Siemens Product Lifecycle Management Software Inc.

Skinner, L, 2012. *Best and Worst Supermini Braking Distances*. Which News. [ONLINE] Available at: <https://www.which.co.uk/news/2012/05/best-and-worst-supermini-braking-distances-285596/>. [Accessed 17 October 2017].

Soden, PD, Hinton, MJ, Kaddour, AS, 1998. A Comparison of The Predictive Capabilities of Current Failure Theories for Composite Laminates. *Composites Science and Technology*, 58 (1998), 1225-1254.

Sun, CT, Quinn, BJ, Tao, J, Oplinger, DW, 1996. *Comparative Evaluation of Failure Analysis Methods for Composite Laminates*. Washington D.C: United States Department of Transportation, Federal Aviation Administration Office of Aviation Research.

Thorntor PH, Jeryan, RA, 1988. Crash Energy Management in Composite Automotive Structures. *International Journal of Impact Engineering*, 7 (2), 167-180.

Tsai, SW, Hahn, HT, 1980. *Introduction to Composite Materials*. 1<sup>st</sup> ed. Pennsylvania, United States of America: Technomic Publishing Company Inc.

van Rijswijk, K, 2017. *Think Composites: Short Course*. Durban University of Technology - Steve Biko Campus, KwaZulu-Natal, 19 May 2017. Durban: Mandela Bay Composites Cluster.

von Koenigsegg, C, 2013. *Carbon Fibre Construction – Inside Koenigsegg*. Interview by Drive [ONLINE]. Available at: [https://www.youtube.com/watch?v=504I\\_hJDFck](https://www.youtube.com/watch?v=504I_hJDFck) [Accessed 22 March 2017].

Walker, M, Reiss, T, Adali, S, 1995. Multiobjective Design of Laminated Cylindrical Shells for Maximum Torsional and Axial Buckling Loads. *Computers and Structure*, 62 (2), 237-242.

Yang, X, Bai, Y, Jia Luo, F, Zhao, XL, He, X, 2016. Fiber-Reinforced Polymer Composite Members with Adhesive Bonded Sleeve Joints for Space Frame Structures. *Journal of Materials in Civil Engineering*, 29 (2). [ONLINE] Available at: <http://ascelibrary.org/doi/10.1061/%28ASCE%29MT.1943-5533.0001737> [Accessed 10 September 2017].

Zielecki, W, Kubit, A, Trzepieciński, T, Narkiewicz, U, Czech, Z, 2016. Impact of Multiwall Carbon Nanotubes on the Fatigue Strength of Adhesive Joints. *International Journal of Adhesion and Adhesives*. [ONLINE] Available at: <http://dx.doi.org/10.1016/j.ijadhadh.2016.11.005> [Accessed 4 May 2017].

## Appendix A

$$v^2 = v_0^2 + 2a \quad (\text{A1-1})$$

$$0^2 = (62 \times 0,447)^2 + 2a(34,2)$$

$$a = -11,2 \text{ m / s}^2$$

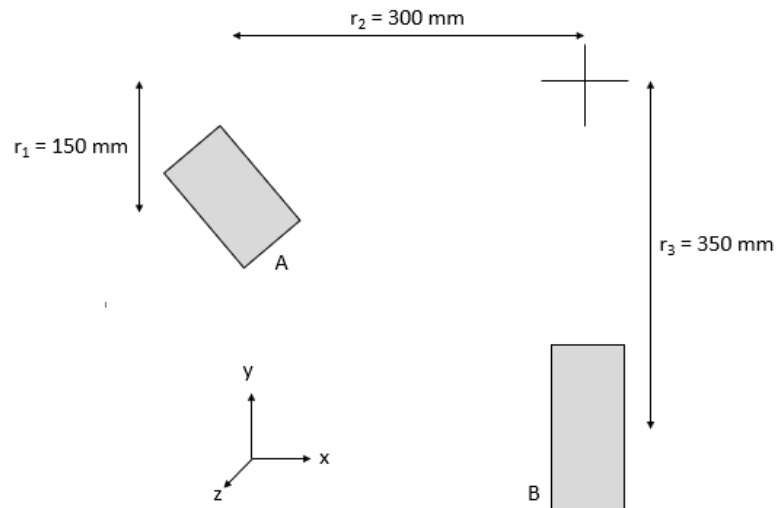


Figure A1-1: Diagram of mass centre relative to chassis mounting points

$$M_x = \frac{m}{2} |a_z| r_1 \quad (\text{A1-2})$$

$$M_x = \frac{100}{2} |7,65| (0,15)$$

$$M_x = 57,4 \text{ Nm}$$

$$M_y = -\frac{m}{2} |a_z| r_2 \quad (\text{A1-3})$$

$$M_y = -\frac{100}{2} |7,65| (0,3)$$

$$M_y = -115 \text{ Nm}$$

$$M_z = \frac{m}{2} |a_x| (0,15) - \frac{m}{2} |g| r_2 \quad (\text{A1-4})$$

$$M_z = \frac{100}{2} |-11,2| (0,15) - \frac{100}{2} |-9,81| (0,3)$$

$$M_z = -63,2 \text{ Nm}$$

$$M_x = \frac{m}{2} |a_z| r_3 \quad (\text{A1-5})$$

$$M_x = \frac{100}{2} |7,65| (0,35)$$

$$M_x = 134 \text{ Nm}$$

$$M_y = 0 \text{ Nm} \quad (\text{A1-6})$$

$$M_z = -\frac{m}{2} |a_x| r_3 \quad (\text{A1-7})$$

$$M_z = -\frac{100}{2} |-11,2| (0,35)$$

$$M_z = -196 \text{ Nm}$$

## Appendix B

This appendix contains the report supplied by DUT regarding the fabrication and testing of all specimens.



TSQ-670-07112017-002



### TECHNOLOGY STATION: REINFORCED & MOULDED PLASTICS

#### MATERIAL TESTING REPORT:

**Client:** Mr Mikhail Narsai of the University of Kwa-Zulu natal.  
**Testing Details:** Testing of Unidirectional carbon fibre samples.  
**Testing Conducted by:** Technology Station (TS), Durban University of Technology  
**Contact Person:** Ebrahim Cassim  
**Tel:** 031 373 2995  
**Email:** [ebrahimc@dut.ac.za](mailto:ebrahimc@dut.ac.za)  
**Date:** 07 November 2017  
**Client Signature:** 

#### 1. INTRODUCTION

The following report details the testing of unidirectional carbon fibre samples manufactured by the client with assistance from the TS. The tests conducted on the samples and their applicable standards are tabulated in Table 1.

No.	Test Conducted	Test Description	Applicable Standards
2.	Tensile	Determines the tensile strength and modulus of the specimen.	ASTM D3039
3.	Compressive	Determines the compressive strength of the specimen.	ASTM D 695/ SRM 1R-94
4.	Tube strength	Determines the strength of a tubular specimen.	-
5.	In-plane shear strength	Determines the in-plane shear strength of a $\pm 35^\circ$ fibre oriented specimen.	ASTM D3518/ D3518M
6.	Fibre content	Determines the required fibre content of the specimen by matrix digestion.	ASTM D3171-99

Table 1: Tests conducted and applicable standards.

**MANUFACTURING AND PREPARATION OF SPECIMENS**

It was required to produce unidirectional carbon fibre laminates and a unidirectional carbon fibre tube all with a similar volume fractions. The laminates and tube consisted of carbon fibre and epoxy resin (Prime 20LV). The lamination process used was vacuum infusion (VARTM), where resin was forced through the laminate at a vacuum pressure of 1 bar. The laminate was then left to cure at room temperature of 25°C for 24hrs, de-moulded and further cured at an elevated temperature of 40°C for 16 hrs. Specimens were CNC machined from the samples in accordance with the specific test geometrical requirements of Table 1. A carbide composite cutter was used to machine the specimens. Where necessary, specimens were cleaned, flash removed and polished with fine sandpaper prior to testing.

<b>Details of matrix, reinforcement and release system</b>	
<b>Matrix Details</b>	
Manufacturer	Gurit
Resin type	Epoxy
Resin Identification	Prime 20 LV
Density ( $\text{kg/m}^3$ )	1200
<b>Matrix hardener</b>	
Product Name	Prime 20 slow hardener
<b>Fibre Details</b>	
Fibre material	Carbon fibre
Fibre orientation	0° -Unidirectional
Material nominal weight ( $\text{g/m}^2$ )	300
Density	1850
<b>Release System</b>	
Wax	Ram Wax

Table 2: Process details.



Figure 1: Vacuum assisted resin transfer moulding of tensile test panel.



Figure 2: Vacuum assisted resin transfer moulding of tube sample.



## **2. TENSILE TEST- ASTM D3039**

The tensile properties of the specimens were determined using the ASTM D3039 testing standard. Rectangular tabbed specimens were prepared to determine the tensile strength and tensile modulus. Testing was performed utilising a Lloyd LR30k tensile testing machine with a 30KN load cell. An Epsilon extensometer with a gauge length of 25.00mm and a maximum travel of 2.50mm was used to determine the extension of the specimen during the test.

### **Note:**

- The ASTM D3039 test standard requires 5 valid failures. 5-7 specimens were machined and tested - 5 results were chosen. Specimens were averaged and standard deviation displayed as per standard requirements, the CV (Coefficient of variation) is also displayed.
- Values that deviated far from the mean or were invalid have been excluded from the average value.



Figure 3: ASTM D3039 Tensile test specimen with extensometer mounted.

**RESULTS**

<b>Laminate Details</b>	<b>Average Width (mm)</b>	<b>Average Thickness (mm)</b>	<b>Testing Speed (mm/min)</b>	<b>Load cell Size (KN)</b>	<b>Tabbed</b>
<b>0° Panel</b>	14.9	0.66	2	30	Yes
<b>90° Panel</b>	15	0.70	2	30	Yes

Table 3: ASTM D3039 average specimen dimensions and testing details.

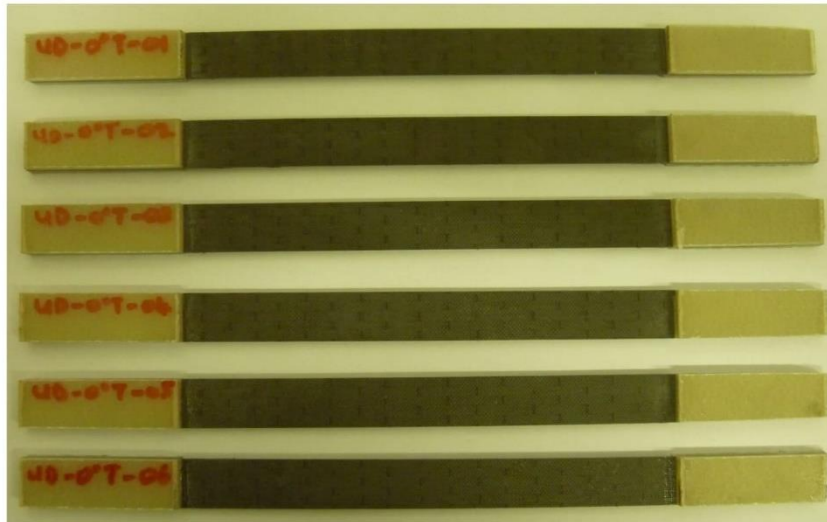
**0° PANEL**

Figure 4: 0° Panel specimens before tensile testing.

Specimen Number	Laminate Details: 0° Panel			
	Maximum Load (N)	Ultimate tensile strength (MPa)	Young's modulus (GPa)	Failure Mode / Details
UD-0T-02	19782.21	2012.96	119.98	VALID FAILURE
UD-0T-03	18986.73	1967.03	106.67	VALID FAILURE
UD-0T-04	19287.23	1991.45	104.69	VALID FAILURE
UD-0T-05	20134.81	2044.72	102.39	VALID FAILURE
UD-0T-06	18990.00	1931.06	110.70	VALID FAILURE
<b>Average</b>	<b>19436.20</b>	<b>1989.45</b>	<b>108.89</b>	
<b>Standard deviation</b>	-	43.37	-	
<b>CV (%)</b>	-	2.18	-	
UD-0T-01	18951.59	2246.51	134.08	VALID FAILURE

Table 4: Tensile properties of 0° Panel.

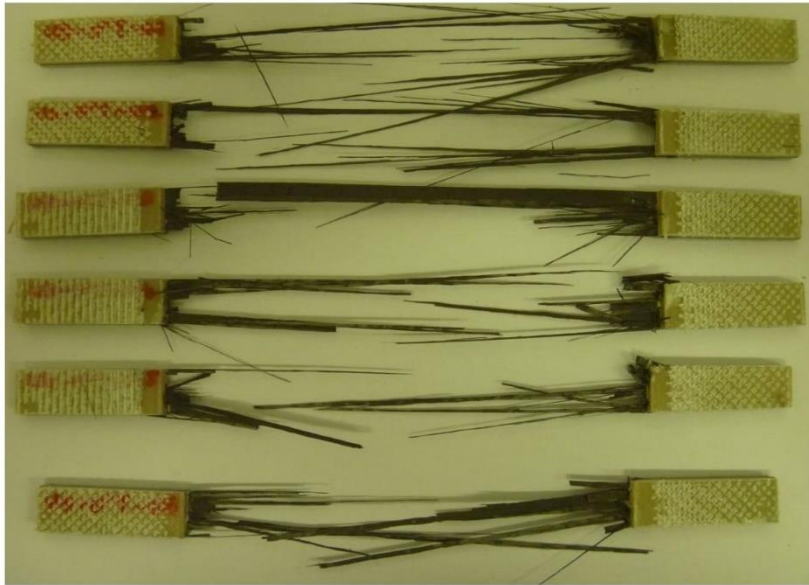


Figure 5: 0° Panel specimens after tensile testing.

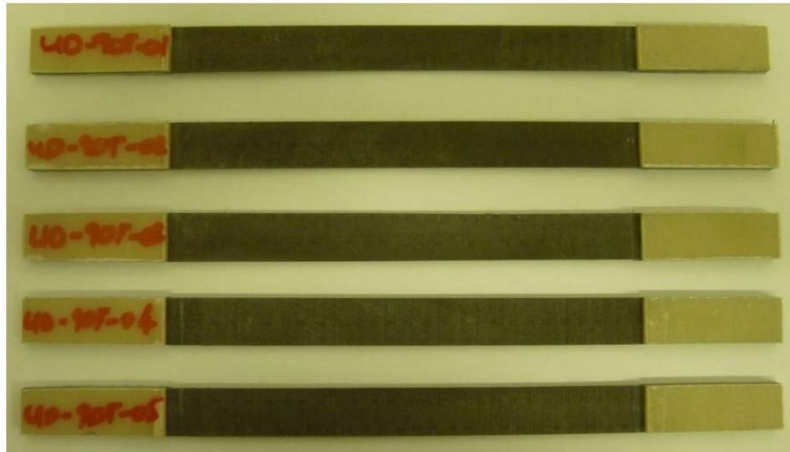
**90° PANEL**

Figure 6: 90° Panel specimens before tensile testing.

Specimen Number	Laminate Details: 90° Panel			
	Maximum Load (N)	Ultimate tensile strength (MPa)	Young's modulus (GPa)	Failure Mode / Details
UD-90T-01	340.75	32.56	6.52	VALID FAILURE
UD-90T-02	303.25	28.88	6.38	VALID FAILURE
UD-90T-03	314.03	30.11	6.58	VALID FAILURE
UD-90T-04	346.95	32.58	6.64	VALID FAILURE
UD-90T-05	243.43	23.18	6.48	VALID FAILURE
<b>Average</b>	<b>309.68</b>	<b>29.46</b>	<b>6.52</b>	
<b>Standard deviation</b>	-	3.86	-	
<b>CV (%)</b>	-	13.09	-	

Table 5: Tensile properties of 90° Panel.

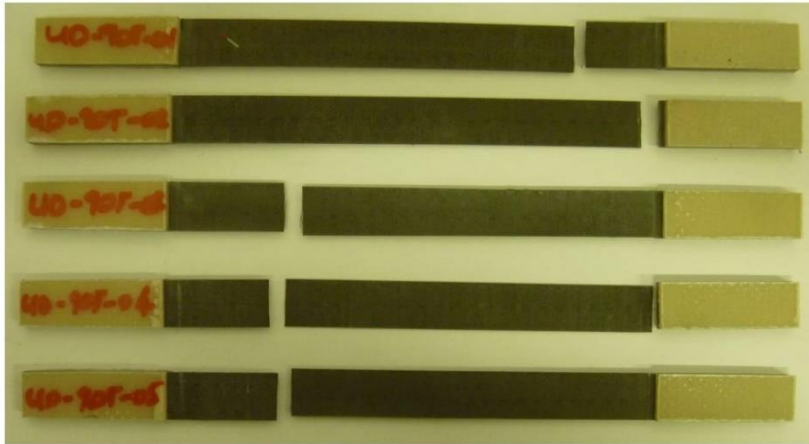


Figure 7: 90° Panel specimens after tensile testing.

### **3. COMPRESSIVE TEST - ASTM D 695/ SRM 1R-94.**

The compressive properties of the specimens were determined using the ASTM D 695/ SRM 1R-94 testing standard. All testing was performed using a Lloyd LR30k universal testing machine running in compressive mode. Specimens were prepared according to ASTM D 695/ SRM 1R-94 to determine the specimen's compressive strength. The specimens were placed in the modified ASTM D 695 Boeing 7260 compression test fixture and tested accordingly

**Note:**

- The ASTM D3039 test standard requires 5 valid failures. 6-7 specimens were machined and tested - 5 results were chosen. Specimens were averaged and standard deviation displayed as per standard requirements, the CV (Coefficient of variation) is also displayed.
- Values that deviated far from the mean or were invalid have been excluded from the average value.
- Neither slip promoters nor inhibitors were utilised during testing.



Figure 8: Specimen mounted in ASTM D 695 Boeing 7260 compression test fixture.

**RESULTS**

<b>Laminate Details</b>	<b>Average Width (mm)</b>	<b>Average Thickness (mm)</b>	<b>Testing Speed (mm/min)</b>	<b>Load cell Size (KN)</b>	<b>Tabbed</b>
<b>0° Panel</b>	14.7	0.85	1	30	Yes
<b>90° Panel</b>	14.8	0.90	1	30	Yes

Table 6: ASTM D 695/ SRM 1R-94 average specimen dimensions and testing details.



**0° PANEL**

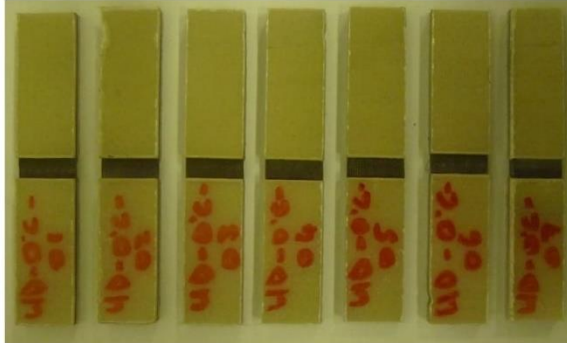


Figure 9: 0° Panel specimens before compressive testing.

Specimen Number	Laminate Details: 0° Panel		
	Maximum Load (N)	Ultimate Compressive strength (MPa)	Failure Mode / Details
UD-0C-01	9090.37	717.76	VALID FAILURE
UD-0C-03	9953.48	796.60	VALID FAILURE
UD-0C-04	10662.52	853.34	VALID FAILURE
UD-0C-05	10959.27	837.67	VALID FAILURE
UD-0C-07	9073.88	746.37	VALID FAILURE
<b>Average</b>	<b>9947.90</b>	<b>790.35</b>	
<b>Standard deviation</b>	-	57.99	
<b>CV (%)</b>	-	7.33	
UD-0C-02	8570.89	623.59	VALID FAILURE
UD-0C-06	10764.10	845.70	VALID FAILURE

Table 7: Compressive properties of the 0° Panel.

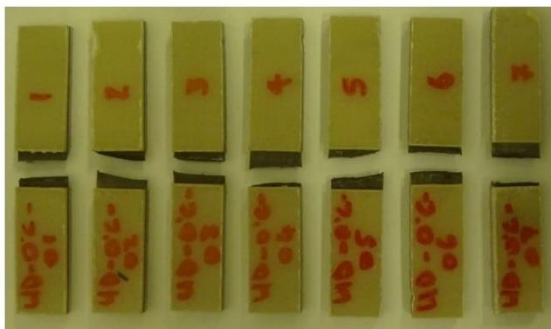


Figure 10: 0° Panel specimens after compressive testing.

**90° PANEL**

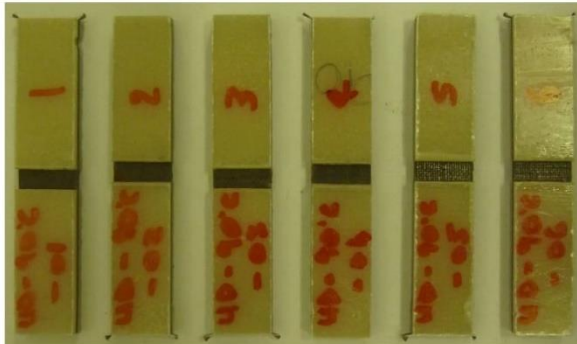


Figure 11: 90° Panel specimens before compressive testing.

Specimen Number	Laminate Details: 90° Panel		
	Maximum Load (N)	Ultimate Compressive strength (MPa)	Failure Mode / Details
UD-90C-01	1703.73	117.99	VALID FAILURE
UD-90C-02	1538.66	107.98	VALID FAILURE
UD-90C-03	1606.06	121.40	VALID FAILURE
UD-90C-04	1451.86	109.85	VALID FAILURE
UD-90C-05	1699.35	129.01	VALID FAILURE
<b>Average</b>	<b>1599.93</b>	<b>117.25</b>	
<b>Standard deviation</b>	-	8.61	
<b>CV (%)</b>	-	7.35	
UD-90C-06	1389.61	102.93	

Table 8: Compressive properties of the 90° Panel.

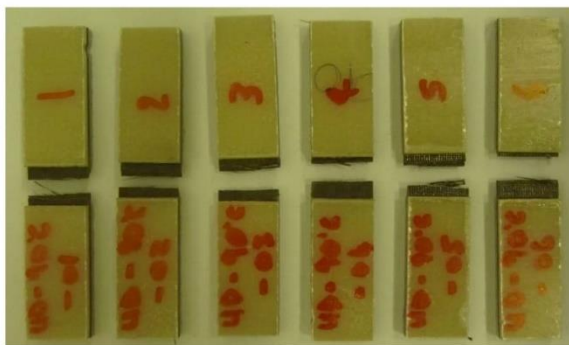


Figure 12: 90° Panel specimens after compressive testing.

#### **4. TUBE STRENGTH**

Carbon fibre tubes, with fibres orientated at 35° were tested in order to find the breaking load. All testing was performed using a Lloyd LR30k universal testing machine running in compressive mode. 3 specimens were tested.

**Note:**

- A metal ring was used at the bottom of the specimen to prevent crushing.
- Sand paper was used at the top and the bottom of the specimen to prevent slippage.

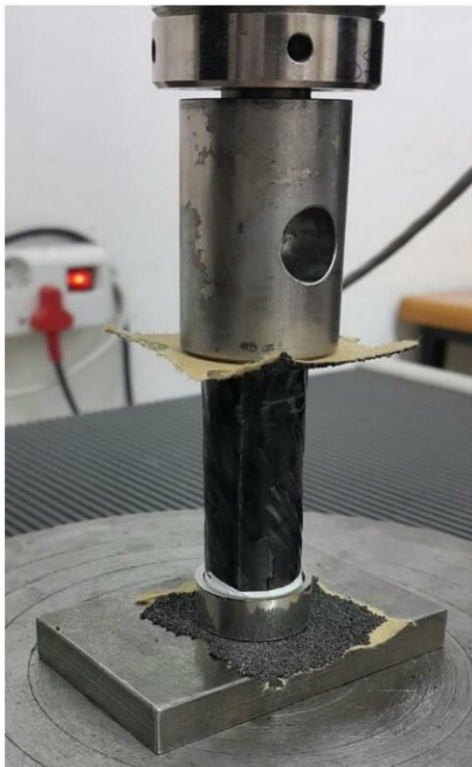


Figure 13: Manner in which specimens were tested.

**RESULTS**

Specimen No	Specimen length (mm)	Inner diameter (mm)	Average wall thickness (mm)	Failure load (N)
1	58.39	19.50	0.72	3449.1
2	55.26	18.42	0.61	2680.9
3	56.60	19.79	0.68	3405.5

Table 9: Test results.



Figure 14: Failure mode of tube specimen.

**5. IN-PLANE SHEAR STRENGTH TEST ASTM D3518/ D3518M**

The ASTM D3518/ D3518M standard was followed to determine the in-plane shear strength of the specimens. All testing was performed using a Lloyd LR30k tensile testing machine with a 30KN load cell. An Epsilon extensometer with a gauge length of 25.00mm and a maximum travel of 2.50mm was used to determine strain measurement in the axial direction (0°). Due to strain gauging equipment not being available at the DUT TS, Lateral strain measurement was conducted using a micrometre, although this method is not as accurate as a strain gauge, it was still used to get an approximate value of the change in lateral strain.

The shear modulus values were found for 2 specimens only.

- The ASTM D3518/ D3518M test standard requires 5 valid shear failures per batch.
- 5-7 Specimens were machined and tested. Specimens were averaged and Coefficient of variation (CV) displayed as per standard requirements.
- Values that deviated far from the mean have been excluded from the average value.

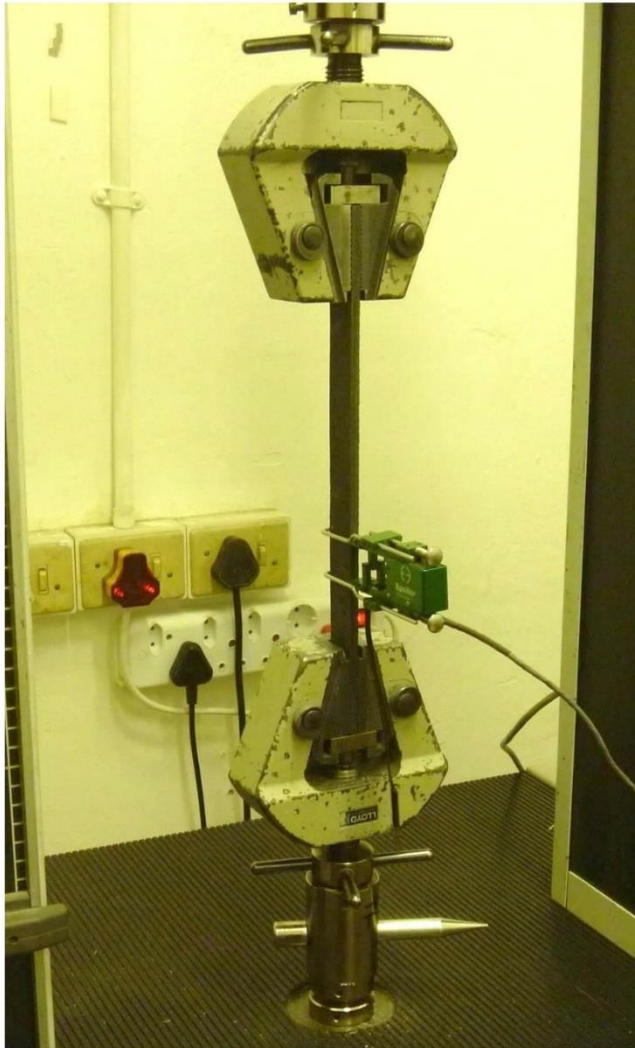


Figure 15: Carbon fibre UD specimen during tensile test.  
(Specimen un-tabbed at time of picture).

I

**RESULTS**

Laminate Details	Average Width (mm)	Average Thickness (mm)	Testing Speed (mm/min)	Load cell Size (KN)	Tabbed
±45° Panel	24.8	4.8	2	30	Yes

Table 10: Dimension of test specimens.

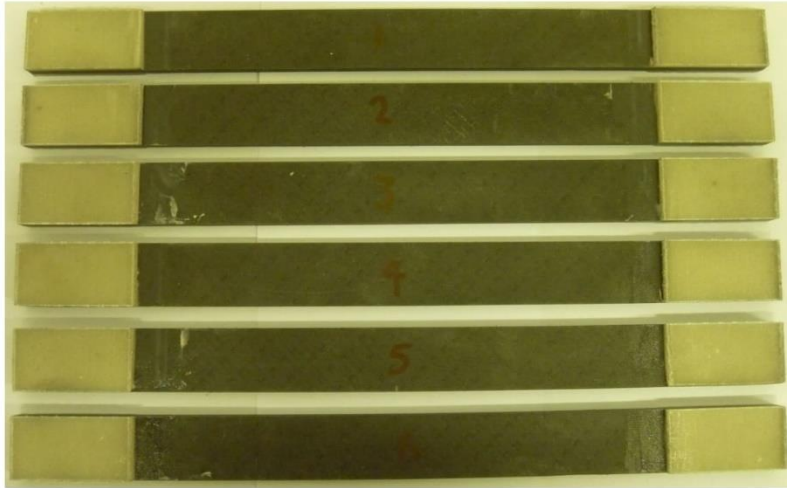
**±45° PANEL**

Figure 16: ±45° Panel specimens before In-plane shear testing.

Specimen Number	Laminate Details: ±45° Panel			
	Maximum Load (N)	In-plane shear strength (MPa)	Shear modulus (GPa)	Failure Mode / Details
1	19496.08	83.08	-	VALID FAILURE
2	19996.60	84.62	-	VALID FAILURE
3	19900.55	84.45	2.93	VALID FAILURE
4	19477.70	83.89	-	VALID FAILURE
5	20686.64	83.73	2.70	VALID FAILURE
<b>Average</b>	<b>19911.51</b>	<b>83.95</b>	-	
<b>Standard deviation</b>	-	0.61	-	
<b>CV (%)</b>	-	0.73	-	
6	19527.44	82.52	-	VALID FAILURE

Table 11: In-plane shear properties of the ±45° Panel specimens.



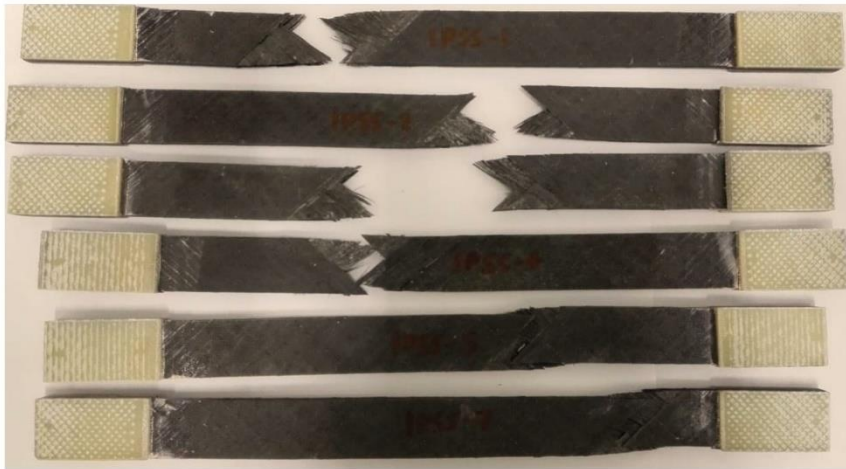


Figure 17:  $\pm 45^\circ$  Panel specimens after In-plane shear testing.

**6. FIBRE CONTENT- ASTM D3171-99**

The fibre content by mass of the specimens was determined using the ASTM D3171-99 testing standard, Procedure B, using sulphuric acid and hydrogen peroxide. Measurement of the mass was performed on a KERN and Sohn GmbH electronic balance with a resolution of 0.1mg.

- Specimens were tested from the tensile, compressive, shear strength and tube samples.

**RESULTS**

<b>Fibre content of specimen by mass (%)</b>				
<b>Samples</b>	<b>Specimen 1</b>	<b>Specimen 2</b>	<b>Specimen 3</b>	<b>Average</b>
<b>Tensile</b>	68.31	73.63	72.12	<b>71.35</b>
<b>Compressive</b>	67.51	69.57	71.87	<b>69.65</b>
<b>Shear</b>	65.56	66.63	67.22	<b>66.47</b>
<b>Tube</b>	65.49	66.61	73.08	<b>68.39</b>

Table 12: Fibre content of specimen by mass (%).

<b>Fibre content of specimen by volume (%)</b>				
<b>Samples</b>	<b>Specimen 1</b>	<b>Specimen 2</b>	<b>Specimen 3</b>	<b>Average</b>
<b>Tensile</b>	58.3	64.42	62.66	<b>61.79</b>
<b>Compressive</b>	57.41	59.73	62.37	<b>59.84</b>
<b>Shear</b>	55.25	56.43	57.08	<b>56.25</b>
<b>Tube</b>	55.18	56.4	63.78	<b>58.45</b>

Table 13: Fibre content of specimen by volume (%).

**7. CONCLUSION**

- Tensile testing conducted according to ASTM D3039. High CV noted in the 90° specimens. All failures are valid.
- Compressive testing conducted according to ASTM D 695/ SRM 1R-94. High CV noted in both 0° and 90° specimens. All failures are valid.
- Tube strength testing was conducted to no applicable standard.
- In plane shear strength testing conducted according to ASTM D3518/ D3518M. Shear stress results are consistent. All failures are valid.
- Fibre content testing conducted according to ASTM D3171-99.